AUS DER ABTEILUNG GENVEKTOREN
DES HELMHOLTZ ZENTRUM MÜNCHEN
VORSTAND: PROF. DR. WOLFGANG HAMMERSCHMIDT

DISSERTATION

ZUM ERWERB DES DOKTORGRADES DER NATURWISSENSCHAFTEN

AN DER MEDIZINISCHEN FAKULTÄT DER

LUDWIG-MAXIMILIANS-UNIVERSITÄT ZU MÜNCHEN

Notch2 signaling in B cell plasticity

VORGELEGT VON
MARKUS LECHNER
AUS
WEILHEIM I.OB

JAHR

2021

Mit Genehmigung der Medizinischen Fakultät

der Universität München

Betreuerin:	PD Dr. rer. nat. Ursula Zimber-Strobl
Zweitgutachter(in):	Prof. Dr. rer. nat. Olivier Gires
Dekan:	Prof. Dr. med. Thomas Gudermann
Tag der mündlichen Prüfung:	17.11.2021

Table of Contents

Publication based on the results of this dissertation and copyright statement:

Lechner, M., Engleitner, T., Babushku, T., Schmidt-Supprian, M., Rad, R., Strobl L. J. & Zimber-Strobl, U. **Notch2-mediated plasticity between marginal zone and follicular B cells**. *Nature Communications* (published 17.02.2021). doi:10.1038/s41467-021-21359-1 (Lechner et al. 2021)

In part, components of figures are shared between this thesis and the above publication. All used figures were created by Markus Lechner, unless otherwise stated.

ABSTRACT

B cells are a type of lymphocyte immune cells with important functions in humoral immunity of the adaptive immune system and are responsible for the production of antibodies. B cells also account for malignancies and autoimmune disorders. For a better understanding and treatment of these diseases, the respective B cell functions and last not least their development and origin are of crucial importance.

Murine peripheral B cells can be separated into B1 and B2 cells, with B2 cells constituting the vast majority of B cells in the secondary lymphatic organs such as the spleen. B2 cells in the murine spleen are composed of follicular B (FoB) and marginal zone B (MZB) cells, which are two functionally and spatially distinct mature B cell populations. It has been shown before that Notch2 signaling plays a key role in the cell fate decision of immature transitional B cells after influx into the spleen to terminally differentiate into either a FoB or MZB cell. This process is mediated by Notch2 activation via binding its ligand DLL-1 on follicular fibroblasts. To study the effect of Notch2 activation on B cells in this follicular niche, this work makes use of a transgenic mouse model with an inducible expression of a constitutively active intracellular signaling domain of the Notch2 receptor, specifically in mature FoB cells.

This work answered the open questions of what happens if a mature FoB cells receives an enduring Notch2 signal and whether this fate-decisive signaling pathway might suffice to induce a trans-differentiation towards the MZB lineage. It was observed that Notch2 activation triggered the slow process of re-programming FoB cells into bona fide MZB cells within a time window of two weeks with regard to their surface phenotype, splenic localization, immunological function and transcriptomic profile. The second part of this thesis answered the question whether the observed trans-differentiation can also occur physiologically in a non-transgenic setting of wild type mice. For this, purified FoB cells were transplanted into congenic recipient mice and their phenotype was followed up over the same time window of two weeks. The results of the adoptive transfer experiments confirmed our theory and proved a remarkable dynamic plasticity between mature FoB and MZB cells.

ZUSAMMENFASSUNG

B-Lymphozyten oder kurz B-Zellen stellen einen wichtigen Teil der Immunzellen dar und zeigen sich hauptverantwortlich für die humorale Immunantwort des adaptiven Immunsystems durch die Produktion und Sekretion von Antikörpern. B-Zellen sind in die Entstehung maligner Erkrankungen und Autoimmunkrankheiten involviert. Um diese Erkrankungen in Zukunft besser therapieren zu können, ist es von immenser Bedeutung, die einzelnen Untergruppen der B-Zellen, deren spezifische Funktionen und nicht zuletzt die Entwicklungswege der B-Zellen zu verstehen.

Murine periphere B-Zellen lassen sich grob in die zwei Unterklassen der B1 und B2-Zellen teilen, wobei letztere den Großteil der B-Zellen in den sekundären Lymphorganen wie der Milz stellen. Die B2-Zellen wiederum spalten sich in Follikuläre (Fo) und Marginalzonen (MZ) B–Zellen auf, zwei Zelltypen mit unterschiedlicher immunologischer Funktion und räumlicher Lokalisation innerhalb der Milz. In der Entwicklung dieser beiden reifen B-Zell Subpopulationen hat sich der Notch2 Signalweg als entscheidender Schalter herausgestellt, mit dem sich unreife Vorläuferzellen aus dem Knochenmark bei ihrer Ankunft in der Milz zur finalen Ausdifferenzierung in entweder FoB oder MZB-Zelle entscheiden. Dabei wird der Notch-Rezeptor durch Bindung mit dem Liganden DLL-1 aktiviert, der auf follikulären Fibroblasten exprimiert wird. Um den Effekt der Aktivierung des Notch2 Signalwegs in B-Zellen in dieser follikulären Nische zu untersuchen, wurde in dieser Dissertation ein transgenes Mausmodell verwendet, in dem die Expressionen eines konstitutiv aktiven Teils des Notch2-Rezeptors spezifisch in reifen FoB-Zellen induziert werden kann.

In der vorliegenden Dissertation wurde der Effekt eines andauernden Notch2 Signals auf reife FoB-Zellen untersucht, um die Frage zu beantworten, ob dieses Notch2 Signal ausreicht, um eine Transdifferenzierung zur MZB-Zellidentität anzustoßen. Die Induktion des konstitutiv aktiven Notch2 Signals war in der Tat der Auslöser eines relativ langsamen Prozesses der Transformation von FoB-Zellen in bona fide MZB-Zellen innerhalb eines Zeitfensters von zwei Wochen. Die MZB-Zell Identität konnte hinsichtlich des zellulären Phänotyps, der räumlichen Lokalisierung der Zellen innerhalb der Milzarchitektur, ihrer immunologischen Funktion sowie des Transkriptionsprofils bestätigt werden. Im zweiten experimentellen Teil dieser Arbeit wurde die Frage beantwortet, ob diese Transdifferenzierung auch im physiologischen Kontext in Wildtyp-

Mäusen stattfindet. Dazu wurden aufgereinigte FoB-Zellen in nicht-transgene Empfängermäuse transplantiert und deren Phänotyp über einen Zeitraum von zwei Wochen analysiert. Die Ergebnisse des adoptiven Transfers konnten unsere Theorie bestätigen, dass eine bemerkenswerte dynamische Plastizität zwischen reifen FoB und MZB-Zellen vorliegt.

1. Introduction

1.1 The two arms of the immune system

The mammalian immune system is constantly challenged by pathogens such as bacteria, viruses, fungi and parasites. Two arms of immune responses have evolved to counter these attacks: The innate and adaptive immune system. The innate immune system provides protection against a wide variety of foreign microorganisms and in general acts as a first line defense against pathogens during early days after an infection, bridging the gap before the adaptive immune response takes effect after a delay of 4-7 days. The innate immune system mainly comprises cells of the myeloid cell lineage, while the adaptive immune system is mostly executed by cells of the lymphoid lineage. Both lineages of immune cells derive from a common bone marrow-resident hematopoietic stem cell during hematopoiesis (Figure 1).

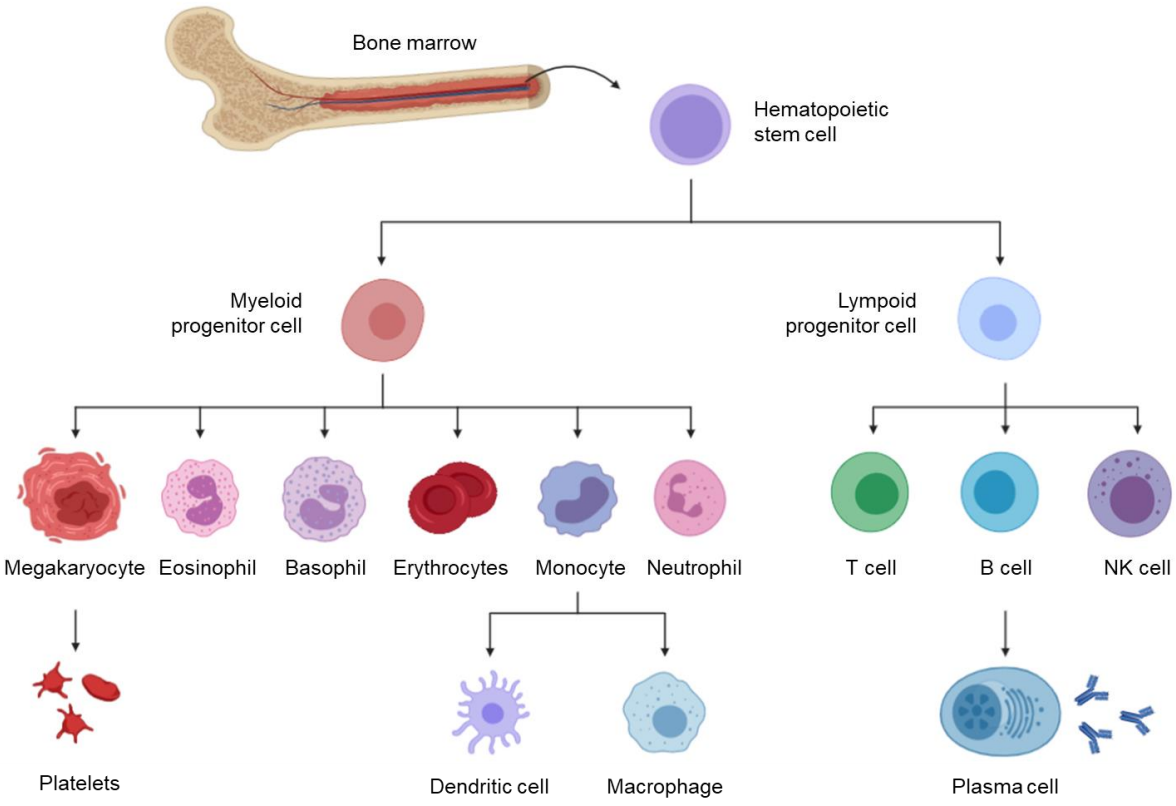

Figure 1: Simplified diagram of hematopoiesis. Hematopoietic stem cells are homed in the bone marrow and can develop into either a myeloid or lymphoid progenitor cell. These lineage-determining progenitors can give rise to the array of terminally differentiated myeloid or lymphoid cell types. (Illustration created in BioRender Basic, biorender.com

1.1.1 The innate immune system

The main mature myeloid effector cells are tissue-resident macrophages and different granulocytes (basophils, eosinophils and neutrophils) circulating in the blood stream. Macrophages are equipped with pattern recognition receptors such as toll-like receptors (TLRs), which can bind structurally conserved molecules, commonly found on microbes such as the bacterial cell wall component lipopolysaccharide (LPS). Pattern recognition receptor binding triggers phagocytosis of the pathogen and subsequent release of inflammatory cytokines and chemokines. Moreover, the so-called complement system is activated: plasma proteins initiate a cascade of proteolytic reactions on microbial surfaces, thus additionally coating and marking the pathogen. Cytokines, chemokines and complement proteins recruit and activate other cell types of the innate immune system from the blood stream to the site of acute infection, such as neutrophils, which further engulf and destroy the pathogens.

Inflammatory responses later involve lymphocytes, which have to be activated by pathogen-specific antigens that have drained from the infected site via afferent lymph vessels to the lymphoid tissues, in case the innate immune system has not succeeded in clearing the infection within a short period of time. Macrophages that have phagocytosed bacteria can also serve as antigen-presenting cells (APCs) to activate other immune cells. The cells that are highly specialized in antigen presentation to lymphocytes and therefore mainly account for the activation of the adaptive immune system are dendritic cells (DCs). APCs ingest and process pathogen-specific proteins and present antigens on their cell surface on major histocompatibility complex (MHC) proteins. DCs are the third class of phagocytic immune cells and can be derived from common myeloid or lymphoid progenitor cells. DCs have long finger-like processes, similar like dendrites of a nerve cell, which gave them their name. In contrast to other phagocytic cells like macrophages, the role of DCs is not the clearance of pathogens, but the presentation of pathogen-specific antigens to bridge the gap to the cells of the adaptive immune system – T and B lymphocytes (Murphy 2012; Taylor 2014).

1.1.2 The adaptive immune system

B cells and T cells are main effectors of the adaptive arm of the immune system. Cells of the adaptive immune system are mostly unable to rapidly respond to pathogens. However, the delayed activation and specification of B and T cells initiate powerful and highly specific mechanisms to not only fully eradicate the pathogen, but also to provide future protection by its memory function. Two major subsets of T cells have specialized for different tasks: $CD4^+$ T-helper cells (T_H-cells) and $CD8^+$ cytotoxic T lymphocytes (CTLs). Once activated by an antigen presented from APCs, T_H-cell can activate CTLs that subsequently migrate to the site of infection and execute the cellular immune response (Figure 2): CTLs release soluble factors to destroy the microbes or an infected body cell. T_H cells remain in the lymphoid organs and cooperate with B cells to initiate the humoral immune response: naïve B cells with a specific B cell receptor (BCR), a membrane-bound immunoglobulin (Ig), can bind the incoming antigen, process it and present it on MHC (major histocompatibility complex) class II surface proteins to T_H cells. T-helper cells, which possess a specific T cell receptor (TCR) against the presented antigen on the MHC class II molecule can bind to the MHC-antigen complex and further activate the B cells via direct surface receptor interaction and cytokine release. Activated effector B cells proliferate and differentiate to plasma cells, which secrete antibodies (released Ig) that circulate in the blood and specifically bind and coat pathogens, thus marking them for efficient phagocytosis and clearance. A more detailed description of B cell activation and plasma cell differentiation is presented in a later section of this work. Moreover, some activated B cells differentiate to memory B cells that serve as future protection against the encountered antigen (Silverstein and Bialasiewicz 1980).

Antibodies are the main effectors of the humoral immune response: These Y-shaped glycoproteins (see Figure 2, lower left side) are comprised of two large heavy chains and two small light chains and act via a highly variable antigen-binding region at the tip of the two “Y”-arms. The lower part is only comprised of heavy chain residues and termed Fc region and is structurally conserved to a limited number of so-called Ig-isotypes (IgM, IgD, IgE, IgG, IgA) (Murphy 2012).

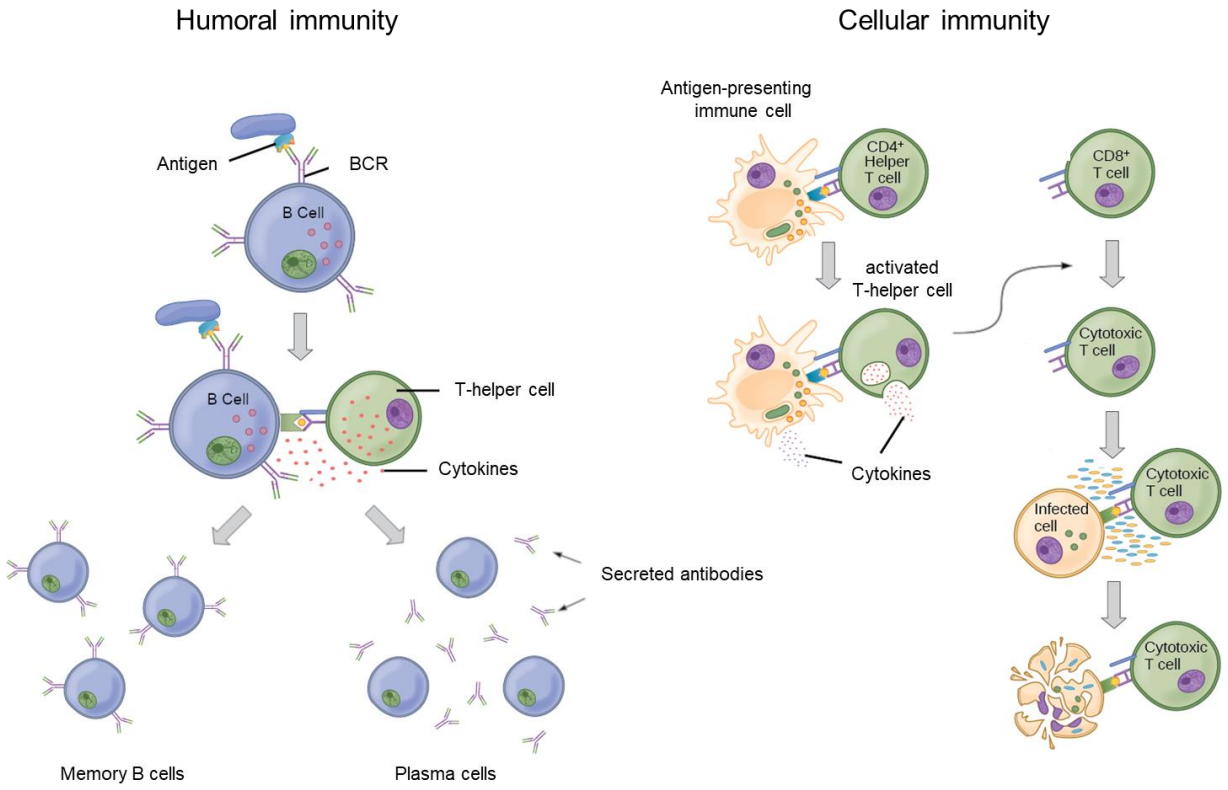

Figure 2: Simplified scheme of mechanisms during adaptive immune response. (adapted from Adaptive Immune Response by Charles Molnar and Jane Gair. License: CC BY 4.0; https://opentextbc.ca/biology/chapter/23-2-adaptive-immune-response/)

The process of T-cell dependent B cell activation takes several days until effective numbers of specific antibodies are secreted. In contrast to cells of the innate immune system, B and T cells do not have to rely on the binding of conserved pathogen structures. The capacity of B and T cells to respond to a virtually unlimited number of antigens in a highly specific way can only be established through processes of maturation and selection during immune responses and diversity of recombination in the generation of TCRs and BCRs during lymphopoiesis. The latter process is described as V (D)J recombination and occurs in the primary sites of lymphocyte maturation (bone marrow for B cells and thymus for T cells) and provides the functional basis for the adaptive immune system. Here, a very limited number of genes encoding for the variable (V), joining (J) and – in some cases – diversity (D) segments can be almost randomly rearranged and combined to generate millions of possible antigen-binding regions of TCRs and BCRs.

1.2 B cell development

T lymphocytes got their name from "thymus" - the mammalian organ they finalize their differentiation after influx of bone-marrow derived common progenitor cells. Most assume that B lymphocytes got their name because they mature in the bone marrow. Interestingly, the "B" in B cells is actually derived from *"bursa fabricii"*, a specialized organ of hematopoiesis in birds which is missing in mammals and was first described to be the site of antibody-producing cells in 1956 (Glick, Chang, and Jaap 1956), many decades after the discovery of antibodies (Cooper 2015). The separation of lymphocytes into *thymus-dependent* and *bursa-dependent* lineages was first introduced in a *Nature* paper in 1965 (Cooper, Peterson, and Good 1965). Since then, advances in animal models, clinical studies and molecular biology helped to understand and characterize the development and function of B cells. Mature functional B cells of mice come in two separated distinct lineages: B1 and B2 cells. B1 cells represent a minor sub-class of B cells that are commonly found in peripheral body cavities and are not considered as a part of the adaptive immune system. B1 cells are produced mainly in the fetal liver and undergo self-renewal in the periphery, unlike conventional B2 cells (Baumgarth 2017).

1.2.1 Early B cell development in the bone marrow

Murine B2 cells are generated from multipotent hematopoietic stem cell in the liver during late fetal development and in the bone marrow after birth and are subjected to multiple selection processes during development. The multipotent progenitors then differentiate into common lymphoid precursor (CLP) cells that can give rise to B, T and natural killer cells (Figure 1) (Kearney et al. 1997; Hardy and Hayakawa 2001). CLP cells still lack the surface expression of lineage-defining markers and can be identified by high expression levels of the interleukin-7 receptor (IL-7R). Earliest stages of B cell lineage commitment can be identified following the CLP stage by the expression of the B220 isoform of the pan-leukocyte molecule CD45 (Allman and Hardy 1999). These pre-Pro-B cells have not undergone immunoglobulin V (D)J rearrangement yet. They still lack CD19, a molecule whose expression characterizes all later stages within the B cell lineage. Pre-Pro-B cells show diminished levels of IL-7R expression when compared to the previous CLP stage and later stages of B lineage cells, which again highly express

IL-7R. Cells of the following Pro-B cell stage are either in a state of active cell division or initiation of immunoglobulin heavy-chain (V_HDJ_H) rearrangements, a state associated with cell cycle arrest. (V_HDJ_H) rearrangements aremediated by recombinase activating genes 1 and 2 (RAG1/2), dependent on transiently oscillating levels of IL-7R signaling. Activation of Il-7R signaling induces STAT5 and Cyclin D3 activation to drive proliferation and this inversely correlates with RAG1/2 gene expression (Johnson et al. 2012; Clark et al. 2014). Positive selection for successful heavy chain V_HDJ_H recombination leads to cell surface expression of the so-called pre-BCR and identifies large pre-B cells. Pre-BCR signaling is crucial for continued development and accounts for clonal expansion of large pre-B cells for several cell divisions. After this proliferative burst, large pre-B cells develop to small pre-B cells that exit the cell cycle and rearrange their immunoglobulin light-chains. Next, successfully rearranged light chain-expressing B cells are selected into the immature B cell pool, which express an antigen-specific BCR. At this stage, self-reactive B cells are either sorted out or edit their light chains via re-expression of RAG genes in order to change BCR specificity and prevent autoreactivity (Clark et al. 2014; Murphy 2012). After having passed this last selection step of clonal deletion or receptor editing, immature B cells can leave the bone marrow and enter the blood stream.

1.2.2 Peripheral B cell maturation and B cell subsets in the spleen

Immature B cells circulate the blood stream after their efflux from the bone marrow. Upon arrival in the largest peripheral lymphoid organ – the spleen – immature B cells pass transitional B cell stages (termed T1 and T2 cells, early papers also discussed a T3 cell stage) during their development into fully mature naïve B cells (Chung et al. 2002; Allman et al. 2001). All developing and transitional B cells express the surface marker of immaturity - CD93 (AA4.1), which is lost upon terminal differentiation to mature B lymphocytes. The transitional stages are considered to keep their identity only for a short time before their final maturation into one of the two distinct mature B cell identities: follicular B (FoB) cells and marginal zone B (MZB) cells (Pillai and Cariappa 2009). FoB and MZB cells represent two distinct mature B cell populations that differ in size, surface protein phenotype, splenic localization and immunological function. FoB cells account for the vast majority of mature peripheral B cells (80-90% in the spleen). MZB cells represent about 5-10% of all splenic B lymphocytes. While FoB cells are known to recirculate

between all other lymphoid tissues, murine MZB cells are sessile in the spleen (Martin and Kearney 2002; Pillai, Cariappa, and Moran 2005). FoB and MZB cells are usually identified by distinct surface marker expression: FoB cells are high in CD23 and IgD, and low in CD21, IgM and CD1d, in contrast to MZB cells, which are low in CD23 and IgD but high in CD21, IgM and CD1d. As the separation of mature FoB and MZB cells according to the aforementioned surface proteins does not distinguish cells in a clearly separated black or white manner, it leaves room for gating on potential intermediate phenotypes. From doing this, two intermediate mature B cell populations are being discussed: Follicular type 2 cells (FoB-II) and marginal zone precursor (MZP) cells. FoB-II cells differ from FoB cells by their high expression levels of IgM, and MZP cells still express higher levels of IgD and CD23 compared to its lineage-defining MZB counterparts (Allman, Srivastava, and Lindsley 2004; Srivastava, Quinn, et al. 2005; Srivastava, Lindsley, et al. 2005; Allman and Pillai 2008; Loder et al. 1999).

Back in 1901, Weidenreich first described a concentric ring of cells surrounding the follicle structures of the human spleen and called this the “Knötchenrandzone” (Weidenreich 1901). The cellular characterization of these cells - the MZB cells - were later described in 1982 in rat spleens (MacLennan et al. 1982). The function of MZB cells and decision of immature B cells to differentiate to a FoB or MZB cell identity have been subject to a plethora of studies ever since, especially in the last two decades. The most accepted model of peripheral B cell maturation is summed up in a review by Pillai and Cariappa (Pillai and Cariappa 2009) (Figure 3): Transitional B cells undergo critical fate-decision events to becoming either a FoB or MZB cell, mediated by the several cell signaling pathways that are thought to act in a tightly regulated interplay.

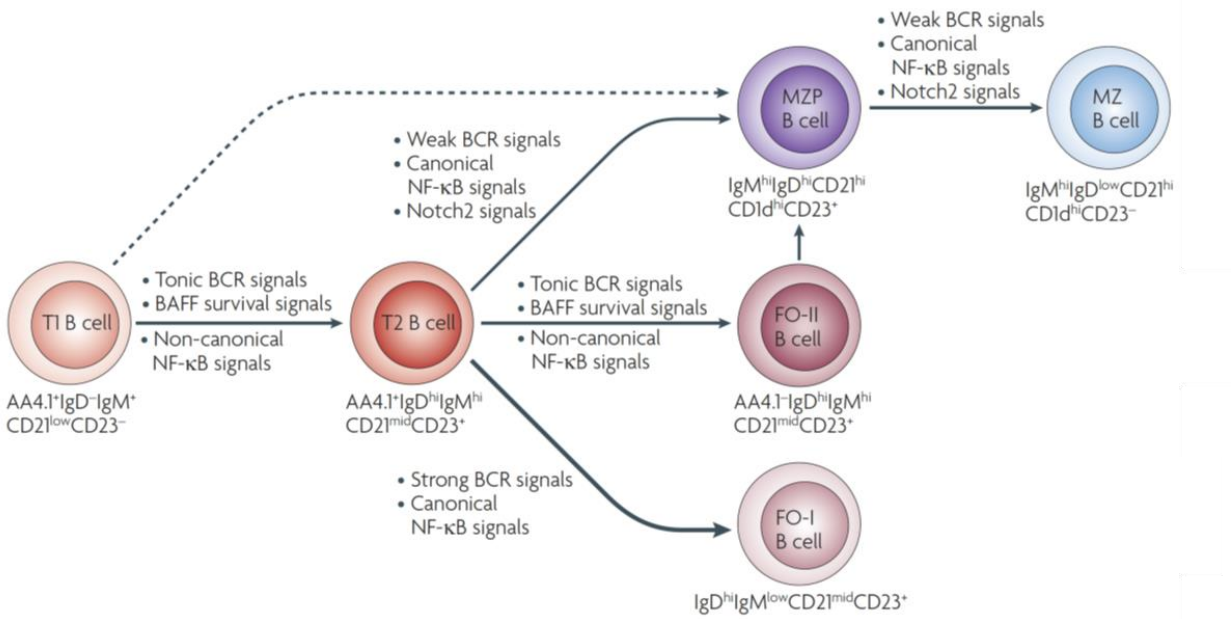

Figure 3: Model of sequential peripheral B cell development. Bone marrow derived immature B cells enter the spleen and develop into transitional (T1 and T2) B cells. They can mature into either follicular type I (FoB-I or here FO-I), follicular type II (FoB-II or FO-II) or marginal zone precursor (MZP) B cells. The cell fate decision depends on the interplay and strength of signaling pathways such as BCR, BAFF, NF-κB and Notch2 signaling. Cells are identified in flow cytometry by levels of surface protein expression of AA4.1, IgD, IgM, CD21, CD23 and CD1d. (Modified figure from a *Nature Immunology* review by Pillai and Cariappa, 2009 (Pillai and Cariappa 2009). Copyright license granted by Springer Nature)

The model describes a crucial cell fate decision event in T2 cells, dependent on BCR signal-strength and activation of the Notch2 receptor: Based on previous data from transgenic mouse models it is suggested that immature T2 B cells that receive a strong BCR signal and avoid activation of the Notch2 signaling differentiate to the follicular B cell lineage (Pillai and Cariappa 2009). Knockout mouse models of components of the BCR-BTK (Bruton's tyrosine kinase) pathway resulted in a loss of FoB cells, while MZB cells were preserved (Hardy et al. 1983; Hikida et al. 2003; Wen et al. 2003). Mice deficient for the transcription factor Aiolos, in which the signal strength of the BCR is strongly increased, showed that FoB cells were preserved while MZB and MZP cell numbers were markedly decreased (Cariappa et al. 2001). A lower BCR signal is considered being beneficial for the development of MZB cells. Transgenic B cells that recognize self antigens with low avidity were shown to preferentially differentiate to MZB cells (Kanayama, Cascalho, and Ohmori 2005; Martin and Kearney 2000; Pillai, Cariappa, and Moran 2005). Another transgenic BCR system was studied in hen egg lysozyme (HEL)-specific BCRs, where antigen-induced weak BCR signaling induced the generation of MZB cells (Wen et al. 2005).

The exact role of BCR signaling strength and the interplay of BCR signaling with other signaling components is still under investigation (Pillai and Cariappa 2009; Hikida et al. 2003). PI3K signaling also seems to be critically involved in FoB-versus-MZB fate decisions. PI3K signaling is activated downstream of the BCR co-receptor CD19 (Otero, Omori, and Rickert 2001; Anzelon, Wu, and Rickert 2003). Ablation of PI3K signaling component p110δ inhibits MZB cell generation (Clayton et al. 2002) while knockout of PTEN, a negative regulator of PI3K signaling, increased MZB differentiation (Anzelon, Wu, and Rickert 2003). Deletion of CD19 also completely blocks MZB development (Sato, Steeber, and Tedder 1995; Martin and Kearney 2000).

BAFF (B cell activating factor) has long been known to be important for overall B cell survival in the follicle (Batten et al. 2000; Schiemann et al. 2001) and BAFFR signaling is known to integrate with BCR signaling by cooperatively activating the non-canonical NF-κB pathway (Cancro 2009). Moreover, BAFFR signaling was shown to activate also the canonical NF-κB pathway, which was described being essential for MZB generation (Siebenlist, Brown, and Claudio 2005). Depletion of canonical NF-κB component such as p50 or c-REL ablated MZB differentiation (Sasaki et al. 2006; Pillai and Cariappa 2009; Cariappa et al. 2000; Ferguson and Corley 2005).

We know from a wealth of such studies that the development of MZB cells was especially dependent on functioning Notch2 signaling, as differentiation to the MZB lineage was defective after inactivation of Notch2 signaling components (Pillai and Cariappa 2009; Cariappa et al. 2001; Hampel et al. 2011; Saito et al. 2003; Hozumi et al. 2004; Kanayama, Cascalho, and Ohmori 2005; Otero, Anzelon, and Rickert 2003; Martin and Kearney 2000; Tanigaki et al. 2002; Tanigaki and Honjo 2007; Oyama et al. 2007; Tan et al. 2009; Gibb et al. 2010). The mode of temporal and spatial activation of Notch2 for a commitment to the MZB fate remains unclear so far, as well as the integration and potential crosstalk between Notch2 and other signaling pathways such as NF-κB or BCR/PI3K (Gutierrez and Look 2007; Osipo et al. 2008; Cornejo et al. 2011; Sangphech, Osborne, and Palaga 2014).

Several authors have however challenged the proposed model of lineage-defining fate decision at the immature T2 stage or tried to extend it with alternative ways. Already in 1999, experiments showed that mature FoB cells are direct precursors of MZB cells in rats (Dammers et al. 1999),

while others hypothesize a potential plasticity between a common precursor stage and MZB and FoB cells (Allman, Srivastava, and Lindsley 2004). As depicted in Figure 3, FoB-II cells are discussed to feed into the MZP pool, thus acting as potential reservoir for the MZB lineage (Pillai and Cariappa 2009). The origin, function and potential plasticity of these less-defined intermediate FoB-II and MZP cell population are still under discussion (Srivastava, Quinn, et al. 2005; Allman and Pillai 2008; Wang et al. 2010; Cariappa et al. 2007; Kleiman et al. 2015; Pillai and Cariappa 2009).

1.3 B cell functions

1.3.1 B cell localization sites within the murine spleen

For a better understanding of the distinct functional properties of FoB and MZB cells, it is necessary to gain a deeper insight into their respective spatial localization within the main peripheral lymphatic organ, the spleen.

Besides its already discussed role in hematopoiesis, the spleen hosts major immunologic sites of the adaptive immune system within its lymphocyte compartments. The principal physical architecture of the spleen is shared by all mammals and enables the organ to execute two major filtering functions at high blood perfusion rates: Clearing blood of old red blood cells (this process is name-giving for the so-called red pulp) and surveillance of blood-borne pathogens (executed in and around the lymphoid follicles, the white pulp). The white pulp is subdivided into T cell zones and B cell zones, which can easily be distinguished by histologic staining using lineage-specific antibodies (Figure 4).

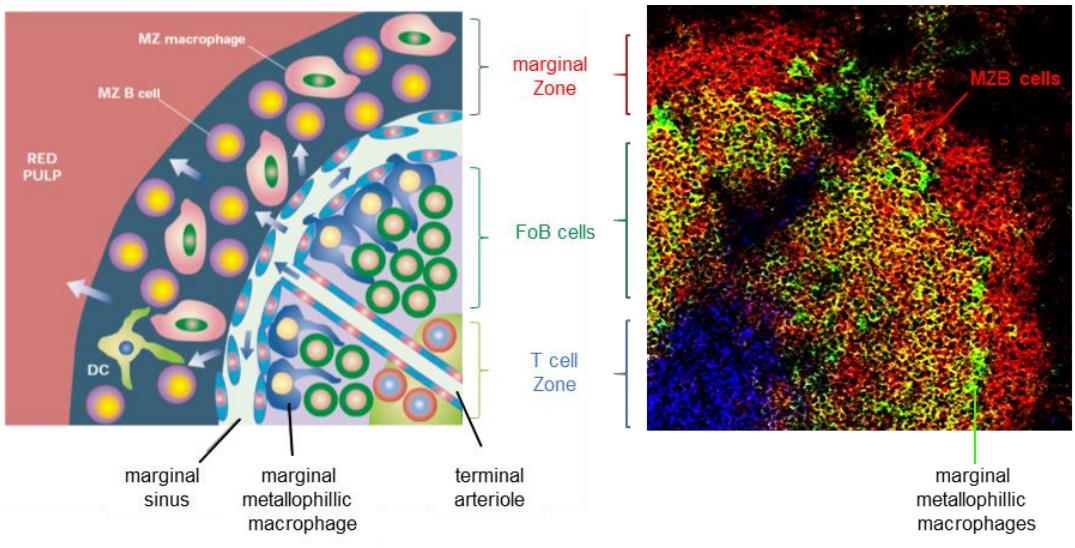

Figure 4: Schematic view (left) and exemplary immunofluorescent staining of a splenic section (right) depicting the murine marginal zone. Modified scheme from Jason G. Cyster's comment: "B cells on the from line" in *Nature Immunology*, 2000 (Cyster 2000)(Copyright license granted by Springer Nature). Immunofluorescent staining was performed with the following antibodies: anti-B220 (red), anti-IgD (green), MOMA-1 (bright green), CD90.2 (blue) (own data)

Blood enters the spleen through the splenic artery located in the lymphocyte follicle and is further distributed throughout the organ via smaller arterioles. The blood flow is thereby bypassing the white pulp, which is densely packed with T- and B-lymphocytes and protected from flow-induced shear stress. Arterioles terminate into the marginal sinus, from where the blood flow drains into an area populated with macrophages, dendritic cells and MZB cells before reaching the red pulp and re-joins circulation via venous sinuses (Cyster 2000; Lewis, Williams, and Eisenbarth 2019). This blood-perfused area is called marginal zone and is name-giving for the specialized MZB cells (Figure 4).

The splenic white pulp follicles were found to be a dynamic microenvironment, with FoB cells being in constant motion and transiently contact to other lymphocytes, follicular dendritic cells (FDCs) and stromal fibroblasts. FoB cells of the white pulp are actively surveying the microenvironment and especially antigen-presenting cells for signs of infection (Cyster 2005; Cyster 2010; Cyster and Schwab 2012). A high motility was also attributed to MZB cells, as they constantly shuttle between the marginal zone and the follicle (Cinamon et al. 2008; Arnon et al. 2013).

The marginal zone is only found adjacent to follicle structures of the murine splenic white pulp, while lymphocyte follicles of lymph nodes lack this specialized microenvironment. While the marginal zone was shown to be larger in rats than in mice and even constitute the major B cell compartment there (MacLennan et al. 1982; Kumararatne, Bazin, and MacLennan 1981), a comparable substructure is slightly different in humans and is generally less studied. Here, additional substructures add some complexity: Lymphocyte follicles in human spleens are surrounded by a marginal zone and a perifollicular zone (Cerutti, Cols, and Puga 2013; Lewis, Williams, and Eisenbarth 2019). The lack of detailed cellular characterization of the human splenic architecture accounts for some ambiguity regarding the comparison between murine and human splenic B cells subsets. Whether the region referred to as MZ in humans is a functional analog to the murine MZ and whether mouse and human MZB cells resemble each other is not well studied so far.

1.3.2 B cell activation

As described above, plasma cells are the antibody-producing effector cells that have differentiated from naïve B cells. Plasmablasts are a short-lived precursor cell type at the transition of activated B cells to plasma cells. The activation of a B cell is clearly dependent on the B cell subtype and the properties of the antigen. Overall, B1 and MZB cells can be functionally grouped together as executers of a rapid first-line defense against common antigens, whereas FoB cells are known to cooperate with T cells in generating a delayed but highly specific antibody response. The different ways of activation will be addressed in the following chapter. Common to all B cells is the cell-intrinsic machinery of transcription factors that are known mediators of plasmablast and plasma cell differentiation: Naïve B cell activation and differentiation to plasmablasts and plasma cells is always driven by the transcription factors Irf4 and Blimp1 (Klein et al. 2006; Savage et al. 2017; Tellier et al. 2016; Shaffer et al. 2002; Ochiai et al. 2013).

The outcome of B cell-derived plasma cell response differs and can generally be separated into the two types of T cell-dependent and T cell-independent immune reactions (MacLennan et al. 1997; Murphy 2012). While TD antigens are usually derived from proteins, TI antigens are diverse, can additionally be comprised of lipid-residues or DNA and often exhibit repetitive,

polymeric structures. TI responses are mainly triggered through antigens derived from common natural pathogens and are potent direct activators of B cells that do not require additional stimulation through T helper cells. TI antigens can further be divided into TI-1 and TI-2 antigens: TI-1 antigens can be bound by both BCRs and TLRs to directly activate the encountering B cell. Examples are LPS or bacterial DNA (Rawlings et al. 2012b). TI-2 antigens mainly consist of highly repetitive epitopes that activate B cells by binding to multiple BCRs simultaneously and cross-linking of a critical number of BCRs (Murphy 2012; Vos et al. 2000; Liao et al. 2017).

1.3.2.1 T cell-dependent immune responses

FoB cells are by far the most abundant population of naïve B cells and execute the T cell-dependent (TD) immune responses. FoB cells recirculate through the blood and lymphatic organs, constantly screening for unprocessed foreign antigens that can be bound by their BCR. The bound antigen is engulfed, processed and presented on MHC class II proteins to epitope-specific T cells. Antigen binding induces BCR signaling, which results in B cell activation. BCR activation further initiates the upregulation of chemokine receptor CCR7, which directs their movement towards the border of T cell zones, following a gradient of CCL19 and CCL21, two chemokines produced in the T cell area (Förster, Davalos-Misslitz, and Rot 2008; Forster et al. 1999). T_H cells with a TCR specific for processed polypeptides of the same antigen are activated by peptide presentation via MHC-II on APCs in the T cell zone, which in turn leads to an upregulation of CXCR5 and migration along the gradient of CXCR5-ligand CXCL13, produced in the B cell area. This parallel movement of B and T cells, specific for a common antigen, positions both lymphocyte cell types at the border between T and B cell zones (Oracki et al. 2010). Activated T_H cells and B cells interact closely in a so called immunological synapse via the polypeptide-mediated TCR:MHC interaction and secondary interactions that involve costimulatory molecules expressed as receptor-ligand pairs on T and B cells. These interaction partners include CD40 ligand (CD40L), CD28, CTLA-4 and ICOS expressed on activated T cells and CD40, CD80, CD86 and ICOS Ligand (ICosL) expressed on B cells (Murphy 2012; Bretscher 1999). Additional accessory signals are also delivered via T-cell secretion of cytokines such as interleukin (IL)-2, 4, 5, 10 and 12 as well as interferon (IFN)-gamma that can act on both B cells and in an autocrine way on T_H cells (Peng et al. 1996; Murphy 2012; Dustin 2014)

This co-activation triggers B cell proliferation and plasma cell differentiation, which can be derived either by rapid extra-follicular differentiation or by the slower germinal center reaction, depending on antigen affinity (Murphy 2012; Fairfax et al. 2008; Oracki et al. 2010; Paus et al. 2006; Chan et al. 2009). The germinal center (GC) forms at the site of T- / B- cell zone border and is a highly dynamic substructure of B and T cell interaction that is important for B cell proliferation and selection, dependent on BCR specificity. The GC is established several days after infection and can be present for weeks. In the GC, phases of extensive B cell proliferation take turns with phases of antibody modification and selection via processes of somatic hypermutation (SHM) of the antigen-binding variable region of immunoglobulin (Ig) genes and Ig-class switch recombination (CSR). SHM is driven by single-base changes that are introduced into the *Ig* regions that encode for the antigen-binding domain of the BCR or the respective secreted antibody. This process is driven by the deamination of cytosine to uracil in the DNA by the enzyme activation-induced deaminase (AID), resulting in a DNA mismatch and error-prone base excision repair (Larson and Maizels 2004; Teng and Papavasiliou 2007). Several rounds of these mutations and selections for BCR specificity dramatically diversify the possible *Ig* repertoire. The constant regions of the *Ig* heavy chain genes undergo a series of modification known as class-switch recombination (CSR). Here, portions of the heavy chain locus are again nicked by AID-mediated lesions and the consequently introduced double-strand brakes allow to be substituted with other constant region gene segments. Recombination results in the class switch and B cell production of different antibody isotypes such as IgG or IgE (Muramatsu et al. 2000; Murphy 2012; Yu and Lieber 2019).

The GC reaction leads to the output of either plasma cells, which produce affinity-maturated antibodies of several Ig-subclasses (IgM, IgG, IgE), or memory B cells that establish a long-term immunological memory. GC-derived antibodies of high affinity were described to be detectable in the blood of immunized mice after several days, usually not before 5 days after immunization (Zhang, Garcia-Ibanez, and Toellner 2016; Mesin, Ersching, and Victora 2016).

1.3.2.2 T cell-independent immune responses

T cell independent (TI) immune responses are important to close the temporal gap before the production of high affinity antibodies derived from GC reactions come into play. The TI immune response is mediated by MZB cells (and B1 cells) and can close this gap via a rapid secretion of

rather unspecific antibodies, which are mostly of IgM isotype (Martin, Oliver, and Kearney 2001). MZB cells interact with antigens exposed on marginal zone-resident macrophages or DCs and rapidly differentiate to short-lived plasmablasts, which produce large amounts of antibodies, thus bypassing the necessity of T cell help. Antigen-dependent activation of MZB cells through BCR ligation and activated TLR signaling induces a rapid re-localization of MZB cells into the splenic follicle (Kraal 1992; Groeneveld, Erich, and Kraal 1985), where they start to differentiate to pre-plasmablasts. Subsequently, they migrate towards the bridging channels between B and T cell zones and leave the follicle into the red pulp where they continue to differentiate to extrafollicular PC (Wehrli et al. 2001). Apart from their secretion of large amounts of IgM-antibodies, MZB cells can produce IgG3 and IgA via class switch recombination in extrafollicular foci (MacLennan and Vinuesa 2003).

1.3.3 Inherent traits of innate-like marginal zone B cells

Being located in a microenvironment of strong blood flow and adjacent to antigen-capturing cells such as macrophages and dendritic cells, MZB cells are prone to respond rapidly to blood-borne pathogens via strategies blurring the classical boundaries of innate and adaptive immunity. Several adaptions enable MZB to localize in the MZ and execute innate-like immune functions (Kraal 1992; Wardemann et al. 2002).

Opposed to the protected white pulp, the MZ is a microenvironment exposed to strong blood flow exposing all MZ cells to shear stress through the strong flow currents (Tedford et al. 2017). The MZ-specific microenvironment is created by stromal cells expressing certain cell adhesion molecules that are not found in the follicle such as ICAM-1 and VCAM-1 expression on fibroblastic reticular cells (FRCs) (Arnon and Cyster 2014; Cyster, Lu, and Lo 2003; Katakai et al. 2004). Moreover, the MZ niche was shown to be specifically defined by the secondary matrix protein laminin α5 (Song et al. 2013) and the presence of spingosine-1-phosphate (S1P), a signaling molecule not or barely found in the white pulp (Ramos-Perez et al. 2015).

MZB cells show several adaptive features enabling them to attach to the extracellular matrix of the MZ and being not washed away with the blood flow. MZB cell express integrins such as α6β1, crucial for binding and holding MZB cells to the laminin-α5-rich MZ (Song et al. 2013).

Moreover, MZB cells express high levels of shear stress-induced integrins such as α4β1 (VLA-4), αLβ2 (LFA-1) to be able to bind and migrate along gradients of respective ligands fibronectin, VCAM-1 or ICAM1-4 (Tedford et al. 2017). FoB cells, which lack a similar integrin machinery get "flushed" away towards the red pulp upon migration to the MZ (Arnon and Cyster 2014). The efforts made in recent years to enlighten the mechanisms of MZB cell migration dynamics were especially driven by Jason Cyster and colleagues. They found that S1P-receptor signaling is the key mediator of lymphocyte migration to and homing in the S1P-rich MZ (Cyster 2000; Cinamon et al. 2004; Cyster 2005; Cinamon et al. 2008; Arnon et al. 2011; Cyster and Schwab 2012; Arnon et al. 2013; Arnon and Cyster 2014). Interestingly, they also describe that MZB cells constantly shuttle between the MZ and the B cell follicle and that this migration is mediated by transient upregulation and desensitization of S1P-receptors 1 and 3 (S1PR1 and S1PR3). The re-entry of S1PR-desensetized B cells into the follicle is guided by CXCR5-mediated binding of CXCL13, the chemokine produced by cells of the B cell follicles.

MZB cells are frequently termed innate-like lymphocytes (Meyer-Bahlburg et al. 2009; Rawlings et al. 2012a; Grasseau et al. 2020). This term is derived from their capability to rapidly respond to common bacterial antigens within hours in a pattern-recognition fashion, mediated by the expression of high levels of TLRs. TLR expression is a trait common to executors of the innate immunity: DCs, macrophages or granulocytes (Treml et al. 2007; Genestier et al. 2007; Cerutti, Cols, and Puga 2013). Functionally, MZB cells are considered important executers of a rapid first-line defense against blood-borne pathogens (Rubtsov et al. 2008). While FoB cells express mono-reactive BCRs, many MZB cells were found to express BCR of polyreactive specificity against multiple microbial patterns, sometimes similar to TLRs, thus additionally blurring the boundaries between innate and adaptive immune systems (Martin and Kearney 2002; Treml et al. 2007).

The rapid response is additionally launched through the pre-activated state of MZB cells. Hence, MZB cells were found to generate effector cells much more efficiently than FoB cells (Oliver, Martin, and Kearney 1999; Martin, Oliver, and Kearney 2001). MZB cells mostly execute T cell independent immune responses by rapid secretion of large amounts of antibodies from the IgM and IgG3 isotype. Moreover, MZB cells produce so-called natural antibodies that are present without any previous infection or vaccination, an immunologic function shared with innate B1 cells (Martin, Oliver, and Kearney 2001; Cerutti, Cols, and Puga 2013). Another trait of MZB

cells is their high expression levels of the MHC-I-like molecule CD1d, enabling them to present lipid antigens to other immune cells such as natural killer T cells (Sonoda and Stein-Streilein 2002; Chaudhry and Karadimitris 2014). This shows their potential as antigen-transporting and -presenting cells, thus broadening the MZB cell-mediated immune responses from only acting independently of T cells. Finally, MZB cells are thought to share intrinsic properties of memory cells such as the potential of self-renewal and longevity (Hao and Rajewsky 2001; Martin and Kearney 2002). Some authors have shown that MZB cells additionally participate in GC reactions in T cell-dependent immune reactions (Song and Cerny 2003).

1.4 Notch2 signaling

Notch signaling pathways are evolutionary conserved and present in most multicellular organisms. Being a regulatory pathway for gene expression, Notch is involved in multiple differentiation processes. The Notch signaling pathway has its name from a gene that, if altered, resulted in a "notched" wing phenotype in the fruit fly *Drosophila*, as described in 1917 by evolutionary biologist Thomas H. Morgan (Morgan 1917).

1.4.1 Structure and activation of Notch receptors

The family of Notch receptors consists of four members (Notch1-4) and five ligands (Delta-like (DLL)-1,2,4 and Jagged-1,2). Notch receptors are heterodimers consisting of an extracellular (NotchEC) part and a transmembrane/intracellular part (NotchTM/IC), which are connected by disulfide bonds. The N-terminal NotchEC contains epidermal growth factor (EGF)-like repeat elements that mediate ligand binding. The C-terminal part of the Notch receptor is comprised of a short extracellular heterodimerization domain, a transmembrane stretch and the intracellular (NotchIC) part containing several functional domains such as a RAM (RBPjκ association module) domain and a transactivation domain (TAD). The TAD contains a nuclear localization sequence (NLS) and conserved proline/glutamic acid/serine/threonine-rich motif (PEST). Notch signaling differs from other conserved signaling pathways in its mechanism of receptor proteolysis. During maturation in the Golgi network, Notch precursor proteins are cleaved at the Site 1 (S1) by furin-like convertases producing the heterodimeric receptor. Activated Notch receptors undergo two

consecutive proteolytic cleavages: The first activating cleavage (S2) executed by ADAM metalloproteases at an extracellular site that is only exposed through ligand binding-induced conformational changes. This S2 cleavage releases NotchEC, which is endocytosed by the ligand-expressing cell. The consecutive S3 cleavage is performed by γ-secretase (at the transmembrane domain) to release the intracellular fragment NotchIC, which then translocates to the nucleus and promotes transcriptional activation (Radtke, MacDonald, and Tacchini-Cottier 2013) through interaction with the DNA-binding protein RBPjκ (recombining binding protein suppressor of hairless, also known as CBF-1) and the transcription factor Mastermind proteins (Mastermind-like 1: MAML1) (Figure 5). In the absence of NotchIC, RBPjκ is bound to DNA but associated with repressor proteins and histone deacetylases, thus acting as a transcriptional repressor of target genes (Kopan and Ilagan 2009; Kovall et al. 2017).

Notch signaling has been shown to play key roles in differentiation and cell fate decision processes at various developmental stages or cell types, such as embryogenesis and hematopoiesis. The different developmental functions of Notch signaling are mediated by different receptor-ligand pairs: prominent examples are Jagged1:Notch1 in embryonic hematopoietic stem cells, DLL-4:Notch1 for T cell development and DLL-1:Notch2 for MZB cell differentiation (Radtke, Fasnacht, and Macdonald 2010).

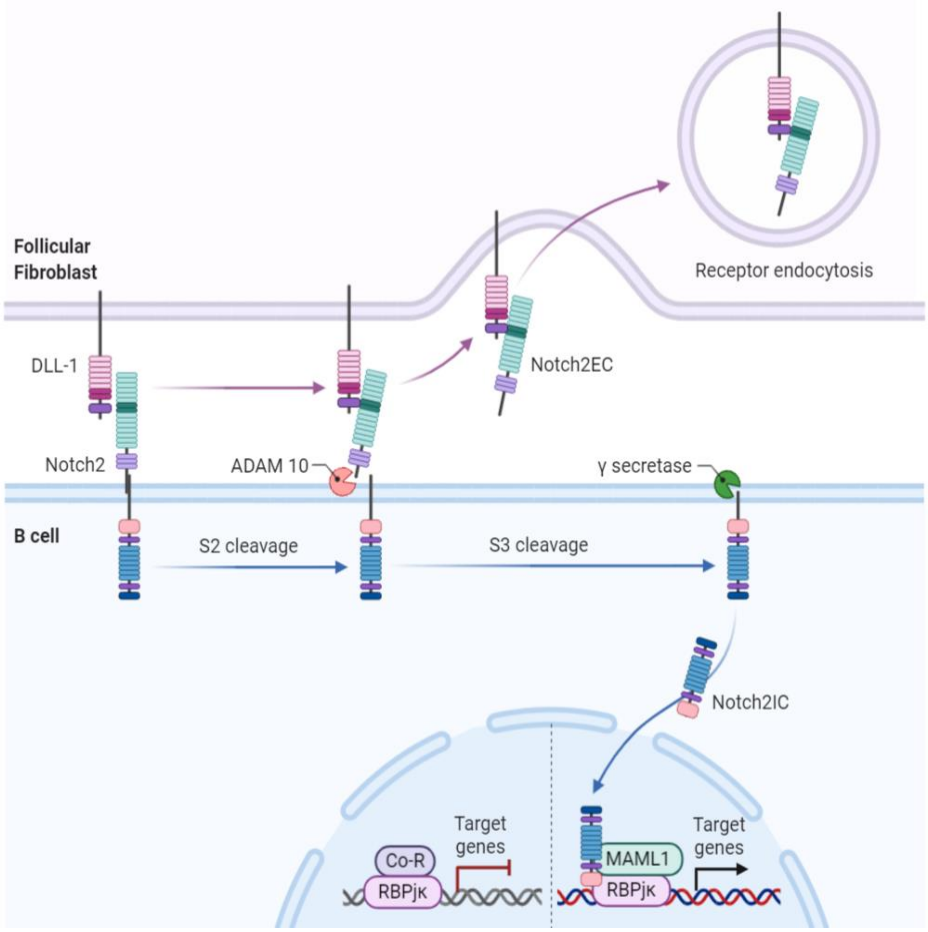

Figure 5: Schematic summary of Notch2 receptor activation. Activation of Notch2 via DLL-1-binding expressed on follicular fibroblasts releases the intracellular Notch2 domain (Notch2IC) after two proteolytic receptor cleavages through ADAM metalloproteases (S2) and γ-secretase (S3). Notch2IC translocates to the nucleus where it binds to RBPjκ, recruits the transcription factor MAML1 to activate target gene expression. (Illustration created in BioRender Basic, biorender.com)

1.4.2 Notch2 signaling in B cell development

As already mentioned earlier, functional Notch2 signaling has been shown in many genetic loss-of-function mouse models to be absolutely essential for MZB development. Knockout of the Notch2 receptor itself (Saito et al. 2003) or RBPJκ (Tanigaki et al. 2002) as well as deletion of essential signaling components such as the Notch2 receptor-cleaving metalloprotease ADAM10 (Gibb et al. 2010; Hammad et al. 2017) or the co-activator MAML1 (Oyama et al. 2007) all inhibit MZB generation, without observable defects in the development or function of mature FoB cells. Moreover, DLL-1 was identified as specific ligand for Notch2 in the context of peripheral B cell

maturation. Knockout or downmodulation of DLL-1 inhibited the successful MZB cell differentiation, while development of other lymphocytes (FoB cells and T cell subsets) was untouched (Hozumi et al. 2004; Moriyama et al. 2008). Fine tuning of Notch2 signaling strength plays a key role in this regard, as MZB differentiation was sensitive to changes in Notch2 receptor expression levels: Inactivation of one allele for Notch2 in B cells was already sufficient to strongly decrease MZB development (Saito et al. 2003). Vice versa, activated Notch2 signaling in B cells from immature stages onwards strongly preferred their differentiation to the MZB over FoB cell fate, even in the absence of CD19 signaling (Hampel et al. 2011).

The splenic site of Notch2 activation has also been investigated in the past. DLL-1 is expressed on various cell types within the spleen and early studies suggested that DLL-1 is expressed on B cells and DCs (Hozumi et al. 2004). Later, DLL-1 was successfully stained on macrophages, DCs and erythroblasts but not on lymphocytes (Moriyama et al. 2008). With the use of a *LacZ* -reporter mouse, DLL-1 expression was found on endothelial cells of venules within the MZ and the red pulp (Tan et al. 2009). An extensive study by the Radtke group performed specific conditional knockouts of Notch ligands on splenic cell types (DCs, endothelial cells, stromal cells). They could disprove the prior hypothesis of DCs and endothelial cells as the important source of DLL-1:Notch2 interaction and finally found DLL-1 expression on fibroblastic stromal cells within the follicle to be the essential site of Notch2 activation for MZB differentiation (Fasnacht et al. 2014) (Figure 5). From this finding, the conclusion can be drawn that incoming transitional B cells receive their threshold Notch2 signal to choose the MZB cell fate within the white pulp of the follicles and not at earlier time points on their migration to the splenic B cell sites.

1.5. The mouse model to study activation of Notch2 in B cells

To investigate the role of Notch2 signaling in B cell biology, a former colleague in the laboratory of Ursula Zimber-Strobl, Franziska Hampel, developed the transgenic mouse strain Notch2IC^{flSTOP} which carries a conditional allele for a constitutively active Notch2 receptor in the *Rosa26* locus (Hampel et al. 2011). This is mediated by the expression of a truncated receptor that

is only comprised of the intracellular signaling domain Notch2IC. As shown in Figure 6, the gene for Notch2IC is upstream accompanied by a loxP-flanked (floxed) STOP cassette. Without further manipulation, the STOP cassette will inhibit transcription of the downstream gene. Upon expression of the loxP-specific recombinase enzyme Cre, the floxed cassette is cut out and the strong CAGGS promoter, a modified chicken actin promoter frequently used in mammalian expression vectors (Jun-ichi et al. 1989), drives the expression of the Notch2IC-allele. The successful Cre activity, deletion of the STOP codon and subsequent expression of Notch2IC can be tracked by staining for a surface marker protein human CD2 (hCD2), which is co-translated as a non-functional receptor with a truncated signaling domain with Notch2IC via an IRES-linker sequence and otherwise absent in murine tissues.

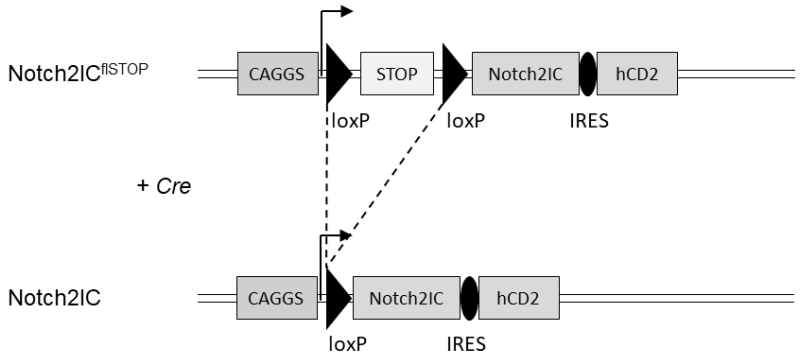

Figure 6: **Generation of Notch2IC^{flSTOP} mice and cell-specific expression of Notch2IC**. The conditional Notch2IC^{STOPfl} allele was inserted together with an IRES-hCD2 coding sequence into the first exon of the murine *Rosa26*-locus. Cre activation results in deletion of the stop cassette and subsequent expression of Notch2IC together with hCD2.

Depending on which cell type expresses the Cre-recombinase, one can restrict the expression of the transgene of interest to a specific cellular context. We initially crossed Notch2IC^{flSTOP} mice with CD19Cre mice. Here, Cre recombinase is expressed by the B-cell specific promoter of CD19, a gene that is exclusively expressed in all B cells from the pro-B cell stage in the bone marrow onwards leading to Notch2IC and hCD2 expression in the majority of all immature and mature peripheral B cells. In order to study the effect of a later onset of Notch2 signaling on B cells in a spatiotemporally controlled model, we crossed Notch2IC^{flSTOP} mice to CD19CreERT2 mice. Here, Cre is fused to the human estrogen receptor binding domain (ERT2) (Feil et al. 1997). In absence

of its ligand tamoxifen, CreERT2 is inactive and retained in the cytoplasm. Binding of tamoxifen to ERT2 results in the translocation of the Cre recombinase fusion protein into the nucleus where it can recombine the loxP-flanked DNA substrate (Feil, Valtcheva, and Feil 2009). Deletion of the STOP cassette drives Notch2IC and hCD2 expression.

1.6. Aims of the study

Activation of Notch2 signaling was already identified as a decisive event in B cell subset differentiation during maturation of immature B lymphocytes, but the role of Notch2 signaling in mature follicular B cells had not been studied so far.

In this work, a transgenic mouse model with an inducible expression of a constitutively active Notch2-receptor signaling domain should be used to study whether a Notch2 signal is sufficient to induce a trans-differentiation of FoB to MZB cells in terms of their surface marker expression, localization, immunological function and transcriptomic profile. Furthermore, the underlying assumption of a general plasticity between FoB and MZB cells should be addressed in transplantation experiments, in which the fate of the transplanted FoB cells should be tracked over time.

2. Methodology

2.1 Materials

All critical reagents, commercial assay kits, genetic mouse models, analytical research devices and software are listed in Table 1.

Table 1: List of critical reagents and recourses

REAGENTS / RESOURCES	SUPPLIER	IDENTIFIER
Antibodies		
Anti-Mouse IL7R (clone A7R34)	Produced in house	N/A
For FACS:		
Anti-Human CD2 APC (clone RPA-2.10)	BD Biosciences	Cat#56064
Anti-Human CD2 BV421 (clone RPA-2.10)	BD Biosciences	Cat#562667
Anti-Human CD2 FITC (clone RPA-2.10)	BD Biosciences	Cat#561759
Anti-Mouse CD45R/B220 PerCP (clone RA3-6B2)	BD Biosciences	Cat#553093
Anti-Mouse CD21/CD35 FITC (clone 7G6)	BD Biosciences	Cat#561769
Anti-Mouse CD23 PE (clone B3B4)	BD Biosciences	Cat#561773
Anti-Mouse CD23 APC (clone EBVCS2)	eBioscience	Cat#17-0238
Anti-Mouse CD97 PE (clone AA4.1)	eBioscience	Cat#12-5892
Anti-Mouse CD1d PE (clone 1B1)	BD Biosciences	Cat#553846
Anti-Mouse CD1d AF647 (clone 1B1)	BD Biosciences	Cat#564706
Anti-Mouse IgM BV450 (clone R6-60.2)	BD Biosciences	Cat#560575
Anti-Mouse IgM APC (clone II/41)	BD Biosciences	Cat#550676
Anti-Mouse IgD FITC (clone 11-26c.2a)	BD Biosciences	Cat#553439
Anti-Mouse CD138 PE (clone 281-2)	BD Biosciences	Cat#553714
Anti-Mouse CD138 BV421 (clone 281-2)	BD Biosciences	Cat#562610
Anti-Mouse IRF4 APC (clone 3E4)	eBioscience	Cat#50-9858-82
Anti-Mouse IgG1 PE (clone A85-1)	BD Biosciences	Cat#550083
Anti-Mouse TACI APC (clone ebio8F10-3)	eBioscience	Cat#17-5942-82
Anti-Mouse CD19 PE Vio770 (clone REA749)	Miltenyi	Cat#130-112-037
Anti-Mouse Notch2 PE (clone HMN2-35)	Biolegend	Cat#130707
For IHC:		
Anti-Laminin (clone L9393)	Sigma-Aldrich	Cat#L9393
Anti-Human CD2 Biotin (clone RPA-2.10)	BD Biosciences	Cat#555325
Anti-Mouse CD90.2 (Thy1.2) Biotin (clone 30-H12)	BD Biosciences	Cat#553011
Anti-MOMA-1 FITC	Abcam	Cat#ab34355
Anti-Mouse IgD FITC (clone 11-26c.2a)	BD Biosciences	Cat#553439
Anti-Mouse IgM (clone 1020-01)	Southern Biotech	Cat#1020-01
Anti-Goat IgG AF647	Invitrogen	Cat#A-21469
Anti-Rabbit IgG Peroxidase	Sigma-Aldrich	Cat#A0545
Critical Chemicals and Recombinant Proteins		
Taq DNA Polymerase, recombinant	Invitrogen	Cat#10342053

Tamoxifen	Sigma-Aldrich	Cat#T5648
NP-LPS	LGC Biosearch Tech.	Cat#N-5065
Corn Oil	Sigma-Aldrich	Cat#C8267
RBC Lysis Buffer	eBioscience	Cat#00-4333
MACS Buffer	Miltenyi	Cat#130-091-221
LPS (E.coli 055:B5)	Sigma-Aldrich	Cat#L2880
F (ab)2 Fragment Anti-Mouse IgM	Jackson Immuno Research	Cat#JIM-115-006-020-1MG
Roti-Histofix 4%	Carl Roth	Cat#P087
Streptavidin, AF594	Invitrogen	Cat#S11227
Streptavidin, Alkaline Phosphatase	Sigma-Aldrich	Cat#S2890
Tissue-Tek O.C.T. Compound	Sakura	Cat#SA62550
ProLong Glass Antifade Mountant	Invitrogen	Cat#P36984
Kaisers Gelatine	Carl Roth	Cat#6474.1
Critical Commercial Assays		
CellTrace CFSE Cell Proliferation Kit	Invitrogen	Cat#C34570
LIVE/DEAD Fixable Blue Dead Cell Stain Kit	Invitrogen	Cat#L23105
APC BrdU Flow Kit	BD Biosciences	Cat#552598
TRIzol LS Reagent	Invitrogen	Cat#10296010
ReliaPrep RNA Cell Miniprep System	Promega	Cat#Z6011
RNA Pico 6000 Kit	Agilent	Cat#5067-1513
B Cell Isolation Kit, mouse	Miltenyi	Cat#130-090-862
MZ and FO B Cell Isolation Kit, mouse	Miltenyi	Cat#130-100-366
Avidin/Biotin Blocking Kit	Vector	Cat#SP-2001
AEC Peroxidase Substrate Kit	Vector	Cat#SK-4200
Blue Alkaline Phosphatase Substrate Kit	Vector	Cat#SK-5300
Experimental mouse strains		
Notch2IC^{STOPfl}	U. Zimber-Strobl (PI) (Hampel et al. 2011)	N/A
R26/CAG-CARΔ1^{STOPfl}	M. Schmidt-Supprian (PI) (Heger et al. 2015)	N/A
CD19CreER^{T2}	M. Schmidt-Supprian (PI) (Yasuda et al. 2013)	JAX Stock No 027116
CD19Cre	K. Rajewsky (PI)	JAX Stock No 006785
C57BL/6J	Charles River Germany	JAX Stock No 000664
BALB/c	Charles River Germany	JAX Stock No 000651
B6.SJL-Ptprc^{a} Pepc^{b}/BoyJ (CD45.1)	Lab of V. Heissmeyer (PI)	JAX Stock No 002014
Analytical Research Instruments		
Quantum ST-4 UV chamber	Vilber Lourmat	Cat#101141731
FACSCalibur Flow Cytometer	BD Biosciences	N/A
LSRFortessa Flow Cytometer	BD Biosciences	N/A
FACSAria III Cell Sorter	BD Biosciences	N/A
2100 Bioanalyzer	Agilent	Cat#G2939BA
Confocal Microscope TCS-SP5 II	Leica	N/A
Software and Algorithms		
FlowJo V10	FlowJo LLC	https://www.flowjo.com
ImageJ 1.46r	NIH	https://www.imagej.net
GraphPad Prism8	GraphPad Software	https://www:graphpad.com

GSEA v4.0.1	Broad Institute, Inc.	http://software.broadinstitute.org/gsea
Dropseq tools v1.13	Broad Institute, Inc.	https://github.com/broadinstitute/Drop-seq
R v3.4.4	The R Foundation	https://cran.r-project.org/
DESeq2 v1.8	Love et al., 2014	https://bioconductor.org/packages/release/bioc/html/DESeq2.html
ImmGen	Immunological Genome Project	http://rstats.immgen.org/PopulationComparison/index.html
Other		
reference genome GRCm38	The GENCODE Project	ftp://ftp.ebi.ac.uk/pub/databases/gencode/Gencode_mouse/release_M19/GRCm38.primary_assembly.genome.fa.gz
Gencode gene annotation release M19	The GENCODE Project	ftp://ftp.ebi.ac.uk/pub/databases/gencode/Gencode_mouse/release_M19/gencode.vM19.basic.annotation.gtf.gz

2.1.1 Mouse models

Notch2IC/CD19CreERT2

The previously described Notch2IC^{STOPfl} mice (Hampel et al. 2011) carrying a heterozygous *Notch2IC*$^{STOPfl/wt}$ allele in the *rosa26* locus were crossed with the tamoxifen-inducible Cre strain CD19CreERT2 (Yasuda et al. 2013) to generate either Cre-homozygous Notch2IC/CD19CreERT2:hom (predominantly used in this study) or Cre-heterozygous Notch2IC/CD19CreERT2:het mice. In all mice, the Notch2IC transgene was heterozygous. Homozygous expression of CD19CreERT2 in Notch2IC/CD19CreERT2:hom mice leads to a CD19-knockout due to the disruption of both wild type CD19 alleles while Notch2IC/CD19CreERT2:het are CD19-proficient. These mouse strains were bred in a mixed C57BL/6J x BALB/c background

CAR/CD19CreERT2

R26/CAG-CARΔ1^{STOPfl} reporter mice (Heger et al. 2015) were also crossed to CD19CreERT2 and serve as a control strain for the Notch2IC/CD19CreERT2 strain with the similar C57BL/6J x BALB/c background to indicate Cre-deletion efficiency after tamoxifen treatment in the absence of Notch2IC. Here, a human CAR (Coxsackievirus and adenovirus receptor) serves as a non-

functional reporter gene. CAR is expressed on the cell surface of all B cells responding to the tamoxifen treatment with Cre activation resulting in the deletion of the STOP-cassette deletion upstream of CAR.

CD45.1

The B6.SJL-Ptprc^{a} Pepc^{b}/BoyJ (CD45.1) mouse strain is frequently used for adoptive lymphocyte transfer experiments, as the only difference to the commonly used C57BL/6J wild type-like strain is the expression of the allele variant 1 of the pan-leukocyte marker gene CD45, whereas 'normal' C57BL/6J mice express variant CD45.2. This allele variances enables the tracking of transplanted cells within the recipient by separating the donor from recipient cells with a co-staining for CD45.1 and CD45.2. CD45.1 mice were used as donor mice for B cell transplantation experiments.

C57BL/6J

The most commonly used inbred strain of laboratory mice was purchased by Charles River Germany and served as recipient strain for transfer of purified congenic CD45.1^{+} B cells.

BALB/c

BALB/c is a commonly used albino inbred mouse strain. This strain was used to breed F1 mixed-background C57BL/6J x BALB/c mice, which served as controls in RNA Sequencing. With this, strain-specific genetic differences were reduced as Notch2IC/CD19CreERT2 mice are of a mixed C57BL/6J x BALB/c background.

2.2 Method details

2.2.1 Mouse genotyping

Polymerase chain reaction (PCR) was used for genotyping of transgenic mice. DNA was routinely purified by Krisztina Zeller from ear punched tissues and one or multiple PCR reactions were performed to identify the specific transgenes of interest. Primers (Table 2) were ordered from Metabion (Planegg, Germany) and PCR reactions (Table 3) were run in thermal cyclers from

Biometra (AnalyticJena, Jena, Germany). PCR products were subsequently analyzed in agarose gel electrophoresis and visualized via ethidium bromide intercalation in a Quantum ST-4 UV detection chamber (Vilber Lourmat, Eberhardszell, Germany).

Table 2: primers used for genotyping PCR

PCR	Primers	Sequence 5'-3'
Notch2IC	Notch2 se	GAG AAG CAG AGA TGA GCA GAT A
	Notch2 as	GTG AGA TGT GAC ACT TCT GAG C
CD19CreERT2	3 Cre	ATGTTTAGCT GGCCCAAATG
	5BamEx1	GGATCCATCTCCTCTCCCTGTCTC
	Cd19d	CCA GAC TAG ATA CAG ACC AG
ROSA26	Rosa for	CTC TCC CAA AGT CGC TCT G
	Rosa rev	TAC TCC GAG GCG GAT CAC AAG C
CAR	CAR for	CAG CCA CTC GAT GAT GTA CAG CGG
	CAR rev	CAG GAG CGA GAG CCG CCT AC

Table 3: Genotyping PCR programs

	Notch2IC	CD19CreERT2		ROSA26	CAR
		(**1**)	(**2**)		
1 *Initialization*	5' 95°C	3' 95°C		5' 95°C	3' 95°C
2 *Denaturation*	45'' 94°C	30'' 95°C	30'' 95°C	45'' 95°C	15'' 95°C
3 *Annealing*	45'' 59°C	30'' 65°C (-1°C cycle)	30'' 53°C	45'' 58°C	30'' 62°C
4 *Elongation*	1' 72°C	30'' 72°C	20'' 72°C	1' 72°C	1' 72°C
5 *Final Elongation*	10' 72°C		5' 72°C	10' 72°C	10' 72°C
Cycles (Step 4 to 2)	32	12	20	33	32

2.2.2 In vivo experiments

To induce Cre-recombinase, mice were gavaged with 5 mg tamoxifen, dissolved in 200µl corn oil (Sigma-Aldrich, Merck group, Burlington, USA). Treatments were either a single dose (day 1) or on five consecutive doses (day 1-5). In single dose experiments, mice were additionally pre-treated with four doses of 250µg (250µl) anti-IL7R antibody, which was administered intraperitoneally (i.p.) every second day. T-cell independent (TI) immune responses were triggered via i.p. immunization using 10µg NP-LPS. For *in vivo* detection of cycling cells, BrdU was provided via drinking water at 0.8 mg/ml according to the manufacturer's protocol (BrdU Flow Kit, BD, Becton Dickinson GmbH Deutschland, Heidelberg, Germany) for 7 days subsequently to tamoxifen treatment, with the BrdU-water solution renewed every other day.

2.2.3 Flow cytometry

Single cell suspensions from spleen, bone marrow, lymph nodes or peritoneal cavity lavage were transferred into 15ml falcon tubes and washed by filling up the tubes with MACS buffer (Miltenyi, Bergisch Gladbach, Germany) and centrifugation for 10 minutes at 4°C and 1200rpm (Rotanda 460-R, Hettich, Tuttlingen, Germany). Erythrocytes were depleted from splenic and bone marrow samples by resuspending the cell pellet in 1ml red blood cell (RBC) lysis buffer (eBioscience, Thermo Fisher Scientific, Waltham, USA) and incubation for 3 minutes at room temperature. After a repeated washing step in MACS buffer and centrifugation, usually 5-10 x 10^5 cells were transferred into single wells of a round-bottom 96-well plate for subsequent staining. Surface staining of lymphocytes was performed in 25µl of antibody mix diluted in MACS buffer on ice for 20 minutes. For intracellular FACS-staining, cells were subsequently fixed in 2% formaldehyde (1:2 PBS-diluted Histofix) and permeabilized in ice-cold 100% methanol for 10 minutes on ice. After washing with MACS buffer, cells were then stained for 45 minutes at room temperature in MACS buffer. After staining, samples were again washed with MACS buffer, centrifugated for 5 minutes and transferred into FACS tubes for analysis. Cytometric analyses were executed on a FACSCalibur or LSRFortessa (BD Biosciences). FlowJo V10 was used to analyze and visualize the results.

2.2.4 Histology

Splenic tissues were prepared by embedding into Tissue-Tek O.C.T. compound (Sakura Finetek, Torrance, USA) for freezing of tissue specimen, snap frozen and stored at -20°C. 7 µm sections were then cut and mounted onto glass slides and stored at -80°C for immunohistochemical (IHC) analysis.

For chromogenic IHC, samples were first fixed for 10 minutes with ice-cold acetone, washed in PBS 3 x 5 minutes, blocked for 20 minutes in PBS-based blocking solution containing 1% BSA and 5% goat serum. Subsequently, endogenous biotins within the sample were blocked using the Avidin/Biotin blocking kit (Vector Laboratories, Burlingame, USA) according to the manufacturer's protocol. Expression of the surface marker hCD2 was detected by

immunohistochemical staining using biotinylated mouse anti-human CD2 antibody (dilution 1:100) and rabbit anti-laminin antibody (1:1000) overnight in 1% BSA/PBS at 4°C. Samples were washed in PBS 3 x 5 minutes before secondary staining was performed using streptavidin-coupled alkaline phosphatase and peroxidase-coupled anti-rabbit IgG (1:250) for 1 hour at room temperature. Enzymatic chromogenic detection was performed using the AEC substrate kit and Blue AP substrate kit (Vector) according to the manufacturer's protocol. Slides were eventually embedded in Kaiser's Gelatine (Carl Roth, Karlsruhe, Germany) and analyzed using an Axioscope (Zeiss, Oberkochen, Germany) equipped with an Axiocam MRc5.

For immunofluorescent (IF) staining, samples were fixed for 10 minutes with 3% Histofix in PBS (Carl Roth), rinsed with PBS, rehydrated for 5 minutes in PBS + 50 mM NH_4Cl and then blocked in a PBS-based blocking solution containing 1% BSA, 5% rat serum and 5% chicken serum for 30 minutes. Again, endogenous biotins were blocked using the Avidin/Biotin blocking kit (Vector) according to the manufacturer's protocol. Primary (goat anti-mouse IgM (1:200), anti-Thy1.2-Biotin (1:100)), secondary (chicken anti-goat IgG AF647 (1:500)) and fluorophore-coupled antibodies (anti-IgD FITC (1:100), anti-MOMA FITC (1:100)) as well as Streptavidin-AF594 (1:500) were incubated for 1 hour at room temperature in 0.5% BSA/PBS. Slides were embedded in ProLong Glass Antifade (Invitrogen, Waltham, USA). Immunofluorescent analyses were performed using a TCS SP5 II confocal microscope (Leica, Wetzlar, Germany). Picture stacks were composed using ImageJ.

2.2.5 In vitro B cell activation assay

Purification of naïve B cells from splenic cell suspensions was performed using the CD43 depletion B cell Isolation Kit (Miltenyi) according to the manufacturer's instructions. Purified B cells were stained with CellTrace Carboxyfluorescein succinimidyl ester (CFSE) (Invitrogen) according to the manufacturer's protocol to monitor cell division. B cells were seeded into flat-bottom 96 well plates at of $5x10^5$ cells/ml in RPMI-1640 (Gibco, Fisher Scientific) supplemented with 10% FCS, 1% L-glutamine, 1% non-essential amino acids, 1% sodium pyruvate, 50 µM β-mercaptoethanol and stimulated with 50 µg/ml lipopolysaccharide (LPS, Sigma) for 48 hours. Finally, cells were stained with anti-hCD2-APC and anti-CD138-PE antibodies and analyzed by

flow cytometry. Dead cell discrimination was done with the fixable dead cell staining kit (Invitrogen).

2.2.6 Cell sorting and RNA purification for RNA-sequencing

Mice were pre-treated with anti-IL7R antibody and Notch2IC-expression was induced by application of a single dose of tamoxifen as described above. Splenic B cell samples of Notch2IC/CD19CreERT2:hom mice were stained with anti-AA4.1-PE (1:100), anti-hCD2-APC (1:200), anti-B220-PerCP (1:100) in 1ml MACS buffer. $hCD2^{+}B220^{+}$ cells were sorted from splenic cell suspensions of n=5 mice per time point. The following cell populations served as controls: $hCD2^{-}B220^{+}$ B cells from tamoxifen-treated mice of different time points (n=6 samples) as well as FoB ($B220^{+}AA4.1^{-}CD23^{high}CD21^{+}$) and MZB ($B220^{+}AA4.1^{-}CD23^{low}CD21^{high}$) cells from 5 untreated C57BL/6J x BALB/c F1 mice stained with AA4.1-PE (1:100), anti-CD23-APC (1:200), anti-B220-PerCP (1:100) and anti-CD21-FITC (1:200). Cell sorting was performed using a 70µm nozzle at a sorting speed of around 15.000 events/sec on a FACSAria III (BD). $5x10^4$ cells were sorted into tubes containing 1ml of cooled (4°C) TRIzol LS (Invitrogen), mixed by vortexing after sorting, then snap frozen on dry ice and stored at -80°C. Purification of RNA was performed using a previously established hybrid TRIzol/column-wash protocol. TRIzol samples were thawed and after addition of 200µl chloroform, centrifuged at 12,000 x g for 15 minutes at 4°C. The aqueous phase containing RNA was mixed with an equal amount of 100% ethanol and samples were subsequently loaded on ReliaPrep RNA Cell Miniprep columns (Promega, Madison, USA). Further purification of RNA was done according to the supplied protocol. RNA purity was confirmed using a 2100 Bioanalyzer with RNA Pico chips (Agilent Technologies, Santa Clara, USA). RNA with an integrity number (RIN) of 9.7 (SD=0.4) was used for library preparation and RNA sequencing.

2.2.7 RNA Sequencing

Whole transcriptome RNA sequencing, quality control and initial bioinformatic analyses (MDS analysis and heatmap) were performed by Dr. Rupert Öllinger and Dr. Thomas Engleitner at the TranslaTUM, Munich as described in the collaborative publication (Lechner et al. 2021).

2.2.8 Bioinformatics I (Dr. Thomas Engleitner)

After bioinformatic processing as described in detail in Lechner et al. 2021, multidimensional scaling (MDS) was the initial output figure provided by Thomas Engleitner. As an input for the MDS, the 10% most variant expressed genes were selected based on the rlog transformed expression values across all samples.

The RNA sequencing data sets are available through the European Nucleotide Archive (ENA) accession code PRJEB35207. https://www.ebi.ac.uk/ena/browser/view/PRJEB35207

2.2.9 Bioinformatics II (Markus Lechner)

For the generation of the MZB signature gene sets, the gene list for differentially regulated genes between wild type MZB and FOB cells were downloaded from the ImmGen Population Comparison tool (Heng, Painter, and Immunological Genome Project 2008) (microarray data GSE11961 (Kaji et al. 2012)) and intersected with the respective comparison in this dataset. Gene set enrichment analysis (GSEA) was performed using the GSEA v4.0.1 software. For GSEA the log2 fold changes were used as ranking metric for genes. The GSEA algorithm generates an enrichment score (ES), which reflects the degree to which a given gene set is overrepresented at the top or bottom of the ranked list of genes. The GSEA algorithm walks down this ranked list of genes and increases a running-sum statistic for the ES whenever a gene is also found in the provided gene set (Figure 7). If the gene is not found, ES is decreased. A positive ES indicates that the gene set is enriched at the top of the ranked list, a negative ES indicates an enrichment at the bottom end of the list.

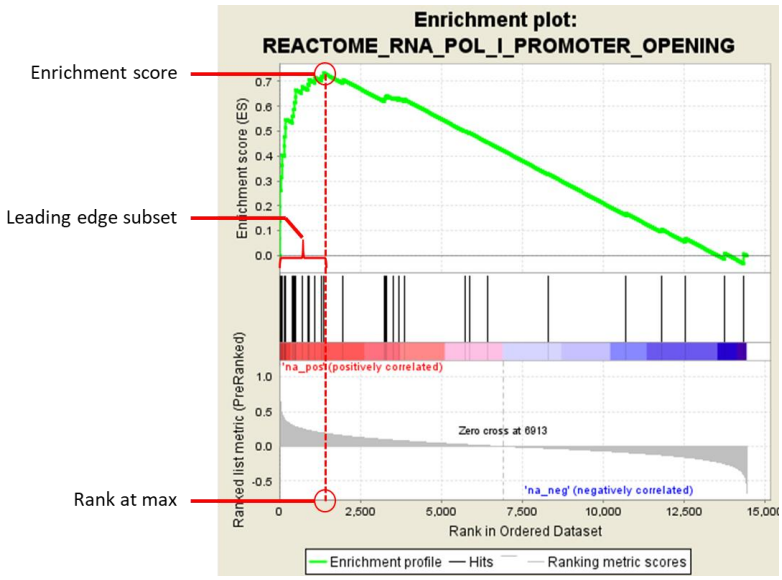

Figure 7: Explanatory GSEA Enrichment plot. The top portion of the plot shows the running enrichment score (ES) for the gene set "REACTOME_RNA_POL_I_PROMOTER_ OPENING" as the algorithm walks down the ranked gene list. The score at the peak of the plot is the ES. The middle portion of the plot shows where members of the gene set appear in the ranked list. The subset of gene set members that contribute most to the positive ES are termed "leading edge" subset. The bottom portion of the plot shows the value of the ranking metric scores moving from top to bottom of the ranked gene list. A positive value indicates correlation with the phenotype profile while a negative value indicates inverse correlation with the profile. Modified from the GSEA website (https://www.gsea-msigdb.org/gsea/doc/GSEAUserGuideFrame.html; 27.03.2020).

2.2.10 Adoptive transfer experiments

Suspensions of splenocytes from 2-4 sex-matched CD45.1 donor mice were pooled and stained with 0.5-1ml of the following antibody cocktail: CD21-FITC (1:200), AA4.1-PE (1:200), B220-PerCP (1:100) and CD23-AF647 (1:100). Mature FoB cells ($B220^{+}$, $AA4.1^{-}$, $CD23^{high}$, $CD21^{low}$) or MZB cells ($B220^{+}$, $AA4.1^{-}$, $CD23^{neg\text{-}low}$, $CD21^{high}$) were sorted into 4°C cooled 10% FCS supplemented RPMI-1640 medium. Cells were then pelleted, washed in sterile PBS and resuspended in 200µl PBS with a cell count of 5-6x10^{6} FoB cells or 1x10^{6} MZB cells per tube. Cells were then transplanted into the lateral tail veins of congenic and sex-matched recipient $CD45.2^{+}$ C57BL/6J mice. Due to the expectably low percentage of $CD45.1^{+}$ cells within the stained splenic cell suspension samples, 2-5 million cells were recorded on a LSRFortessa to ensure a faultless representation in contour plots of at least 1x10^{3} $CD45.1^{+}$ cells. Splenocytes were

stained with a consistent flow cytometry protocol at all time points after transfer to guarantee comparability.

2.2.11 Statistics

GraphPad Prism7 was used to determine p-values of indicated one-way or two-way ANOVA with multiple comparison tests. The p-value for linear regression analysis of fold-changes between MZB/FoB and $hCD2^{+}/hCD2^{-}$ sample pairs was executed in Microsoft Excel using the "Analysis ToolPak" Add-In.

3. Results

3.1 The instructive role of Notch2 in mature peripheral B cell plasticity

3.1.1 Establishment of a protocol for Notch2 induction in mature follicular B cells

The effects of a constitutively active Notch2 signaling pathway on the developmental routes of B lymphocytes have been studied in our lab for several years. Notch2IC/CD19Cre mice, that expressed a constitutively active Notch2IC protein from bone marrow stages onwards, showed enhanced MZB cell development at the expense of the FoB lineage (Hampel et al. 2011). To learn more about the fate-decisive power of Notch2 signaling and its influence on mature B cells, we developed an experimental setup to be able to investigate the effect of switching on Notch2 signaling in mature naïve follicular B cells. To follow MZB cell development in the absence of pre-existing MZB cells, we made use of CD19-deficient mice which we generated by combining the Notch2IC^{STOPfl} mice with a homozygous CD19CreERT2 transgene (Notch2IC/CD19CreERT2:hom). This resulted in the disruption of both wild type CD19 alleles and subsequent inhibition of MZB cell development (Figure 8).

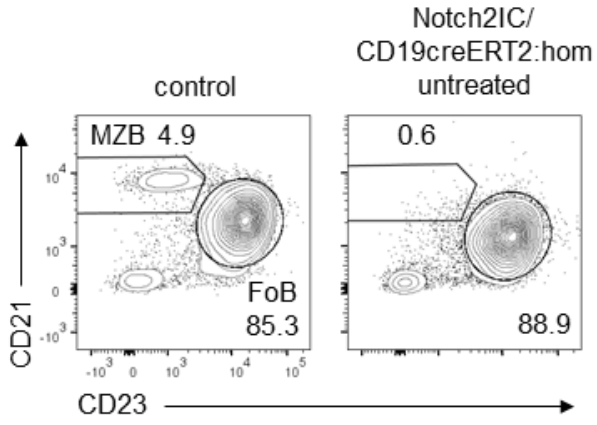

Figure 8: untreated Notch2IC/CD19CreERT2-mice lack a marginal zone B cell compartment. CD19-knockout in Notch2IC/CD19CreERT2:hom mice lacks the CD23^{low} CD21^{high} marginal zone B cell (MZB) compartment. Plots are gated on B220^{+} B cells. Numbers indicate percentages of gated follicular B (FoB) and MZB cells. Representative figure for CD19^{+} control and untreated Notch2IC/CD19CreERT2:hom mice that were both frequently used as positive and negative controls for MZB / FoB stainings. Similar figure in Lechner et al. 2021.

The remaining B2 cell subsets in the spleen of Notch2IC/CD19CreERT2:hom mice were mostly mature follicular B cells (~90%) with some remaining immature transitional type 1 (T1) or type 2 (T2) cells, which are negative for CD21 and CD23.

To find the sites and B cell types that respond to tamoxifen with deletion of the stop cassette and expression of hCD2 and Notch2IC, a single dose of tamoxifen was administered to Notch2IC/CD19CreERT2:hom mice. $hCD2^+$ B cells were analyzed in different lymphatic organs 48 hours after treatment. As shown in Figure 9, $hCD2^+$ cells were found in the spleen, lymph node, peritoneal cavity lavage and in the bone marrow. In all cases, $hCD2^+$ cells also co-expressed the B cell marker B220, while being negative for the immature B cell marker AA4.1. With one exception: the rather small proportion of bone marrow-located $B220^+$ $hCD2^+$ cells was separated by half into $AA4.1^+$ and $AA4.1^-$ B cells. This suggests that not only mature B cells responded to tamoxifen and expressed hCD2, but also a small fraction of bone marrow-homed, immature ($AA4.1^+$) developing B cells.

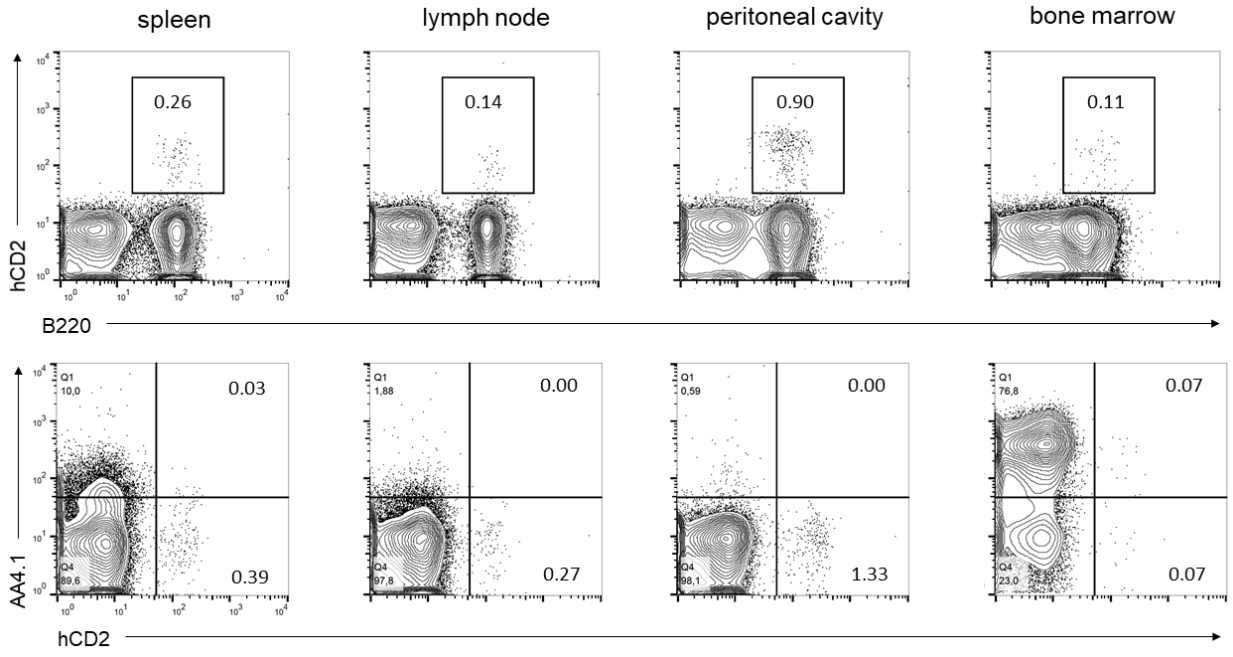

Figure 9: Expression of hCD2 in different lymphatic organs was mainly found in mature B cells. Notch2IC/CD19CreERT2:hom mice were treated with a single dose of tamoxifen. 48 hours after tamoxifen treatment cell suspensions were made from spleen, lymph node, peritoneal cavity lavage and bone marrow preparations and subsequently stained for B220 and hCD2 (top row), as well as hCD2 and immature B cell marker AA4.1 (bottom row) and analyzed by FACS. Plots of the top row were gated on lymphocytes by FSC/SSC characteristics. Plots of the bottom row were additionally pre-gated on $B220^+$ B cells. Representative result of two experiments.

To restrict Notch2IC expression to mature follicular B cells, early B cell development in the bone marrow and subsequent efflux of immature B cells into the peripheral lymphatic organs, where those bone marrow-derived cells feed into the transitional T1 and T2 cell pool, was inhibited by anti-IL-7R injection. As mentioned in the introduction, pro-B cells express high levels of the interleukin 7 receptor (IL7R) and binding of IL7 is required for their further development into pre-B cells. It has been shown earlier that application of an anti-IL7R antibody blocks B cell development at this stage. In a series of pre-experiments, a four-time treatment with 250µg anti-IL7R antibody every other day was shown to be sufficient to deplete $AA4.1^+$ IgM^+ immature B cells in the bone marrow, as well as $AA4.1^+$ $CD23^-$ peripheral transitional B cells in the spleen (Figure 10).

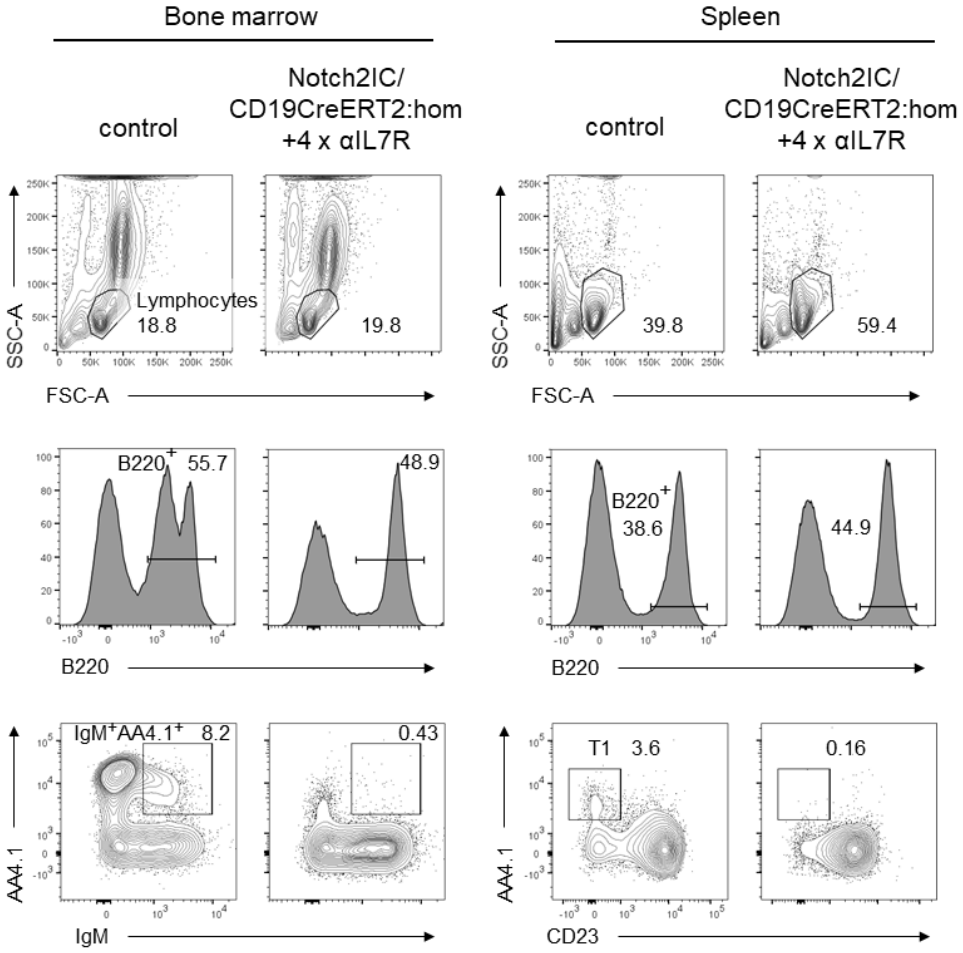

Figure 10: Pretreatment with anti-IL7R antibody blocks B cell development in the bone marrow and transitional B cell influx into the spleen. Notch2IC/CD19CreERT2:hom mice were 4x treated with 250µg anti-interleukin 7 receptor antibody (αIL7R) every two days. Flow cytometric analyses of bone marrow cells and splenocytes were

performed 7 days after the last antibody application. Untreated wild type mice served as control. Bone marrow: Block of AA4.1^{+} B220^{mid} developing B cells. The latest development stage before efflux to the periphery, namely AA4.1^{+} IgM^{+} immature B cells, is completely absent while AA4.1^{+} IgM^{-} precursors are strongly reduced. Spleen: Subsequently, influx of AA4.1^{+} CD23^{-} transitional type 1 (T1) B cells was absent. FACS plots are gated consecutively from top to bottom rows. Numbers indicate percentages of cells within the drawn gates. Representative data for n=3 mice. Similar figure in Lechner et al. 2021.

Later experiments showed a long-term blocking effect of the anti-IL7R treatment, enduring until 30 days after anti-IL7R and tamoxifen treatment (Figure 11). While AA4.1^{+} IgM^{-} cells started to regenerate, AA4.1^{+} IgM^{+} immature B cells were still absent in the bone marrow as well as AA4.1^{+} CD23^{-} transitional B cells in the spleen.

With this successful pre-treatment scheme, we were now able to guarantee tamoxifen-induced Notch2IC-expression specifically in mature follicular B cells and established the protocol depicted in Figure 12. Application of a single dose of tamoxifen enabled us to follow up the effect of Notch2IC expression over time in a subset of tamoxifen-responsive cells with a narrow temporal resolution, as the serum half-life of tamoxifen and its active metabolite 4-OHT was identified to be around 12 and 6 hours, respectively (Robinson et al. 1991).

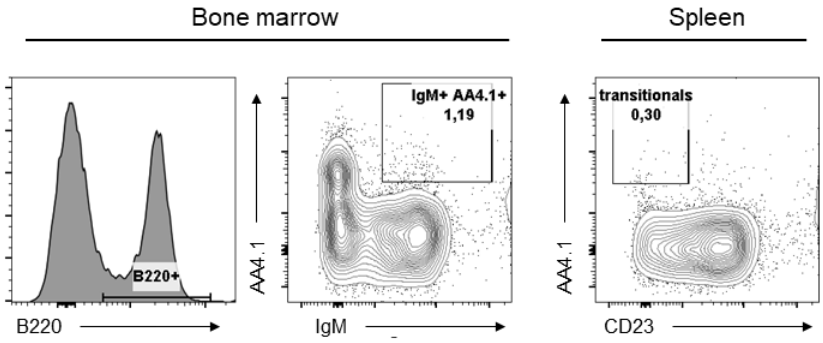

Figure 11: Analysis of long-term effects after anti-IL7R antibody treatment shows enduring blockage of B cell development, 30 days after tamoxifen treatment. Notch2IC/CD19CreERT2:hom mice were treated four times with 250µg anti-interleukin 7 receptor antibody (αIL7R) every other day. 30 days after the last treatment cell suspensions of the BM and the spleen were analysed by FACS. Newly generated B cells (B220^{mid}) were still absent in the bone marrow (left), so are IgM^{+} AA4.1^{+} late immature B cell stages (middle). Subsequently, splenic AA4.1^{+} CD23^{-} transitional T1 B cells are still strongly reduced (right). Relevant staining of untreated controls is depicted in the previous Figure 10. All plots are gated on lymphocytes. Contour plots are additionally pre-gated on B220^{+} B cells. Data are representative for n=3 mice. Similar figure in Lechner et al. 2021.

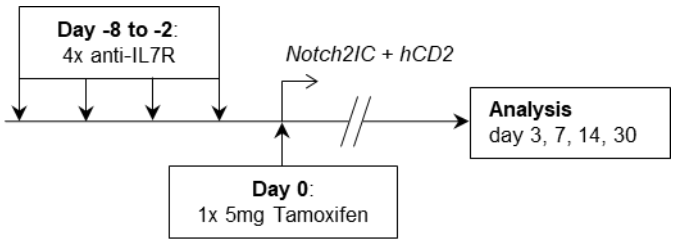

Figure 12: Protocol for the induction of Notch2IC-expression via 1x tamoxifen treatment. A four-time pre-treatment with anti-IL7R antibody was used to ensure depletion of immature transitional B cells. Oral administration of tamoxifen induces expression of Notch2IC and hCD2. Mice were analyzed at indicated time points after tamoxifen treatment. Similar figure in Lechner et al. 2021.

Mainly Notch2IC/CD19CreERT2:hom mice with homozygous expression of CD19CreERT2 were analyzed. CAR/CD19CreERT2:hom were used as controls to verify Cre-mediated deletion efficiency and to analyze Notch2-specific gain of function effects of $hCD2^+$ cells in comparison to CAR^+ cells. In an additional set of experiments, Notch2IC mice carrying a heterozygous Cre allele insertion into the *Cd19* locus (CD19CreERT2:het) were used. These Notch2IC/CD19CreERT2:het mice still possess one functional *Cd19*-allele and therefore still have MZB cells. With this we wanted to challenge the effects of Notch2IC-induction and its influence on follicular B cells in a competitive setting, where a fully developed marginal zone was still present.

3.1.2 Tamoxifen treatment and efficiency of the induction of Notch2IC expression

Using a single dose of tamoxifen application, I found that the induction efficiency of tamoxifen-mediated excision of the STOP cassette and subsequent expression of Notch2IC and hCD2 was low, with only around 1% of splenic B cells being $hCD2^+$ three days after tamoxifen treatment (Figure 13). Percentages of $hCD2^+$ B cells increased over time with a maximum of around 3-7% two weeks after induction.

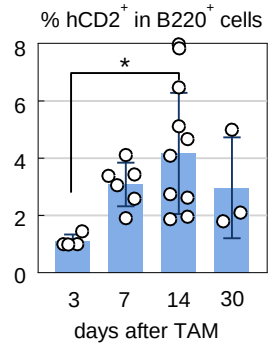

Figure 13: Percentages of Notch2IC-expressing (hCD2$^+$) splenic B cells increased over a one-month time course. Splenic B cells were identified as B220$^+$. Plotted are individual values, the average percentage and SD of hCD2$^+$ cells among B220$^+$ splenocytes for each time point after a single tamoxifen (TAM) treatment. *p=0.0223, d3 n=4, d7 n=6, d14 n=9, d30 n=3. one-way ANOVA, Tukey's multiple comparisons test. Similar figure in Lechner et al. 2021.

Repeated doses of tamoxifen on five consecutive days increased the percentage of hCD2$^+$ B cells. The peak of percentages of Notch2IC-expressing B cells was also reached two weeks after initial treatment, similar to kinetic using a single dose of tamoxifen, but the relative percentages of hCD2$^+$ cells were increased with repeated tamoxifen dosing (Figure 14). hCD2$^+$ cells could be identified up to 3 months after gene induction.

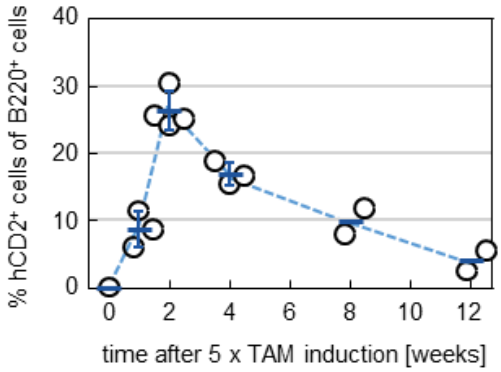

Figure 14: Repeated doses of tamoxifen resulted in increased percentages of Notch2IC-expressing cells and enabled a prolonged follow up. Mean percentages, SD and single values of hCD2$^+$ among splenic B220$^+$ B cells are plotted over a time window of 12 weeks after repeated administration of tamoxifen (TAM) on five consecutive days. Similar figure in Lechner et al. 2021.

3.1.3 Expression of Notch2IC promoted B cell proliferation

To explore whether the initial increase of hCD2$^+$ cells among splenic B cells was a result of Notch2-driven B cell proliferation, a series of BrdU incorporation experiments was executed. BrdU is a synthetic thymidine analog and is frequently used to track proliferating cells. When offered to mice via drinking water, BrdU gets incorporated into DNA of replicating cells, substituting thymidine. If administered to mice, cycling cells can be identified as BrdU$^+$. BrdU is passed to daughter cells upon replication. Notch2IC/CD19CreERT2:hom, CAR/CD19CreERT2

and Notch2IC/CD19CreERT2:het mice were treated with 1x tamoxifen and subsequently offered BrdU via drinking water for 7 days as depicted in the treatment scheme below. As a readout, purified splenic B cells of those mice were stained for BrdU and the proliferation marker Ki67.

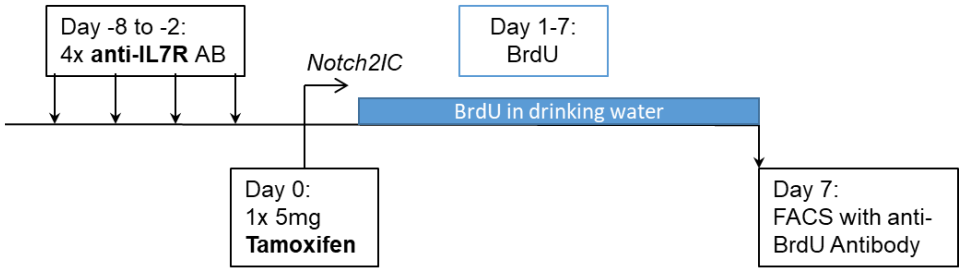

Figure 15: Treatment scheme for BrdU-incorporation assay.

The results showed that indeed the expression of Notch2IC, but not CAR, promoted a significant increase of $BrdU^+$ cells that simultaneously expressed Ki67 when compared to reporter-negative B cells (Figure 16, Figure 17). It was further found that $hCD2^+$ B cells from homozygous Notch2IC/CD19CreERT2:hom mice displayed higher percentages of cycling cells than their CD19-proficient, Cre-heterozygous Notch2IC/CD19CreERT2:het counterparts.

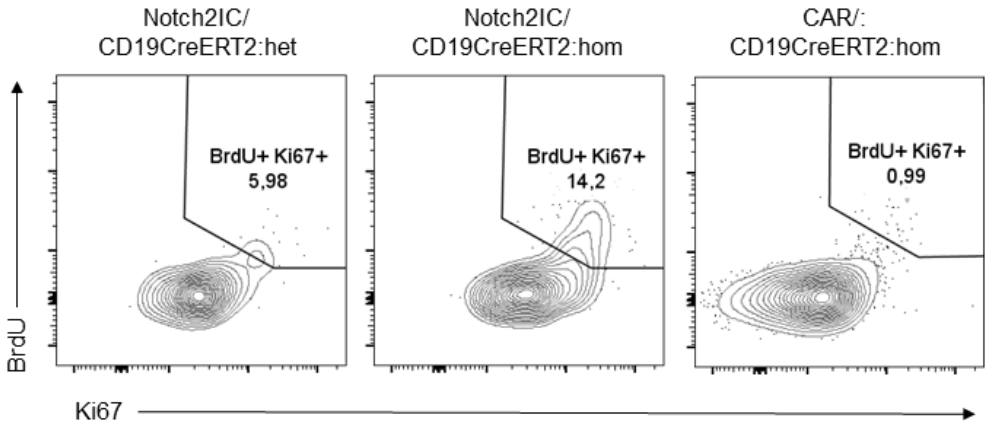

Figure 16: Expression of Notch2IC, but not CAR induced proliferation in a subset of reporter$^+$ B cells. Representative contour plots of reporter$^+$ ($hCD2^+$/CAR^+) $B220^+$ splenic B cells of Notch2IC or CAR expressing mice, 7 days after tamoxifen induction and subsequent BrdU treatment as described in Figure 15. Similar figure in Lechner et al. 2021.

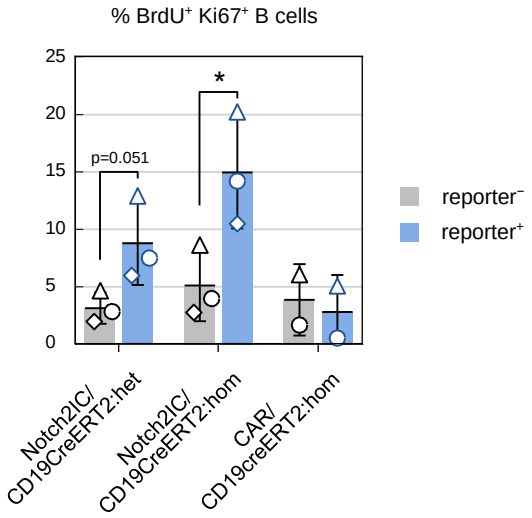

Figure 17: Expression of Notch2IC promotes B cell proliferation. Summary and quantification of BrdU$^+$Ki67$^+$ double positive B cells among hCD2- or CAR-reporter-positive B cells from Notch2IC- and CAR-expressing B cells, 7 days after tamoxifen induction and subsequent BrdU treatment. All individual data points, mean values and SD are shown. n=3 for Notch2IC mice, n=2 for CAR mice, 2 independent experiments, *p=0.0128, paired t-tests, two tailed. Similar figure in Lechner et al. 2021.

3.1.4 Expression of Notch2IC mediated surface marker conversion of follicular B cells to marginal zone B cells

To analyze the phenotypic changes within the B cell compartment of Notch2IC/CD19CreERT2:hom mice after tamoxifen treatment, further flow cytometric experiments were conducted. To phenotype early responding cells after tamoxifen treatment, the expression of hCD2 (or the CAR reporter) was used to identify Cre-recombinase activated cells and it was found that as early as two days after induction of Notch2IC or CAR expression, all reporter-positive B cells resembled the mature FoB cell phenotype (Figure 18).

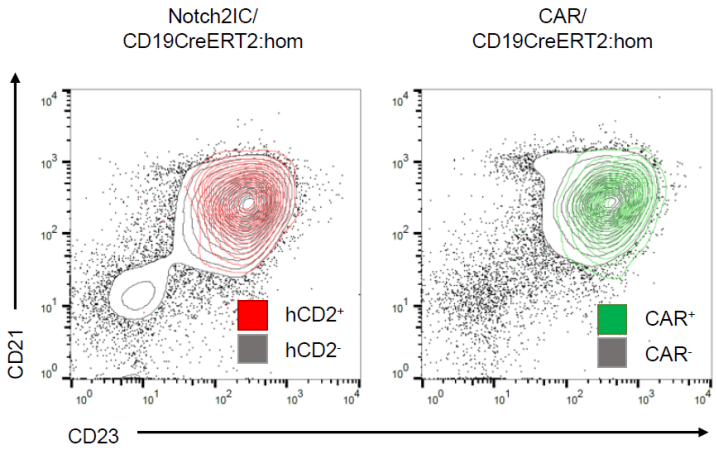

Figure 18: Reporter^{+} B cells 48h after tamoxifen treatment are CD23^{+}CD21^{mid} follicular B cells. Phenotypes of Notch2IC-expressing, hCD2^{+} cells and CAR^{+} control cells were analyzed 48h after TAM induction for their CD21/CD23 surface phenotype. Cells are pre-gated on B220^{+} B cells and separated in an overlay plot for reporter-negative (hCD2^{-}, CAR^{-}; gray) and reporter-positive (hCD2^{+}, red; CAR^{+}, green) cells. Representative figure for two experiments.

By analyzing the changes within the splenic B cells compartment in a time course experiment after tamoxifen treatment in Notch2IC/CD19CreERT2:hom mice, it became apparent that a population of previously absent CD23^{low} CD21^{high} MZB cells was gradually reappearing within a time frame of two to four weeks (Figure 19, top row). To specifically ascribe this observed surface marker alterations to the induction of Notch2IC expression, the phenotype of hCD2^{+} cells was then analyzed. hCD2^{+} cells initially started to upregulate CD21 three days after tamoxifen application, followed by downregulation of CD23 on day 7-14 (Figure 19, bottom row), thereby completing the shift to a surface MZB-phenotype. 30 days after Notch2IC induction, the vast majority of hCD2^{+} cells completed the conversion to the MZB surface marker phenotype. As all hCD2^{-} cells remained in the FoB cell phenotype at all time points, the re-appearance of cells in the MZB surface marker gate was exclusively mediated by hCD2^{+} cells.

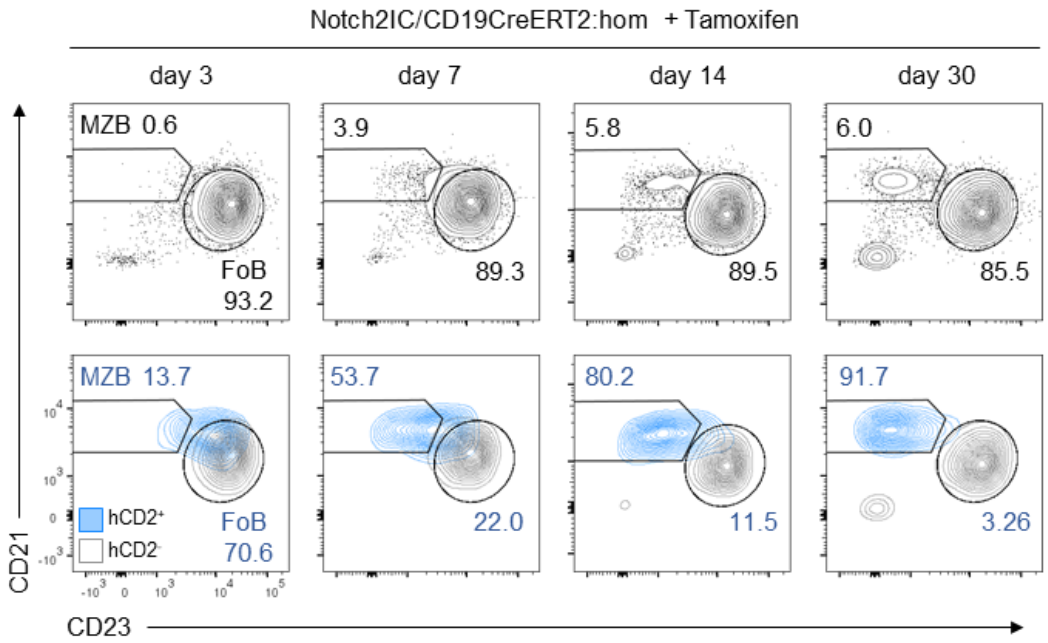

Figure 19: Conversion of the surface marker expression phenotype from FoB- to MZB cells in Notch2IC-expressing B cells over a time course of 30 days. Representative contour plots at different time points of time series experiments are shown. Top row shows all B220$^+$ splenic B cells at the indicated time points after a single tamoxifen treatment leading to Notch2IC-induction. Note the appearance of a wild type-like MZB population from day 14 after treatment onwards. Cells in the bottom row were separated into hCD2$^+$ (blue) and hCD2$^-$ (gray) cells. The majority of hCD2$^+$, Notch2IC-expressing B cells gained a MZB surface phenotype two weeks after Notch2IC induction. Numbers indicate percentages of cells gated as MZB or FoB cells in total B cells (top row) or hCD2$^+$ only (bottom row). Representative contour plots of at least 3 mice per time point. Similar figure in Lechner et al. 2021.

The surface marker conversion of hCD2$^+$ cells was verified through additional stainings for other known flow cytometry markers that are used to distinguish FoB- and MZB cells. As mentioned in the introduction, MZB cells differ from FoB cells in expression of CD1d, IgD and IgM. At day 30 after tamoxifen treatment, hCD2$^+$ cells were CD1d^{high} IgM^{high} IgD^{low}, thus resembling wild type MZB expression levels of all markers (Figure 20). Notch2IC-expressing MZBs also increased in cell size – as indicated by a higher forward scatter area (FSC-A) value – another property matching their wild type MZB counterparts. The kinetic of this Notch2-mediated surface marker conversion over time was shown to be consistent (Figure 21), with around 80% of hCD2$^+$ cells having adopted the MZB surface marker expression phenotype by day 14 after tamoxifen treatment.

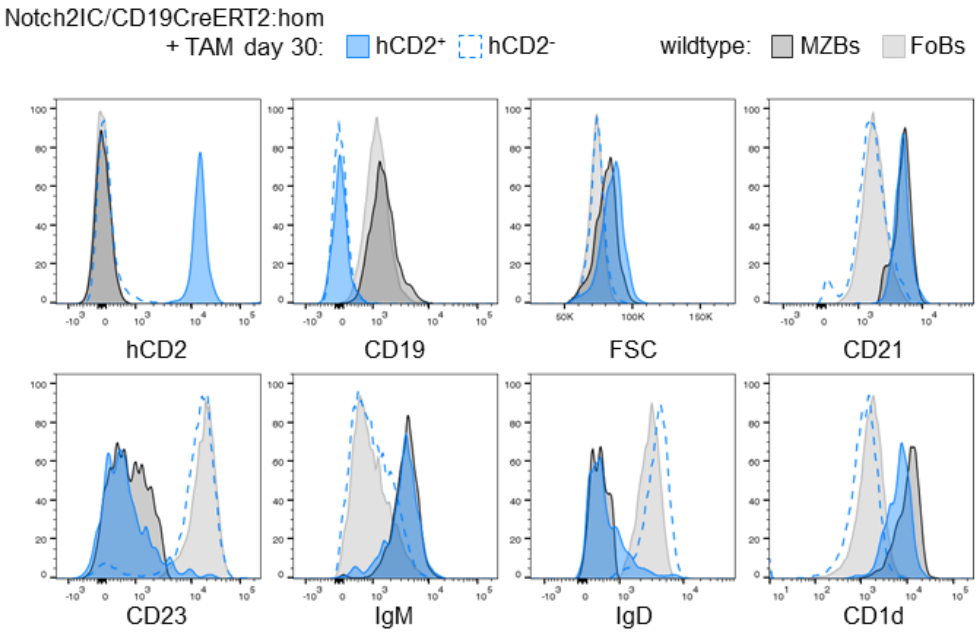

Figure 20: Additional surface markers separating FoB from MZB cells verified the complete phenotypic adaption of the MZB surface marker expression phenotype of all hCD2$^+$ cells. FACS analysis of Notch2IC-expressing cells 30 days after a single tamoxifen treatment and induction of Notch2IC-expression. B cells of Notch2IC/CD19CreERT2:hom mice were separated into hCD2$^+$ (filled blue) and hCD2$^-$ (dotted blue line), as shown in the first histograms. Histogram for CD19 expression was included to visualize the CD19 depletion in Notch2IC/CD19CreERT2:hom mice. FoB cells are CD21$^+$ CD23^{high} IgM^{low} IgD^{high} CD1d$^+$ while MZB cells are CD21^{high} CD23^{low} IgM^{high} IgD^{low} CD1d^{high}. Wild type MZB and FoB cells were added as controls. As MZB and FoB cells also differ in size, FSC was included to the analysis. All histograms were pre-gated on B220$^+$ B cells. Representative data of n=3 mice. Similar figure in Lechner et al. 2021.

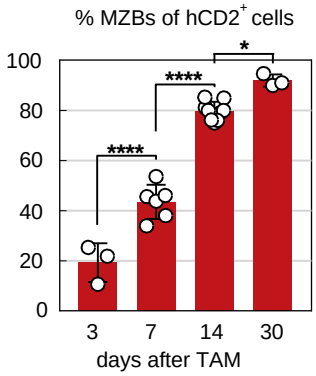

Figure 21: Quantification of hCD2$^+$ cells with completed MZB surface phenotype over time. Plotted are the percentages of MZB cells (B220$^+$, CD23^{low} CD21^{high}, as gated in Figure 19) among hCD2$^+$ cells at the indicated days after a single tamoxifen (TAM) treatment. Individual data points, mean and SD are shown. ****p=3.0E−05 (d3 vs d7), ****p=1.6E−09 (d7 vs d14), *p=0.0144. d3 n=3, d7 n=5, d14 n=7, d30 n=3. one-way ANOVA with Tukey's multiple comparisons test. Similar figure in Lechner et al. 2021.

In an additional set of experiments, tamoxifen dosing was increased to oral administration of 5 mg on five consecutive days. This repeated application did not alter the kinetic and qualitative percentages of FoB-to-MZB phenotype conversion (Figure 22) although the total numbers of $hCD2^+$ cells as well as newly generated MZBs within $B220^+$ splenic B cells were increased (Figure 14).

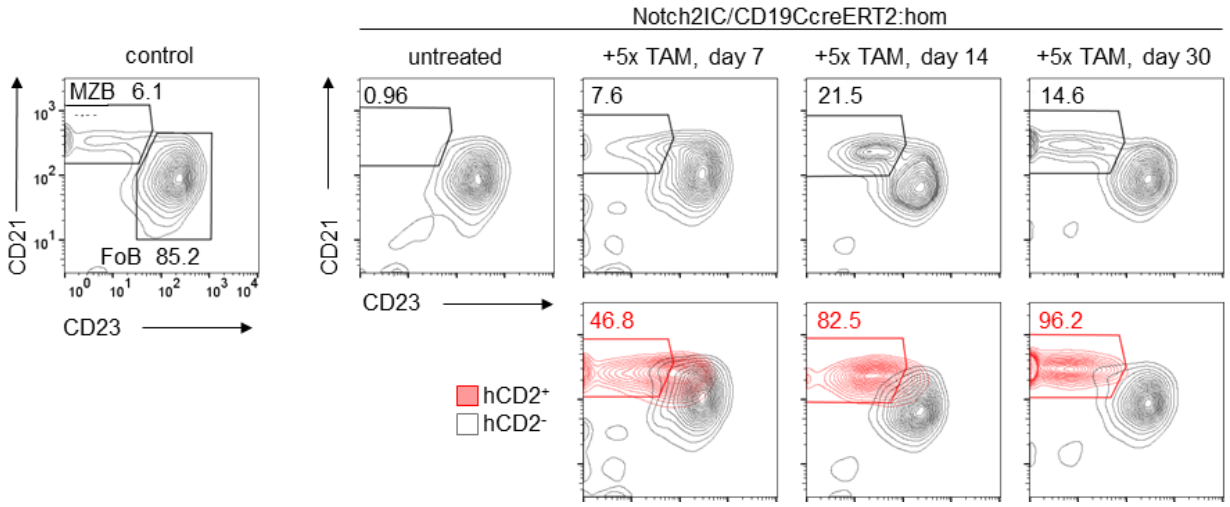

Figure 22: Repeated doses of tamoxifen administration resulted in higher total numbers of $hCD2^+$ cells as well as newly formed MZB cells. Notch2IC/CD19CreERT2:hom mice were treated with 5 mg tamoxifen (TAM) on five consecutive days and analyzed at indicated time points. Contour plots are gated on $B220^+$ B cells. B cells shown in the bottom row were additionally separated into $hCD2^+$ (red) and $hCD2^-$ (gray) cells and then overlaid. Numbers indicate percentages of cells gated as MZB cells in total B cells (top row) or $hCD2^+$ only (bottom row, red). The kinetic of phenotypic conversion did not differ from single treatment mice. Representative data for n>3 mice per time point. Similar figure in Lechner et al. 2021.

3.1.5 Notch2IC-expression initiated spatial homing to the marginal zone

Fully differentiated MZB cells are characterized by their distinct localization in the name-giving marginal zone – strictly separated from FoB cells. To investigate, whether the phenotypic conversion of FoB-to-MZB cells mediated through Notch2IC expression was also accompanied by B cell migration and altered homing, histological analyses were performed. The blood-perfused marginal zone surrounds the lymphoid follicle, which is comprised of a T cell zone and a B cell zone where follicular B cells are located. The border between the follicle and marginal zone is demarked by the marginal sinus, which is lined with Laminin-expressing endothelial cells.

Metallophilic macrophages are located directly at the marginal sinus and can be stained as marker cells for the follicular border with the antibody MOMA-1.

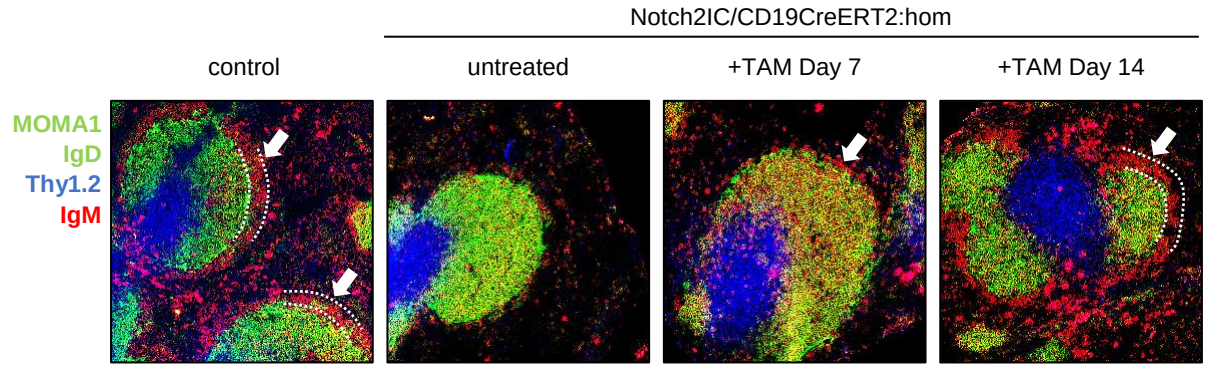

Figure 23: The splenic MZB compartment was progressively repopulated by IgM^{high} B cells after Notch2IC-induction. Splenic sections of CD19^{+} proficient control and Notch2IC/CD19CreERT2:hom mice, without or at days 7/14 after 1x tamoxifen (TAM) treatment, were stained for FoB cells (IgD^{high}, green), metallophilic macrophages (MOMA-1^{+}, bright green ring around follicle), T cells (Thy1.2, blue) and MZB cells (IgM^{high}, red). The IgM-bright MZB cells are highlighted with white arrows. A complete marginal zone is additionally delineated with dotted lines. Representatives of splenic sections of n=2 per group. Similar figure in Lechner et al. 2021.

While wild type sections displayed a distinct ring-like structure of IgM^{high}IgD$^{low/-}$ MZB cells surrounding the IgD^{high} FoB cell zone, no IgM^{high} ring was found in untreated Notch2IC/CD19CreERT:hom mice (Figure 23). MZB cells started to localize at their defined anatomic site 7 days after tamoxifen treatment, while a ring-like population of IgM^{high} B cells was completed 14 days after treatment. Chromogenic immunohistochemical staining using an alkaline phosphatase-coupled secondary antibody allowed for the staining of hCD2^{+} cells. Again, 7 days after tamoxifen, only some cell clusters where stained outside of the laminin^{+} sinus ring, while a full ring of MZ-localized hCD2^{+} cells was completed from day 14 onwards (Figure 24).

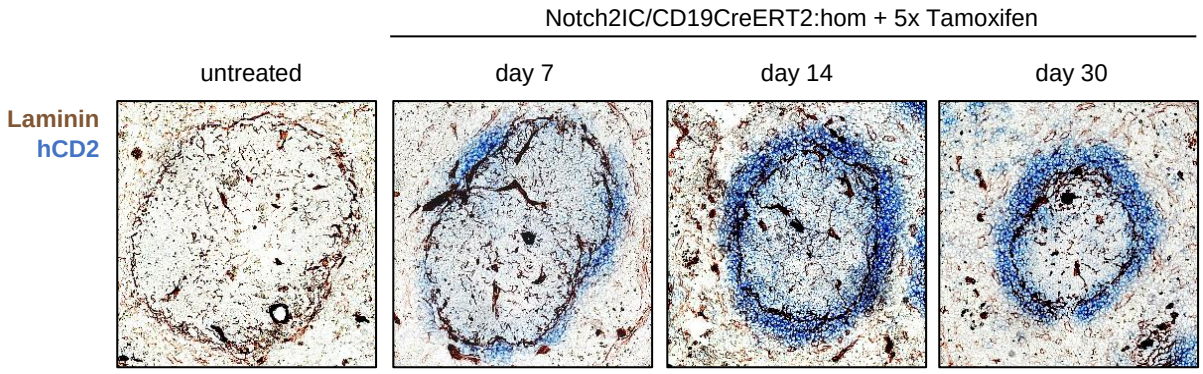

Figure 24: hCD2$^+$ B cells were mainly found in the marginal zone. Immunohistochemical staining of splenic sections from Notch2IC/CD19CreERT2:hom mice at indicated time points after the first day of five consecutive tamoxifen treatments are depicted. Laminin$^+$ endothelial cells line the ring-like marginal sinus, which separates the inner follicular zone (white pulp) from the marginal zone and red pulp. hCD2$^+$ (blue) B cells increasingly repopulated the marginal zone. Similar figure in Lechner et al. 2021.

In conclusion, it was found that induction of Notch2 signaling in mature FoB cells not only mediated a phenotype-conversion to MZB-like cells, but also dramatically altered the spatial organization of Notch2IC-expressing cells. As hCD2$^+$ cells localized outside of the splenic follicle and therefore regenerated a marginal zone B cell compartment, one could possibly claim that mature follicular B cells had undergone a complete trans-differentiation to become marginal zone B cells in a process driven by Notch2 signaling.

3.1.6 Phenotypic conversion through Notch2IC is unaffected by CD19 expression

To address the question whether Notch2IC-expressing FoB cells similarly convert to MZB cells in a competitive, CD19-proficient environment, we induced Notch2IC expression in NotchIC/CD19creERT2:het mice, where a wild type-like marginal zone was already populated by B cells. In Notch2IC/CD19creERT2:het mice, splenic B cell subsets and the microenvironment are unaltered when compared to wild type mice. Moreover, B cells of Notch2IC/CD19creERT2:het mice still possess a fully functional BCR/CD19 signaling complex. Expressing Notch2IC in this background could potentially result in different outcomes due to the presence or absence of a fully functional BCR signaling pathway.

Induction of Notch2IC expression in Notch2IC/CD19creERT2:het mice resulted in a phenotypic shift from FoB to MZB cells in comparable kinetic and frequency to CD19-deficient mice (Figure 25). Interestingly, a similar mature B cell subsets seemed to respond to tamoxifen treatment when comparing Notch2IC/CD19creERT2:het mice to Notch2IC/CD19creERT2:hom mice within the same set of gene induction experiment: at three days after tamoxifen treatment, the Notch2IC-expressing, $hCD2^+$ cells were predominantly found in the FoB cell gate. The percentage of $hCD2^+$ cells that fully converted the phenotype to $CD23^{low}CD21^{high}$ MZB cells over time after tamoxifen treatment is shown in Figure 25B and very much resembled the outcome of Notch2IC/CD19creERT2:hom mice as shown in Figure 21.

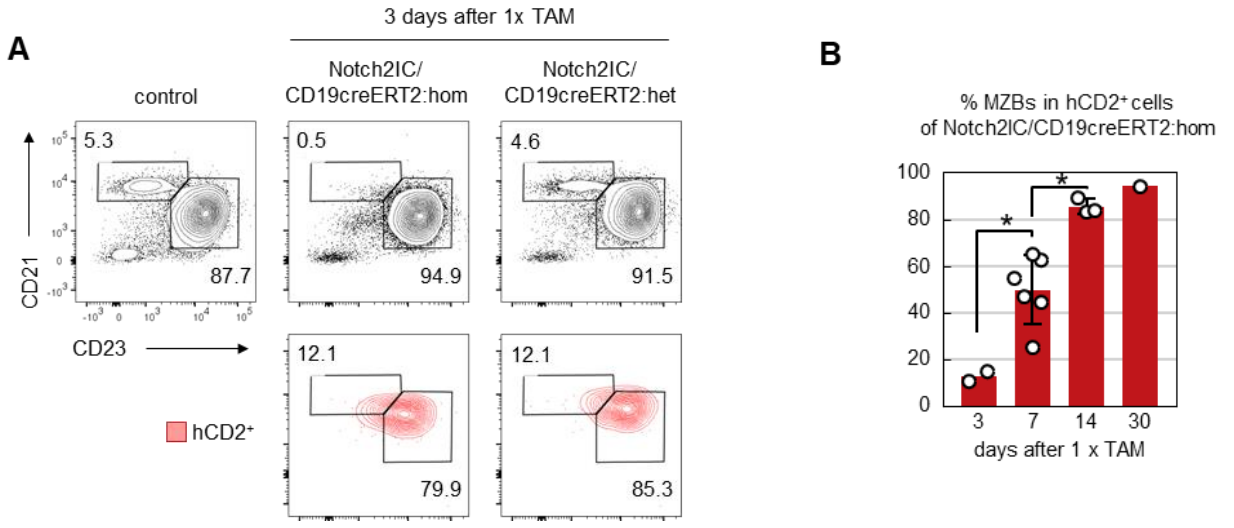

Figure 25: FoB-to-MZB transition is not affected by CD19 expression. (A) Representative flow cytometric analysis of CD19-proficient Notch2IC/CD19creERT2:het mice 3 days after a single tamoxifen (TAM) treatment in comparison to control (left) and CD19-deficient Notch2IC/CD19creERT2:hom mice (middle) as shown in Figure 19. The top row was gated on $B220^+$ B cells and the bottom row in red shows all $B220^+$ $hCD2^+$, Notch2IC-expressing B cells after TAM treatment. Numbers indicate percentages of $CD23^{high}$ $CD21^+$ FoB and $CD23^{low}$ $CD21^{high}$ MZB cells. (B) The graph compiles the percentages of MZB cells within the fraction of $hCD2^+$ B cells in Notch2IC/CD19creERT2:het mice at the indicated time points after treatment with a single dose of tamoxifen. Bars indicate mean values and standard deviations at each time point. Data points represent values for individual mice for n=2 (day 3), n=6 (day 7), n=3 (day 14) and n=1 (day 30) mice. (*p=0.020, *p=0.011, ordinary one-way ANOVA, Tukey's multiple comparisons test). Similar figure in Lechner et al. 2021.

3.1.7 Notch2IC-expressing cells acquired functional properties of MZB cells

MZB cells serve as a first-line defense against blood-borne pathogens and bridge the early days after an infection until the adaptive arm of the immune system has developed to full strength. They come with special traits enabling a rapid response with a broad specificity, one example being high expression levels of TLR4, which recognizes Lipopolysaccharides- (LPS) antigens, outer membrane components of gram-negative bacteria. In contrast to FoB cells, MZB cells have been shown to rapidly respond to LPS stimulation with plasmablast-differentiation within hours *in vivo* and *in vitro* (Oliver, Martin, and Kearney 1999; Martin, Oliver, and Kearney 2001; Fairfax et al. 2008; Martin and Kearney 2002). This rapid blasting behavior of MZB cells can therefore serve as a functional readout for a successful functional conversion of FoB to MZB cells.

The trans-differentiation of mature FoB cells to fully functional MZB cells was tested in *in vitro* and *in vivo* experiments. Proliferation and differentiation to $CD138^+$ plasmablasts and early plasma cells served as readouts in response to LPS stimulation. In a first set of *in vitro* experiments, B cells from wild type controls, as well as untreated and tamoxifen-induced Notch2IC/CD19CreERT2:hom mice were purified and stimulated with LPS for 48h. Untreated B cells from Notch2IC/CD19CreERT2:hom mice showed no response to LPS *in vitro*, while a subset of B cells in control animals responded with proliferation - as indicated by dilution of the CFSE dye – and differentiation to $CD138^+$ plasmablasts (Figure 26). This difference was most likely due to the presence or absence of MZB cells among purified B cells that exclusively mediated the LPS response: MZB cells are present in CD19-proficient control animals but are lacking in the untreated Notch2IC/CD19CreERT2:hom mice. Day 14 after tamoxifen treatment was defined as time point of analysis, as the majority of $hCD2^+$ B cells had completed the trans-differentiation to MZB cells in terms of their surface marker expression and localization at this time point. When B cells from tamoxifen-induced Notch2IC/CD19CreERT2:hom mice were also treated with LPS *in vitro*, the plasmablast response was comparable to that of CD19-proficient control B cells. Gating of live cells after two days in culture into $hCD2^+$ and $hCD2^-$ cells revealed that proliferation and differentiation was exclusive for B cells expressing Notch2IC, which had mostly underwent trans-differentiation from FoB to MZB cells (Figure 27). The *in vitro* experiments showed that the newly generated MZB cells through Notch2-mediated trans-differentiation from FoB cells have

implemented the sensitivity to LPS and subsequent blasting response as a functional trait of wild type MZB cells.

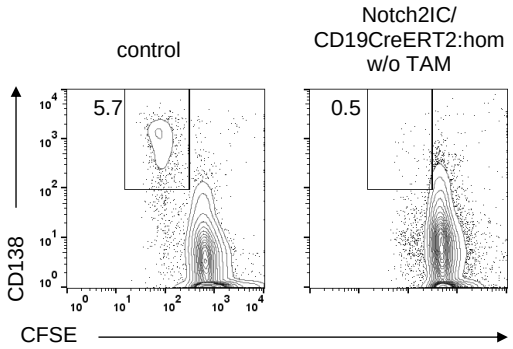

Figure 26: Untreated Notch2IC/CD19CreERT2:hom B cells were non-responsive to LPS stimulation *in vitro.* CFSE-stained purified B cells were stimulated *in vitro* with LPS for 48h and then analyzed in FACS. Cells were gated on living lymphocytes. While a subset of control B cells – most probably the MZB compartment – proliferated and differentiated to CFSE-diluted, $CD138^{+}$ plasmablasts (left), no differentiation or proliferation was detected in CD19-knockout, Notch2IC/CD19CreERT2:hom B cells (right). Numbers indicate the percentages of $CFSE^{low}$ $CD138^{high}$ plasmablasts. Representative data for two experiments. Similar figure in Lechner et al. 2021.

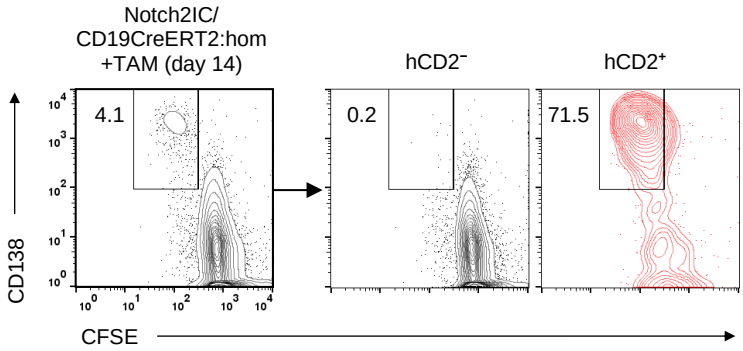

Figure 27: Plasmablast response to LPS was restored in Notch2IC/CD19CreERT2:hom mice through Notch2IC-induction. Same experiment as shown in Figure 26. 14 days after tamoxifen treatment. Notch2IC/CD19CreERT2:hom B cells responded with proliferation and differentiation as shown by a subset of CFSE-diluted, $CD138^{+}$ plasmablasts (left). Separating all B cells into reporter-negative or -positive ($hCD2^{-}$/$hCD2^{+}$, middle and right) showed that this response was exclusively mediated by Notch2IC-expressing $hCD2^{+}$ cells that have undergone trans-differentiation to MZB cells. Numbers indicate the percentages of $CFSE^{low}$ $CD138^{high}$ plasmablasts. Representative data for two experiments. Similar figure in Lechner et al. 2021.

To investigate MZB functionality also *in vivo*, Notch2IC/CD19CreERT2:hom mice were pretreated with anti-IL7R antibody and Notch2IC expression was subsequently induced with a single dose of tamoxifen as described before (Figure 12). 14 days after gene induction, mice were immunized with 10µg NP-LPS. Mice were analyzed 3 days after immunization. Plasmablast response was again used as the readout for functional MZB-mediated response.

Splenocytes of controls and Notch2IC-induced mice were examined for the presence of $CD138^+$, $TACI^+$ plasmablasts and early plasma cells (Figure 28): While CD19-proficient control animals showed a significant plasmablast response after LPS immunization, untreated Notch2IC/CD19CreERT2:hom mice did not. If Notch2IC/CD19CreERT2:hom had been pretreated with tamoxifen to induce FoB-to-MZB trans-differentiation, the generation of plasmablasts was comparable to that of CD19-proficient controls (Figure 28A). Gating on all $hCD2^+$ B cells after immunization showed that a high percentage of Notch2IC-induced cells differentiated to plasmablasts. Additional pre-gating on the plasmablast population illustrated that the vast majority of plasmablasts were $hCD2^+$ (Figure 28C). The rescued plasmablast response was therefore almost exclusively mediated by the newly generated MZB cells (Figure 28, right plot). Additional intracellular FACS staining confirmed the rescue of the wild type-like plasmablast response through trans-differentiated MZB cells: Plasmablasts of Notch2IC-induced mice expressed similarly high levels of the transcription factor IRF4 and downregulated B220 (Figure 29A+B). The intracellular cell staining additionally revealed that most of the identified $IRF4^+$ plasmablasts produced high intracellular levels of unswitched IgM^+ antibodies (Figure 29C).

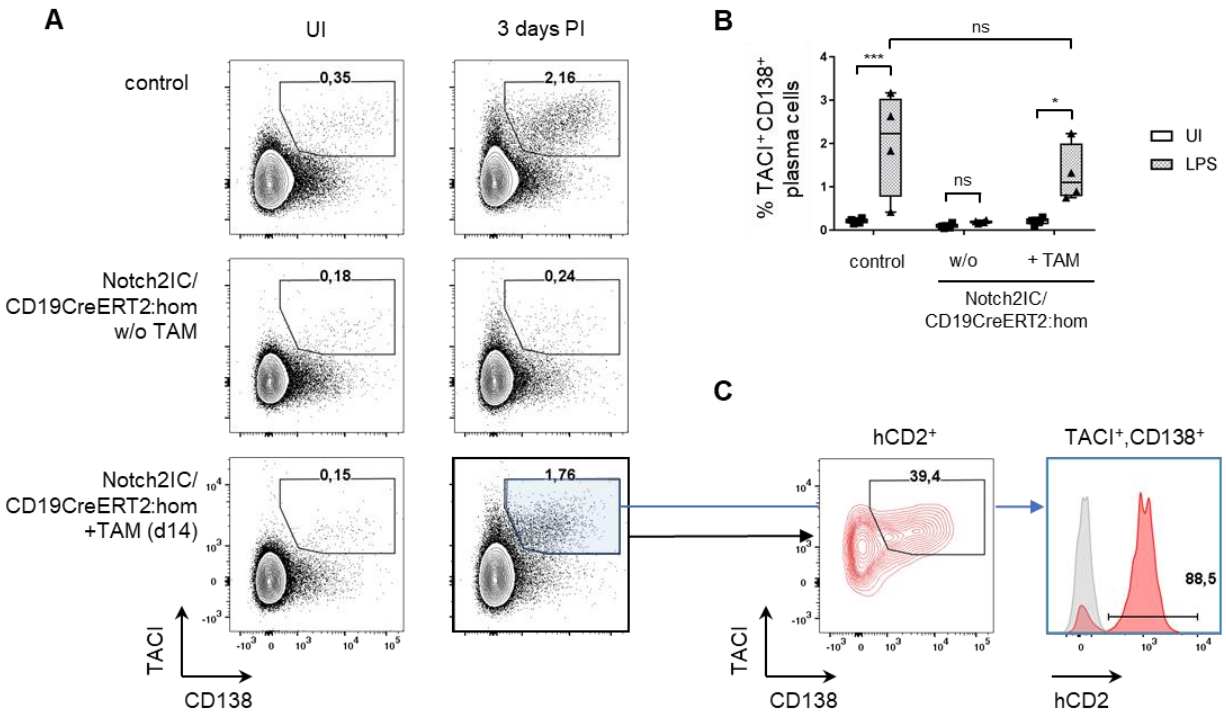

Figure 28: Plasmablast response to LPS immunization was rescued after Notch2IC-mediated MZB differentiation (I). CD19-proficient control mice as well as untreated and tamoxifen-induced Notch2IC/CD19CreERT2:hom mice were immunized with 10µg of NP-LPS. 3 days post immunization (PI), splenocytes were stained for CD138$^+$ TACI$^+$ plasmablasts and early plasma cells (A+B). Differentiation to CD138$^+$ TACI$^+$ plasmablasts in response to LPS immunization was absent in untreated (w/o) Notch2IC/CD19CreERT2:hom mice. Tamoxifen treatment (+TAM) and subsequent FoB-to-MZB trans-differentiation restored a significant proportion of plasmablasts. Numbers indicate percentages of cells gated as plasmablasts among splenocytes. (C) Splenocytes from tamoxifen treated and immunized Notch2IC/CD19creERT2:hom mice were additionally gated on hCD2$^+$ (left) or TACI$^+$ CD138$^+$ cells (right). In the hCD2 histogram, control plasmablasts were added as negative control (gray histogram). Representative data for two independent experiments with a total of n=4 mice per group. Similar figure in Lechner et al. 2021.

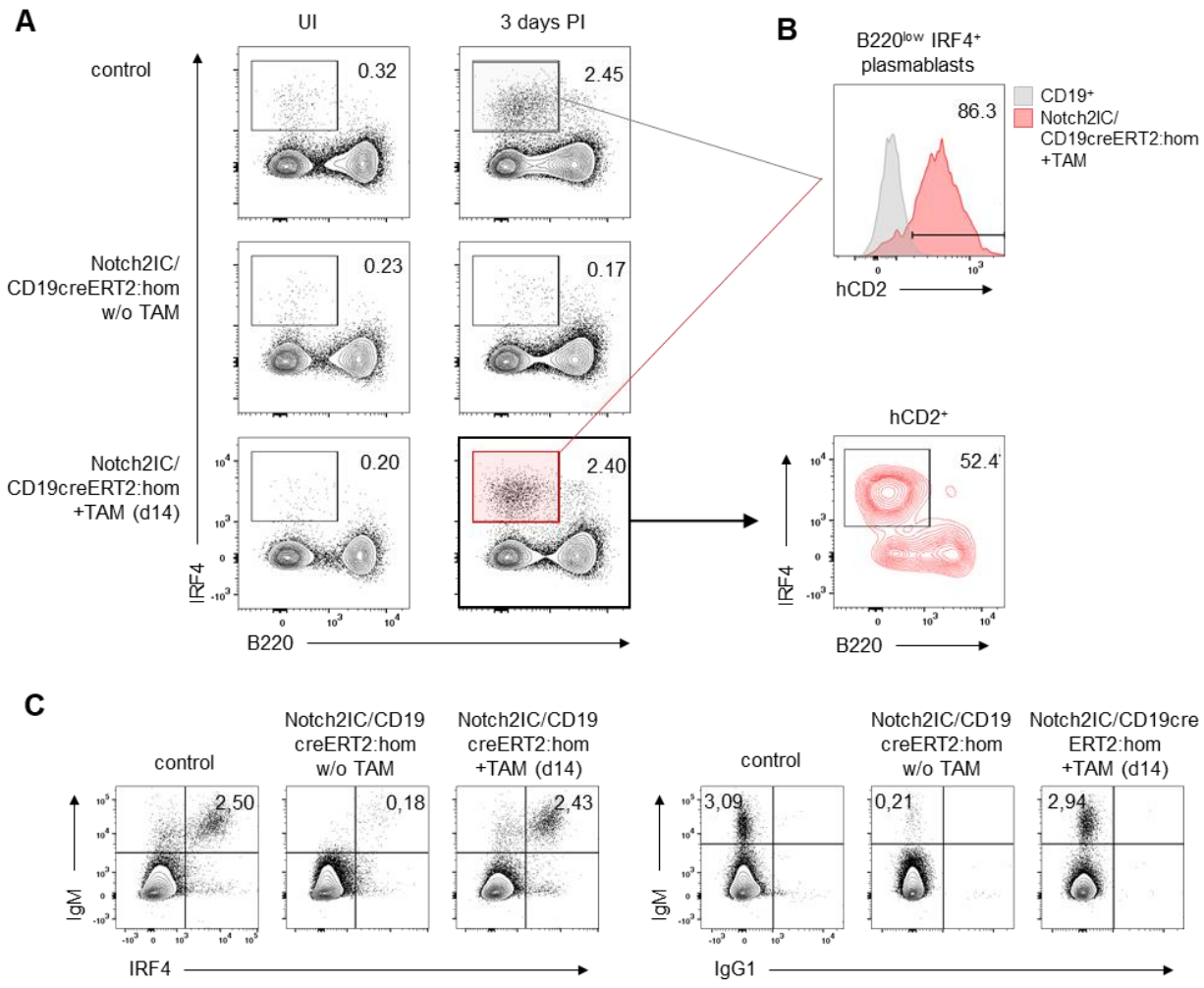

Figure 29: Plasmablast response to LPS immunization was rescued after Notch2IC-mediated MZB differentiation (II). Intracellular FACS analysis of the same experiment as shown in Figure 28. (**A**) The percentages of plasmablasts was confirmed by additional gating on B220^{low} IRF4^{+} cells. Plots are pre-gated on lymphocytes by FSC/SSC characteristics. Numbers indicate percentages of B220^{low} IRF4^{+} plasmablasts. (**B**) Overlay of control and Notch2IC/CD19creERT2:hom (+TAM) B220^{low} IRF4^{+} plasmablasts showed that the regenerated plasmablast differentiation is exclusive to hCD2^{+} cells (upper panel). Additional gating on hCD2^{+} in immunized Notch2IC/CD19CreERT2:hom (+TAM) mice (lower panel) illustrates the strong plasmablast response among Notch2IC-expressing, regenerated MZBs to LPS *in vivo*. (**C**) The majority of IRF4^{+} plasmablasts in control and tamoxifen-induced mice produced large intracellullar pools of IgM, but not IgG1, indicating the generation of unswitched IgM^{+} plasmablasts. Plots were again pre-gated on lymphocytes. Representative data of two independent experiments with a total of 4 mice per group. Similar figure in Lechner et al. 2021.

3.1.8 RNA sequencing revealed a Notch2-mediated transcriptomic shift from FoB to MZB gene expression signature

A collaboration with scientists from the laboratory of Prof. Dr. Roland Rad at the TranslaTUM Munich was initiated to set up a big RNA Sequencing (RNA-Seq) experiment. The goal of this collaboration was to analyze the Notch2-mediated trans-differentiation of FoB to MZB cells on a transcriptomic level. Moreover, we were hoping to identify new Notch2-interaction partners and so far unknown genetic alterations associated with MZB differentiation.

The experimental basis of this RNA-Seq was a large gene induction experiment, where Notch2IC/CD19CreERT2 mice were treated with tamoxifen and B cell samples were collected in a tightly monitored time series. $hCD2^{+}$ cells were FACS-sorted at days 3, 5, 7 and 14 after tamoxifen treatment of Notch2IC/CD19CreERT2:hom mice. The replicates of time points after gene induction were spread over different litters of mice and days of tamoxifen treatments to exclude batch/littermate effects during cell sorting. Wild type FoB and MZB fractions were sorted for transcriptional reference controls. $hCD2^{-}$ non-responding $B220^{+}$ B cells were additionally sorted as negative controls from different time points after tamoxifen treatment. After sorting 50.000 cells of all populations (n=5-6 per group), RNA was purified using an individualized TRIzol LS + Promega column-based protocol. The advantages of this protocol over each of the respective commercial ones were several: The sorting of samples directly in TRIzol LS enabled long-term storage in -80°C without big losses of RNA yield. After thawing, the subsequent RNA purification could be performed in large batches of randomly picked samples. Moreover, the output of this hybrid protocol produced high purity of RNA. RNA quantity and quality of each sample were determined using RNA pico Bioanalyzer chips. The RIN values (RNA integrity number) reached the total average of 9.7, with all used samples being >9.2. Average RNA concentration was around 800 pg/µl with a total elution volume of 15µl.

Samples were then transferred to the collaborating laboratory of Prof. Roland Rad at the TranslaTUM Munich. Library preparation and the sequencing run was performed by Dr. Rupert Öllinger. Dr. Thomas Engleitner analyzed the sequencing data and provided quality controlled and normalized list of differentially expressed genes of each grouped comparison for additional bioinformatic analysis.

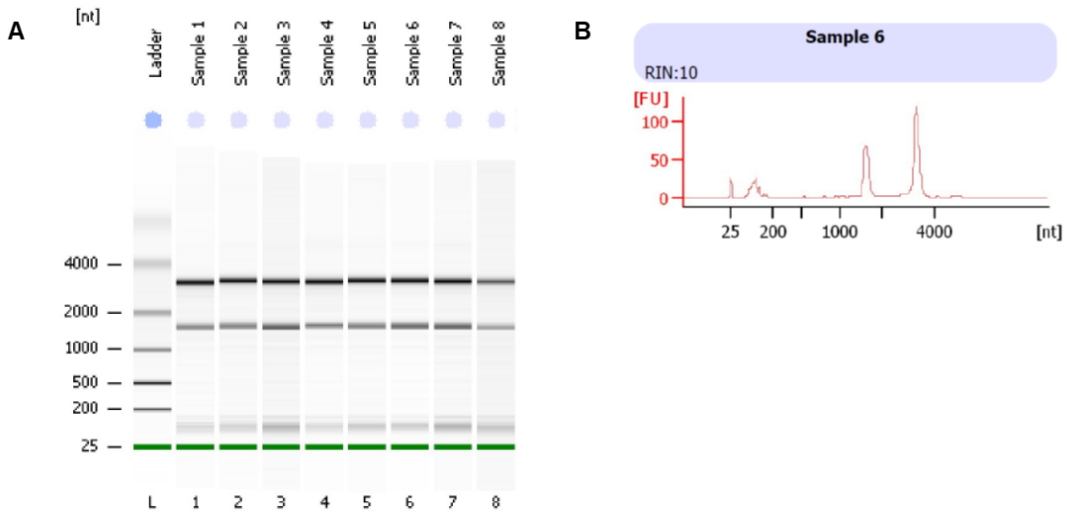

Figure 30: Representative analysis report of purified RNA from 8 samples, as provided from the bioanalyzer RNA pico analysis assay. A) Electrophorese gel-like picture generated by the software for visual overview of all samples and the control ladder run within one chip. RNAs of different nucleotide (nt) length were separated by size from small to large in a capillary gel electrophoresis system. The dark bands indicate accumulation of the similar-sized ribosomal RNAs (rRNAs) within the sample. **B**) Analytical electropherogram, generated as a histogram of fluorescent units (FU) of detected RNA fragments, separated by size. Depicted is a representative sample from the analysis shown in (A): The marker peak at around 25nt followed by a series of small peaks that represent small RNAs such as tRNAs, microRNAs, smaller rRNA (50-200nt). The big peaks are the 18S and 28S rRNAs. The RIN value (RNA integrity number) is generated by an algorithm to enumerate RNA quality from 1-10, based on the ratio of rRNA peaks and additional variables which indicate degradation or impurities. The depicted sample 6 was of highest purity, as indicated by a RIN of 10.

3.1.8.1 Multidimensional scaling analysis visualizes global transcriptomic distances

The method most commonly used to visualize global transcriptome differences between samples is principle component analysis (PCA). Here, a related but preferred method was applied: multidimensional scaling analysis (MDS). MDS output visualizes the level of similarity of individual data points. It is a two-dimensional projection where relative pairwise distances are preserved in comparison to a classic PCA, where data points are projected as individual vectors in an n-dimensional space according to directions of data with most variance (Mead 1992). So, MDS enabled us to draw conclusions on the similarity of transcriptomes between two samples. As depicted in Figure 31, all individual samples of single time points after tamoxifen induction as well as wild type FoB and MZB controls clustered in distinct and well separable groups.

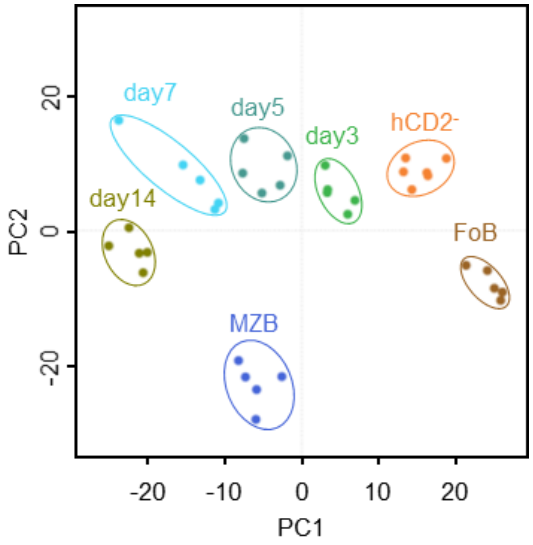

Figure 31: Multidimensional scaling (MDS) plot visualizes relative distances between every possible pair of data points. Indicated sample groups were color-coded and encircled. The two-dimensional distance matrix is defined by transcriptomic differences along the principal component axes PC1 and PC2. MDS data plot was provided by Dr. Thomas Engleitner. Final figure design by Markus Lechner. Similar figure in Lechner et al. 2021.

This unbiased whole-transcriptome MDS model illustrates a directed genetic shift originating from non-responding hCD2^{-} cells over all time points after Notch2IC-induction to the cell cluster of day 14 after treatment as endpoint of this time series experiment. The transcriptomic drift can mainly be attributed to changes in values depicted in the PC1-axis. A second finding from this MDS plot is the basic offset of all samples from Notch2IC/CD19CreERT2:hom mice to the two wild type FoB and MZB clusters. This offset can be attributed to underlying genetic differences of the two mouse strains: In contrast to the sorted FoB and MZB cells from controls, splenic B cells of Notch2IC/CD19CreERT2:hom mice carry the full knockout of CD19, a major signaling component of the BCR signaling axis.

The transcriptomic shift of hCD2^{-} cells to hCD2^{+} cells 14 days after tamoxifen in direct comparison to the transcriptomic differences of FoB and MZB cells is highlighted in Figure 32. Distance and direction of whole transcriptome differences between FoB and MZB cells, as indicated by vector X, matched the endpoints of transcriptomic shift of hCD2^{-} to day14 sample

clusters as shown by the vector copy X'. The basic offset between mouse models (Y = Y') was constant.

In summary: Notch2IC-expression in mature FoB cells in Notch2IC/CD19CreERT2:hom mice successfully triggered a complete transcriptomic shift to an MZB cell-like transcriptome, verifying the final MZB identity. hCD2$^-$ FoB cells and the trans-differentiated MZB cells each closely resembled its wild type benchmarks.

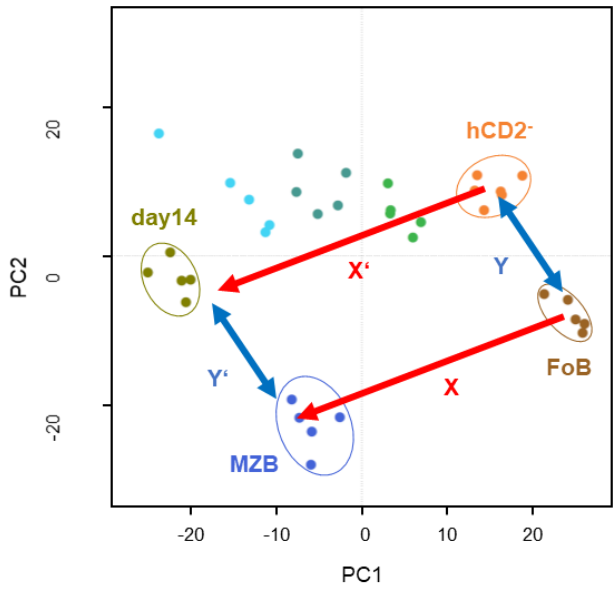

Figure 32: Relative distances between indicated transcriptomic clusters. Distances between two points or clusters can be translated into relative transcriptomic similarity. The relative distance of FoB to MZB was highlighted with a vector X. A copy of vector X, X' applied on the hCD2$^-$ cluster as base, indicates that the genetic relationship of hCD2$^-$ cells to hCD2$^+$ cells, 14 days after tamoxifen (cluster "day14") was comparable to the relationship of FoB to MZB cells. The basic offset Y of the relationship between hCD2$^-$ and FoB cells stays similar if applied to cluster "day14" versus "MZB" (Y'). Similar figure in Lechner et al. 2021.

3.1.8.2 Gene Set Enrichment Analysis verified an MZB-specific transcriptomic signature of hCD2$^+$ cells.

Gene Set Enrichment Analysis (GSEA) is a computational method to verify whether a set of genes - a priori attributed to a certain phenotype of interest - is significantly enriched in the large list of differentially expressed genes between two groups (Subramanian et al. 2005). GSEA experiments

were designed to assess the FoB-to-MZB trans-differentiation of Notch2IC-expressing FoB cells more specifically. For this purpose, MZB signature gene sets were defined by overlapping the top 1000 differentially expressed genes (by p-value) of wild type MZB versus FoB cells from this study with the top 1000 differentially expressed genes of MZB versus FoB cells provided from the ImmGen database (Microarray data) (Heng, Painter, and Immunological Genome Project 2008). This created two gene sets that were either comprised of the top-upregulated genes in MZB-versus-FoB comparison, termed "MZB genes", or top-downregulated, termed "FoB genes" (Figure 33). The signature gene sets are therefore verified via two different technical sequencing approaches and explicitly define the most significant identity genes of MZB cells (176 genes) and FoB cells (210 genes).

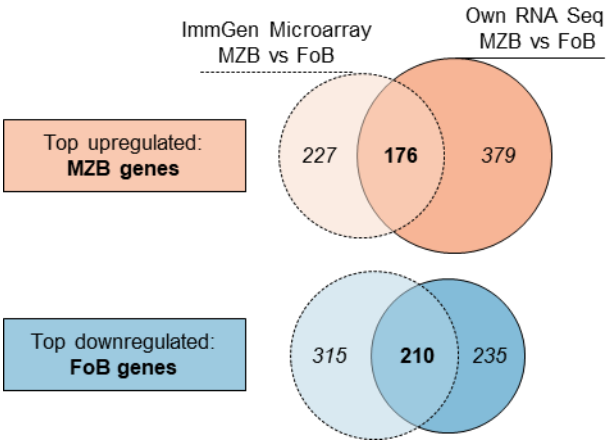

Figure 33: Venn diagrams of gene set design for GSEA analysis. The two genes sets "MZB genes" and "FoB genes" were defined as overlap of the top 1000 most differentially expressed genes between MZB and FoB cells from two sequencing approaches: RNA-Seq from this project and microarray data from ImmGen database. Similar figure in Lechner et al. 2021.

The two gene sets were then used in GSEA algorithms to test their enrichment during the Notch2IC induction time series. Lists of differentially expressed genes from each time point (day3, day5, day7, day14) versus $hCD2^{-}$ were used as ranked list of genes (by fold induction) as a basis for the pre-ranked GSEA algorithm.

GSEA with the gene set "MZB genes", when applied on the ranked gene list of day3 versus $hCD2^{-}$ after Notch2IC-induction, showed that gene set hits were spread along the list of 14450 ranked genes (Figure 34, top left). Yet, 48 genes out of the 176 gene set members were found to be enriched as leading edge at the top of the gene list. This led to an early peak and the overall positive ES of 0.44. Nominal p-value, FDR q-value and FWER p-value were all 0.0. On the contrary, many

genes were also found enriched at the bottom end of the gene list. These MZB genes were downregulated 3 days after Notch2IC-induction and consequently dampened the running score into negative digits. In the following days during the gene induction time series, MZB genes were found to be increasingly enriched at the top end of the gene list and the ES consequently increased. Whereas some MZB genes were still found to be downregulated at day5 and day7, 171 of 176 genes were upregulated at day14, with 141 (80%) in the leading edge, resulting in the very strong ES of 0.90 (Figure 34, left column from top to bottom). FoB genes showed an inversely correlated enrichment at the bottom end of Notch2IC-expressing versus non-expressing cells (Figure 34, right panel). Even at day3 after induction, many FoB genes showed to be already downregulated. In numbers, the ES was -0.71 at day3. The distribution of gene set hits was increasingly concentrated at the bottom end over time after Notch2IC induction, with the ES further decreasing to -0.87 at day14. 165 hits out of the 210 genes (79%) built the core enrichment of the negative leading edge.

Another approach to analyze the FoB-to-MZB trans-differentiation based on the signature gene sets was the calculation of fold-changes for every signature gene, normalized across all samples (FoB, MZB and Notch2IC/CD19CreERT2:hom samples at different time points after induction). The heatmap in Figure 35 illustrates the stepwise loss of a FoB gene expression signature and simultaneous gain of a MZB gene expression signature over time.

To sum up, Gene Set Enrichment Analyses statistically confirmed the FoB-to-MZB trans-differentiation on transcriptomic level. The induction of Notch2IC-expression initiated a gradual and ultimately very strong enrichment of MZB signature genes at the very top end of all regulated genes, while FoB signature genes were comparably downregulated.

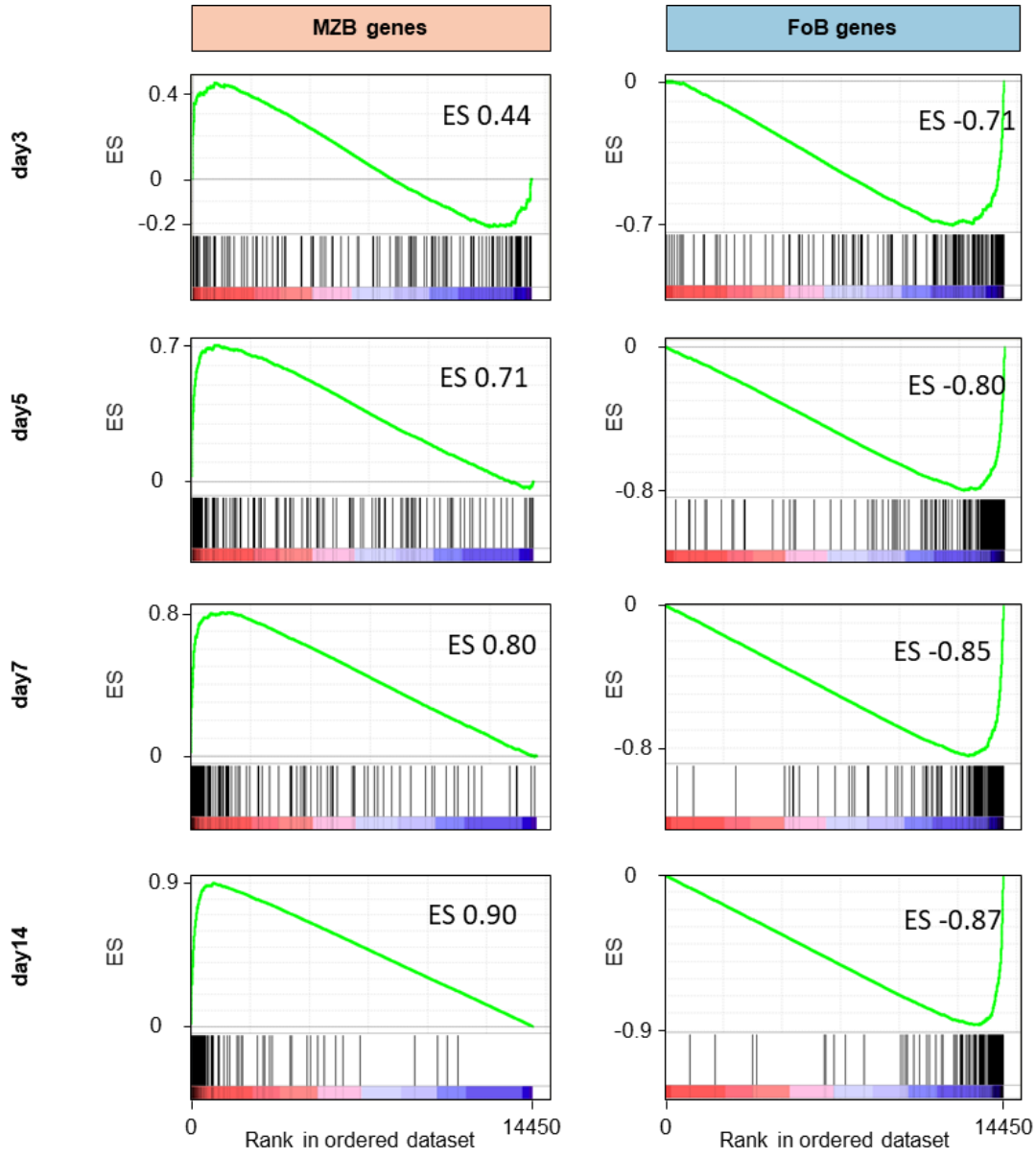

Figure 34: GSEA Enrichment plots for the MZB/FoB signature gene sets applied on ranked differentially expressed gene lists of each time point of Notch2IC-induction versus hCD2^{-}. Enrichment Scores (ES) are additionally depicted for every GSEA analysis using the "MZB genes" set (left column) and "FoB genes" set (right column). Similar figure in Lechner et al. 2021.

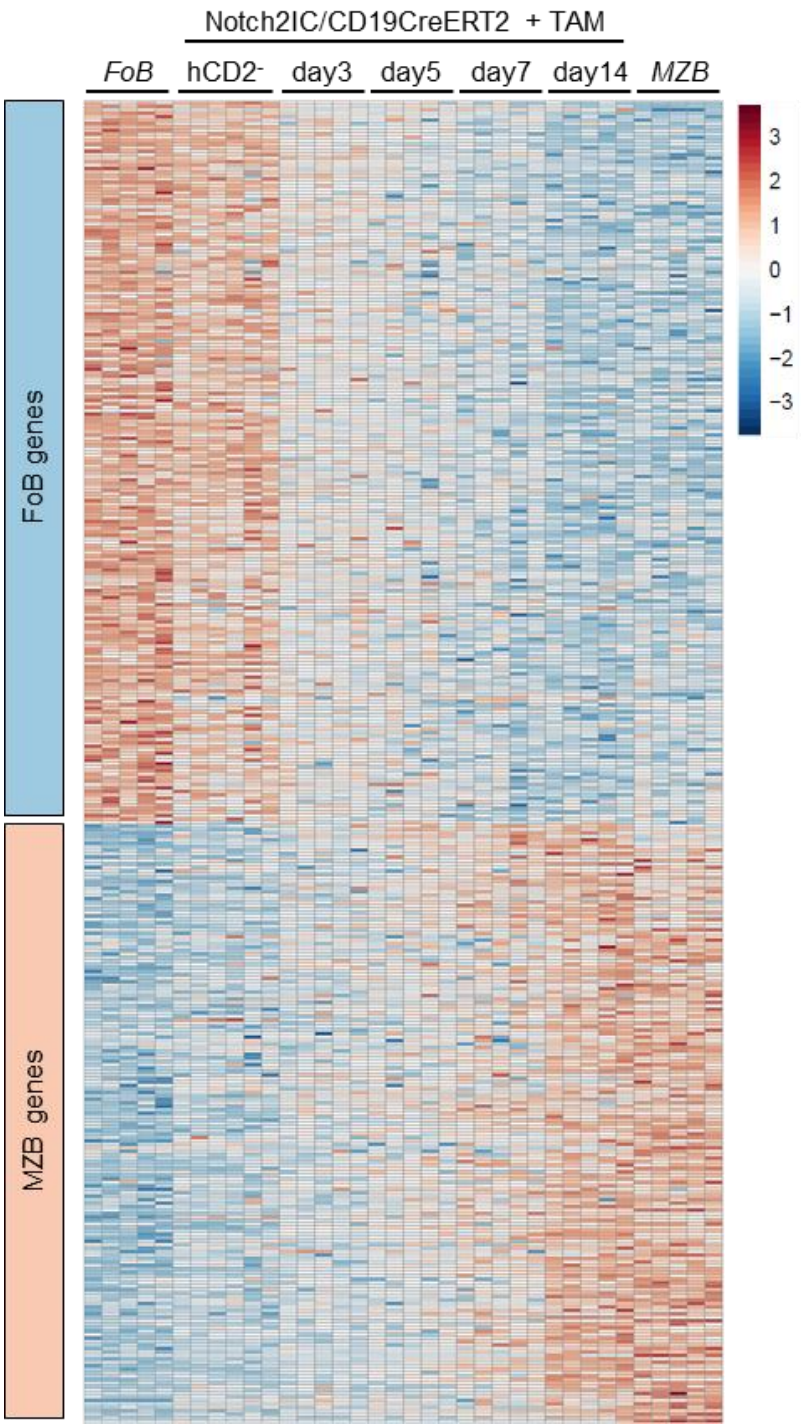

Figure 35: Heatmap of all sequenced samples using the MZB/FoB signature gene sets displays the transcriptomic shift from FoB to MZB signature over time after Notch2IC induction. Sequenced wild type FoB and MZB samples served as controls. $hCD2^+$ cells where sequenced from tamoxifen (TAM)-induced mice at the indicated time points after treatment. $hCD2^-$ cells were also purified from TAM treated animals. The color code legend illustrates relative log2-fold changes normalized across all samples. n=5 samples/group (exception: n=6 for $hCD2^-$). Heatmap data was provided by Dr. Thomas Engleitner, final design by Markus Lechner. Similar figure in Lechner et al. 2021.

3.1.8.3 Transcriptomic changes mediated via Notch2IC induction

A frequently used approach to present the top regulated genes by fold changes and p values was conducted by calculating volcano plots. For this, the most significant differentially expressed genes with a p-value below 0.001 were identified of the sample pairs $hCD2^+$ (day 14 after tamoxifen) versus $hCD2^-$ as well as MZB versus FoB (Figure 36). As many as 732 genes ($hCD2^+$/$hCD2^-$) and 521 (MZB/FoB) fulfilled the cutoff criterium. The volcano plot visualizes the differentially expressed genes by plotting their fold changes against the respective p-values. After labeling the most prominently regulated genes, one can directly determine several genes of interest and possibly identify similarly regulated genes of the two sample pairs. Among the top upregulated genes in both data sets were known Notch2 target genes *Hes1* and *Dtx1* and genes for sphingosine-1-phosphate receptors *S1pr1* and *S1pr3*. On the other side, two of the most prominently downregulated genes were encoding for the surface receptor CD23, *Fcer2a*, as well as for the transcription factor *Klf2*. The function of these genes and many others out of the most significantly regulated genes will be presented and discussed later.

When plotting all regulated genes of $hCD2^{+,}$ day14 versus $hCD2^-$ cells against MZB versus FoB cells by log2-fold changes, an overall correlation of differentially expressed genes through Notch2IC-induction and MZB versus FoB transcriptional profile became visible (Figure 37). Most of the top regulated genes are either co-upregulated (Q1) or co-downregulated (Q3) in MZB versus FoB and $hCD2^+$, day14 versus $hCD2^-$. Some of the strongly regulated genes were additionally marked. From the total of 14450 regulated genes plotted in this figure, only very few popped up to be counter-regulated in Notch2IC-induction in comparison to the MZB versus FoB phenotype. The only gene of interest that is upregulated in wild type MZB cells but significantly downregulated through Notch2IC is *Epcam* (Epithelial cell adhesion molecule). In the opposing quadrant 2, only few genes were upregulated after Notch2IC induction, but downregulated in MZB versus FoB expression data. These genes were either members of immunoglobulin (Ig) identity (*Igl* or *Igk*) or general Ig components (*Jchain*).

Apart from these described outliers, most genes that were up- or downregulated at the endpoint of the Notch2IC mediated trans-differentiation to MZB cells were similarly regulated in wild type MZB versus FoB expression profiles. After a cutoff for differentially expressed genes at +/- 0.5 log2-fold change was applied, the remaining 915 genes strongly correlated in regression analysis,

resulting in diagonal linear fit with a R^2 value of 0.82 (Figure 37, lower plot). The additional calculation of regression statistics showed a p-value of <0.001 (not depicted in the graph). These results provide additional information over GSEA analysis: not only are the same regulated genes from wild type MZB/FoB comparison also found regulated through Notch2IC-expression, but moreover, the most strongly regulated genes show a high correlation in their relative fold changes.

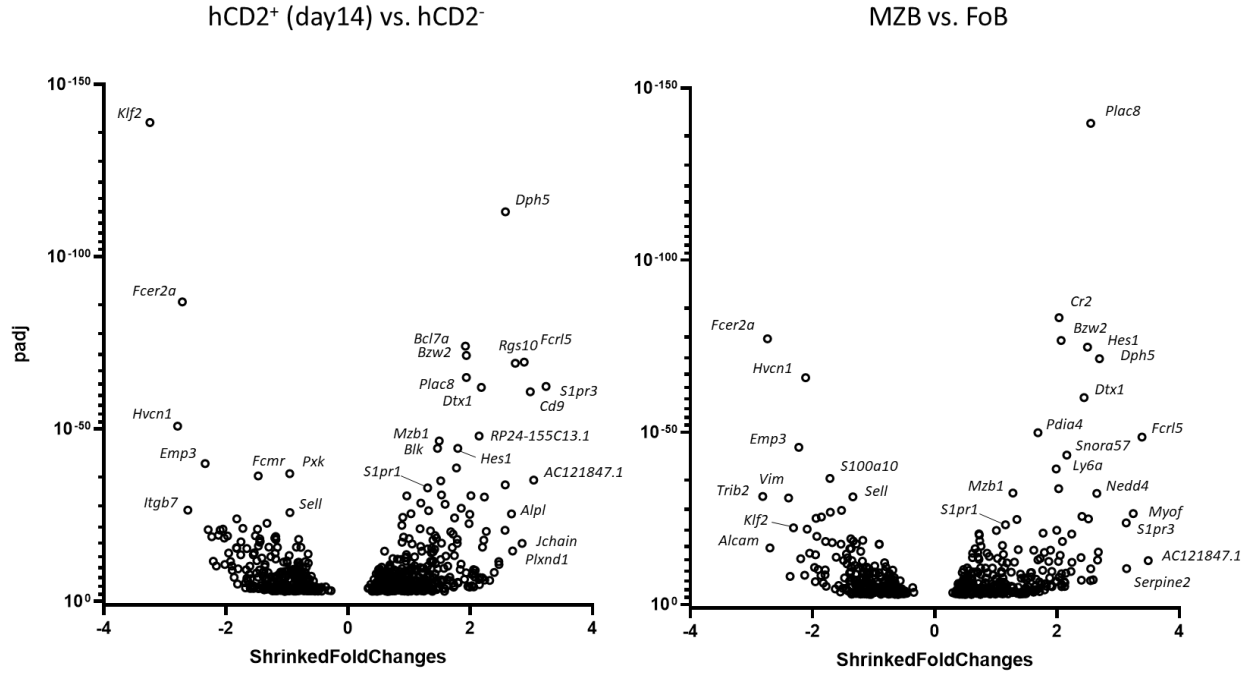

Figure 36: Volcano plots depicting the top differentially regulated genes of time series endpoint cells (hCD2$^+$, day 14 after TAM) versus hCD2$^-$ (left) and wild type MZB versus FoB samples (right). Plotted are log2-fold changes after shrinkage (X-axis) against adjusted p values (padj, Y-axis). A cutoff was set at padj<0.001. 732 genes (hCD2$^+$/hCD2$^-$) or 521 genes (MZB/FoB) fulfilled cutoff criteria. Similar figure in Lechner et al. 2021.

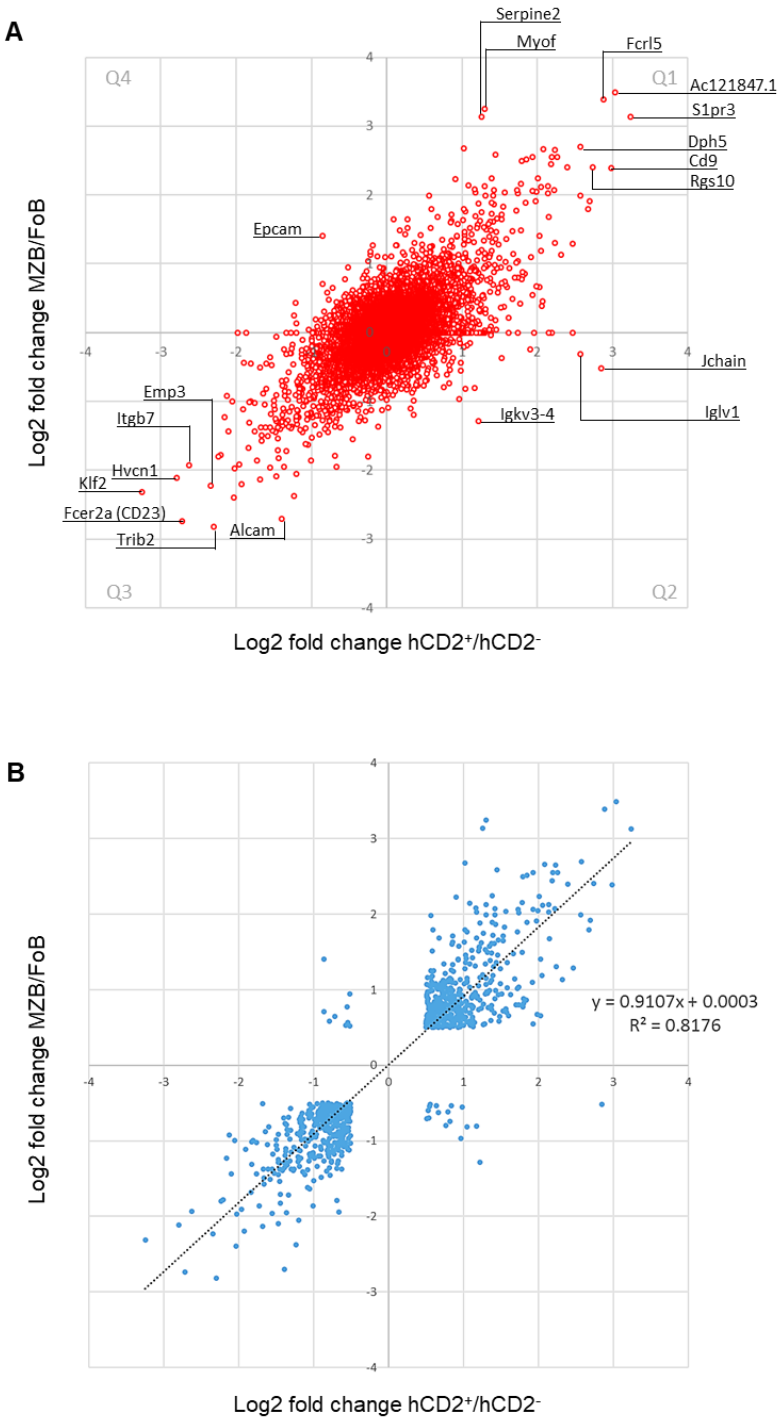

Figure 37: Correlation analysis for all differentially expressed genes of wild type MZB versus FoB cells compared to hCD2$^+$ (day 14 after TAM) versus hCD2$^-$ cells. Top graph: all 14450 genes from differential gene expression profiles are plotted and some top hit genes were additionally labelled. Bottom graph: Cut of at +/- 0.5 log2-fold change was applied for noise reduction. The trend line visualizes a good correlation of differentially regulated genes between wild type MZB/FoB and hCD2$^+$/hCD2$^-$ samples (R^2=0.82, p-value=0). Similar figure in Lechner et al. 2021.

3.1.8.4 Notch2 activation regulated the expression of KLF2 and other transcription factors

As the induction of a single signaling pathway resulted in a plethora of transcriptomic changes, it seemed expectable that other transcription factors (TFs) and epigenetic regulators were activated or repressed after the induction of constitutively active Notch2 signaling. It was indeed found that several known transcription factors and epigenetic modifiers were among the top regulated genes at all time points after induction of Notch2IC expression. Many of the identified relative changes were found to be established directly at the first analysis time point (day 3) of the time series experiment after tamoxifen treatment, suggesting a direct transcriptional regulation via Notch2/RBPj signaling. *Hes1*, *Hes5* and *Bcl7a* were strongly upregulated after the induction of Notch2IC-expression, while *Klf2* was strongly downregulated (Figure 38). Other TFs that were previously described to influence MZB development or homing were found to be downregulated in a less pronounced way: *Irf8* and *Foxo1*. The individual genes of interest will be presented in the following section.

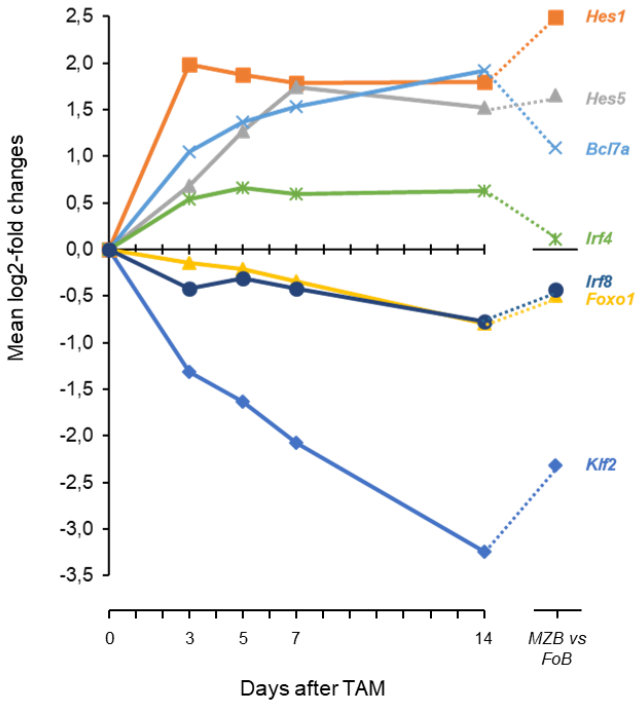

Figure 38: Time series of regulated transcription factors after the induction of Notch2IC expression. Plotted are the mean log2-fold changes of indicated genes against the time axis in days after tamoxifen treatment. Differential gene expression values of the respective genes in wild type MZB versus FoB cells are plotted separately as controls.

The most prominently upregulated TF was the transcriptional repressor *Hes1*. *Hes1* is a known target of Notch activation and RBPj binding (Kageyama and Ohtsuka 1999) and its RNA upregulation is frequently used as a positive marker of active Notch signaling. The direct Notch2 dependency was obvious as relative *Hes1* expression levels reached its maximum at the first analyzed time point after Notch2IC-induction (Figure 38). *Hes5*, the second member of this Notch-targeted TF family (Kageyama, Ohtsuka, and Kobayashi 2007) was also upregulated after Notch2IC expression, but with a delayed kinetic compared to *Hes1*. A regulated gene among the top-3 hits regarding its p-value at all time points was the chromatin modifier *Bcl7a* (Kadoch and Crabtree 2013). Bcl7a could possibly be involved in downstream regulation of gene expression after the onset of Notch2 signaling. The detected downregulation of *Foxo1* was rather weak and only significant at the time point 14 days after tamoxifen. Nevertheless, this factor was included as the role of the TF FOXO1 in B cell biology was subject to many recent high-impact studies (Dominguez-Sola et al. 2015; Inoue et al. 2017; Sander et al. 2015; Lin et al. 2015) and its downregulation matches previous studies on its role in MZB biology (Chen et al. 2010; Dengler et al. 2008). An opposed regulation of the two interferon regulatory factors (IRF) *Irf4* and *Irf8* was found, two TFs that have previously been shown to play roles in MZB versus FoB identity (Simonetti et al. 2013; Feng et al. 2011). When comparing the fold changes between wild type MZB/FoB and day14/hCD2^{-} pairs, it was found that the regulation of all presented TFs was comparable with IRF4 being the only difference: While *Irf4* was directly significantly upregulated through the expression Notch2IC, no changes of *Irf4* mRNA levels were found in wild type MZB versus FoB cells.

The absolute top-regulated gene at all analyzed time points within the Notch2IC time series experiment also belongs to the family of transcription factors: *Klf2* showed the strongest regulation regarding p-value and absolute fold changes. As seen in Figure 38, the strong *Klf2* downregulation after Notch2 induction progressed even further over time. This result was very interesting, as genetic mouse models of KLF2 inactivation alone were found to result in enlargement of the MZB pool and interfering with the regulation of receptors responsible for the regulation of B cell migration (Hart et al. 2011; Winkelmann et al. 2011; Hoek et al. 2010). As the transcriptional modulation of *Klf2* was so prominent and the known genetic downstream effects of a KLF2-knockout resulted in comparable phenotypes to constitutively activated Notch2 signaling (Hart et

al. 2011; Hampel et al. 2011), KLF2 could act as a transcriptionally repressed downstream target of Notch2 activation.

To strengthen this hypothesis, additional GSEA were performed making use of published microarray data by Hart and colleagues (Hart et al. 2011) from KLF2-knockout B cells. In this study, top-differentially expressed genes between wild type B cell subsets (FoB and MZB) and Klf2-deficient FoB cells were identified. After export of those gene names from Supplement Figure 8 of the named publication, two gene sets were defined as "KLF2-KO up" and KLF2-KO down" which were comprised of genes that Hart and colleagues found significantly up- or downregulated in comparison to wild type FoB cells. These gene sets were applied in pre-ranked GSEA on the ranked gene lists from the earliest (day 3) and latest (day 14) time point of differentially expressed genes between $hCD2^{+}$ versus $hCD2^{-}$ cells. It was found that apart from the KLF2-KO up gene set at day 3, all other GSEA results showed highly significant enrichment of KLF2-regulated genes at the top or bottom ends of differentially expressed genes after Notch2IC expression. These results strongly support that *Klf2* downregulation could be one of the key downstream effects of Notch2 activation to regulate that many genes.

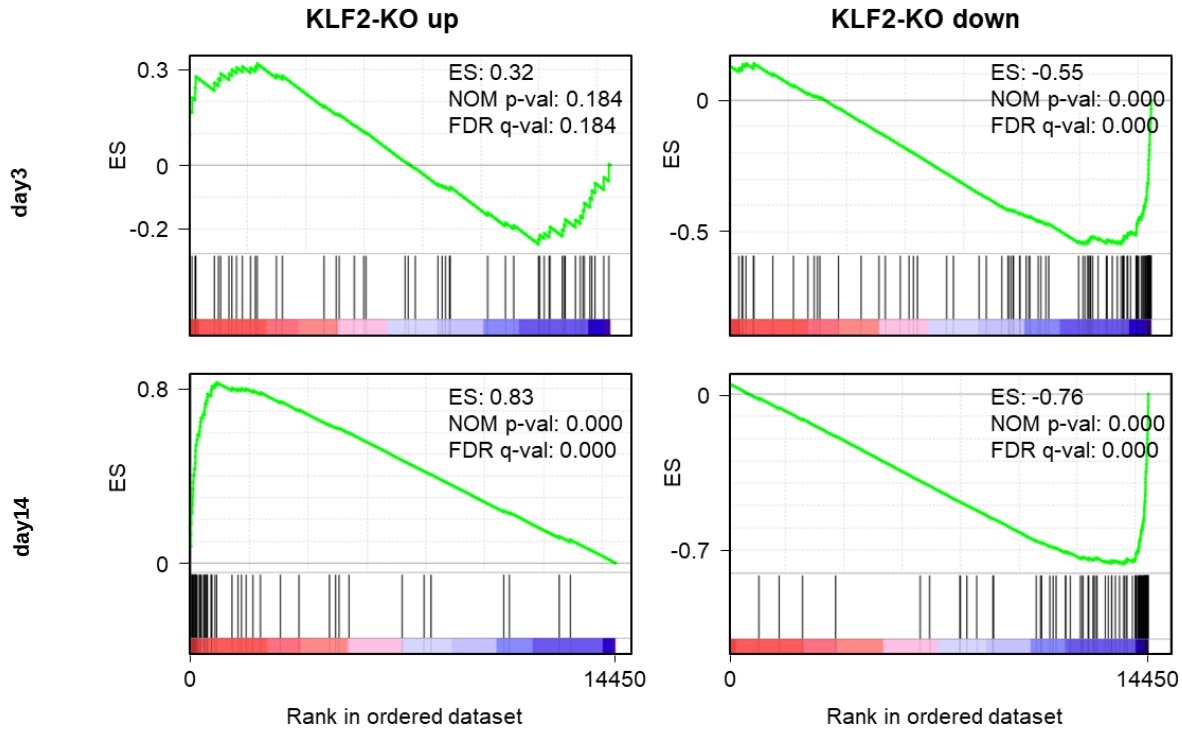

Figure 39: Pre-ranked GSEA analysis results from applying predefined Klf2-knockout target gene sets on the ranked gene lists of the early (day3) and late (day14) time points of the Notch2IC-expression time series experiment. "KLF2-KO up" (62 members) and "KLF2-KO down" (128 members) gene sets were exported from Fig. S8 of Hart and colleagues (Hart et al. 2011). Indicated are the overall enrichment scores (ES), nominal p-values (NOM-p-val.) and false discovery rate (FDR-q-val.). The enrichment of KLF2-KO up at day3 is not significant (p-val > 5%).

3.1.8.5 Notch2 signaling regulates the expression of genes involved in B cell motility and homing

A second functional cluster of genes, which were found to be strongly regulated by the expression of Notch2IC, was comprised of genes responsible for B cell mobility and homing (Figure 40): In this set of genes, two members of the family of Sphingosine-1-phosphate (S1P) receptors were significantly upregulated, namely *S1pr1* and *S1pr3*, while their family member *S1pr4* was downregulated.

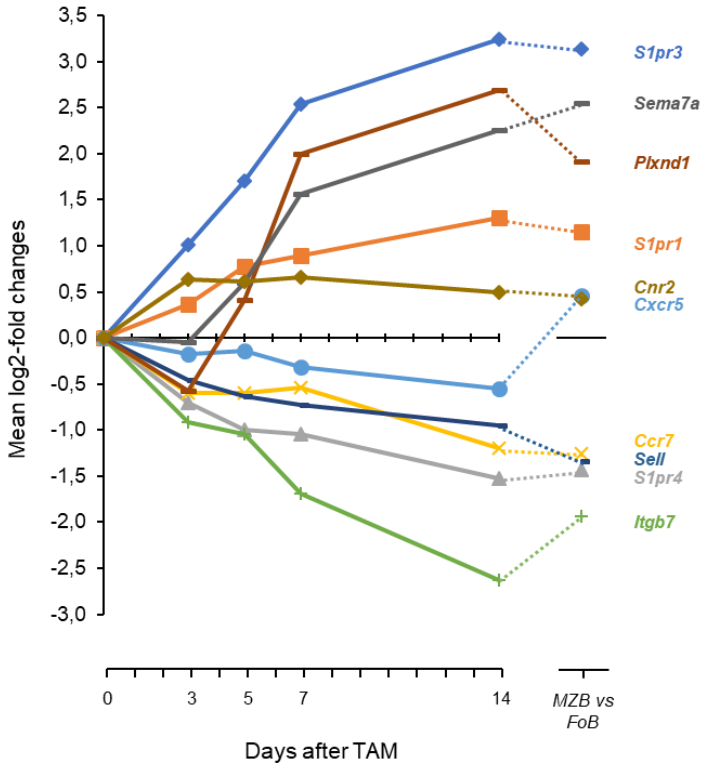

Figure 40: Time series of downstream regulated genes involved in B cell migration and homing after the induction of Notch2IC expression. Plotted are the mean log2-fold changes of indicated genes against the time axis in days after tamoxifen treatment. Differential gene expression values of the respective genes in wild type MZB versus FoB cells are plotted separately as controls.

S1PR1 and S1PR3 are thought to be the key homing receptors for MZB cell homing and their expression forces B cells to migrate along the S1P gradient to the blood-infused and S1P-rich marginal zone (Cinamon et al. 2004; Cyster 2005; Vora et al. 2005; Simmons and Ishii 2014; Cyster and Schwab 2012; Cinamon et al. 2008; Arnon et al. 2011). The progressive increase and final high upregulation of S1PR1 and S1PR3 explain the slow but eventually complete re-localization of $hCD2^{+}$ cells from the S1P-low follicle to the S1P-rich marginal zone (as shown in Figure 23 and Figure 24). Downregulation of the *S1PR4* was also highly significant, yet its role in B cell homing is less studied than the other receptors. S1PR4 is suggested to modulate S1P-mediated chemotaxis in concert with S1PR1 and S1PR2 receptors (Sic et al. 2014).

The third upregulated gene involved in B cell homing was *Plxnd1*. Plexin-D1 is a cell surface receptor for semaphorins, a large family of secreted or membrane-bound glycoproteins that have been implicated in cell migration and regulation of immune responses (Takamatsu and Kumanogoh 2012).

Additional genes of interest, that are known to be involved in B cell migration and homing, were downregulated after the induction of Notch2IC-expression: *Cxcr5*, *Ccr7*, and *Itgb7*.

CXCR5 and CCR7 are both chemokine receptors responsible for binding of CXCL13 and CCL21/CCL19, respectively (Cyster and Schwab 2012; Cyster 2005). These three chemokines are all expressed by lymphoid stromal cells within the splenic follicles, guiding receptor-expressing lymphocytes to the B and T cell zones (Cyster 2010). CXCR5 was additionally required in temporal MZB shuttling to the follicle, in a balanced interplay with the S1P receptors S1PR1 and S1PR3 (Cinamon et al. 2008).

Two additional genes were found to be downregulated, which are suggested to play a role in B cell migration and homing: *Sell* and *Itgb7*. The latter was identified as one of the top-downregulated genes after Notch2IC-expression. It encodes for Integrin-β7, a lymphocyte homing receptor of the integrin family. Nevertheless, Integrin-β7-deficient B cells showed no defects in follicular homing (Cyster, Lu, and Lo 2003). *Sell* encodes for L-Selectin or CD62L, which is a transmembrane glycoprotein and cell adhesion molecule. Both receptors are known to be significantly lower expressed on wild type MZB versus FoB cells and our transcriptome analysis of wild type samples confirmed this. Interestingly, L-Selectin and Integrin-β7 were both found to be downregulated in KLF2-KO FoB cells (Winkelmann et al. 2011; Hart et al. 2011).

To sum up, many of genes involved in B cell migration and homing were regulated in B cells after the onset of Notch2IC expression. These transcriptomic regulations seem to be essential to equip trans-differentiating B cells with a functional tool kit to migrate to and home in the marginal zone.

All results presented in chapter 4.1 merge into the key message, that the activation of Notch2 signaling is sufficient to drive a trans-differentiation program in mature FoB cells to adopt an MZB cell identity. The converted phenotype of FoB cells to MZB cells was confirmed in flow cytometry and in histology, where the proper localization of trans-differentiated cells in the MZ could be shown. *In vitro* and *in vivo* assays were performed to determine the acquisition of MZB cell-specific functional traits. Finally, whole transcriptome sequencing of cells at various stages during 14-day time window of B cell trans-differentiation was crucial to prove this identity conversion also on the level of transcriptomic regulation. Moreover, valuable data could be collected from the RNA sequencing experiment for the identification of possible regulators of the observed B cell trans-differentiation and for a better understanding of the downstream effects of Notch2 signaling in B lymphocytes.

3.2 Plasticity among wild type mature splenic B cell subsets

3.2.1 Transplantation of CD45.1 FoB cells into CD45.2 mice

The results of the previous chapters imply that the potency of a mature FoB cell to adopt the functional phenotype of a MZB cell appears to be cell intrinsic. Nevertheless, the trans-differentiation of mature B cells was shown in a transgenic system utilizing the constitutive activation of a signaling pathway, a process that might not occur physiologically in a similar fashion. The open question remained, whether the aforementioned trans-differentiation could indeed be a physiologically occurring event that was not an artificial product of our Notch2-activating genetic mouse model. We therefore developed a series of transplantation experiments in wild type animals that might help to answer this open question.

To address whether mature FoB cells present the physiological capacity to trans-differentiate into MZB cells, genetically labelled FoB cells were sorted and transferred into congenic recipients to follow up their phenotype over time (day 1, day 4, day 9, day 14). The CD45.1/CD45.2 allele variant model was chosen to differentiate between donor and host cells after transplantation: CD45, also known as protein tyrosine phosphatase receptor type C (PTPRC), Ly5, or LCA (leukocyte common antigen), is a transmembrane protein expressed in various isoforms on all hematopoietic cells (except erythrocytes). While most mice strains – such as the commonly used

C57BL/6 - express the isoform CD45.2 (Ly5.2 historically), some congenic variants express the CD45.1 allele. The CD45.2/CD45.2 system is frequently used in adoptive transfer or mixed bone marrow-chimera experiments for cell identification of donor and recipient cells.

Mature FoB cells ($B220^{+}$ $AA4.1^{-}$ $CD23^{high}$ $CD21^{low}$) from $CD45.1^{+}$ donor mice were FACS-purified (Figure 41, top row). A quality control step was always performed to determine the purity of sorted cell populations (Figure 41, middle and lower row) and confirmed that purity of living FoB cells was always >99%.

$5x10^{6}$ sorted $CD45.1^{+}$ FoB cells were subsequently transferred into CD45.2 recipient mice (2-3 recipient mice per sorted cell batch).

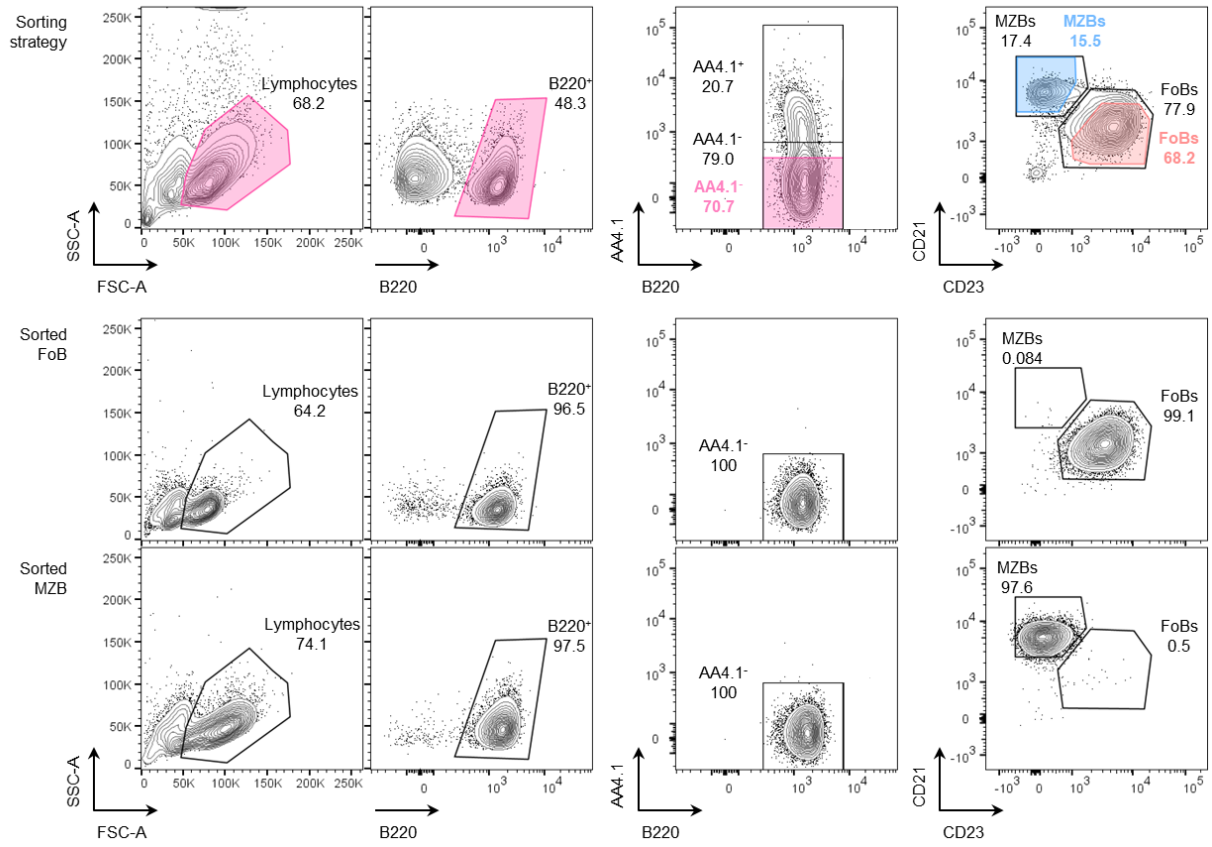

Figure 41: Sorting strategy and purity check of FoB and MZB fractions for adoptive transfer: Splenocytes of 2-4 CD45.1 donor mice were pooled to reduce batch effects and stained with an antibody cocktail to identify and sort $B220^{+}$, $AA4.1^{-}$ mature B cells, subdivided into $CD23^{high}$ $CD21^{low}$ FoB and $CD23^{low}$ $CD21^{high}$ MZB cells. Shaded color gates illustrate the sequential sorting gates, which were set stricter than the analytic gates in black. The corresponding percentages within sorted gates are colored accordingly. Samples from the sorted FoB- and MZB-tubes were recorded directly after sorting process as a re-sort analysis. Similar figure in Lechner et al. 2021.

3.2.2 Phenotyping of follicular B cells over time after adoptive transfer

Engraftment of transferred FoB cells is depicted in Figure 42 as percentage of CD45.1$^+$ cells among total splenic B220$^+$ B cells by separation of CD45.1$^+$ donor from CD45.2$^+$ recipient cells. The number of CD45.1$^+$ cells was comparable at days 1, 4, slightly higher at day 9 and reduced at day 14 after transfer.

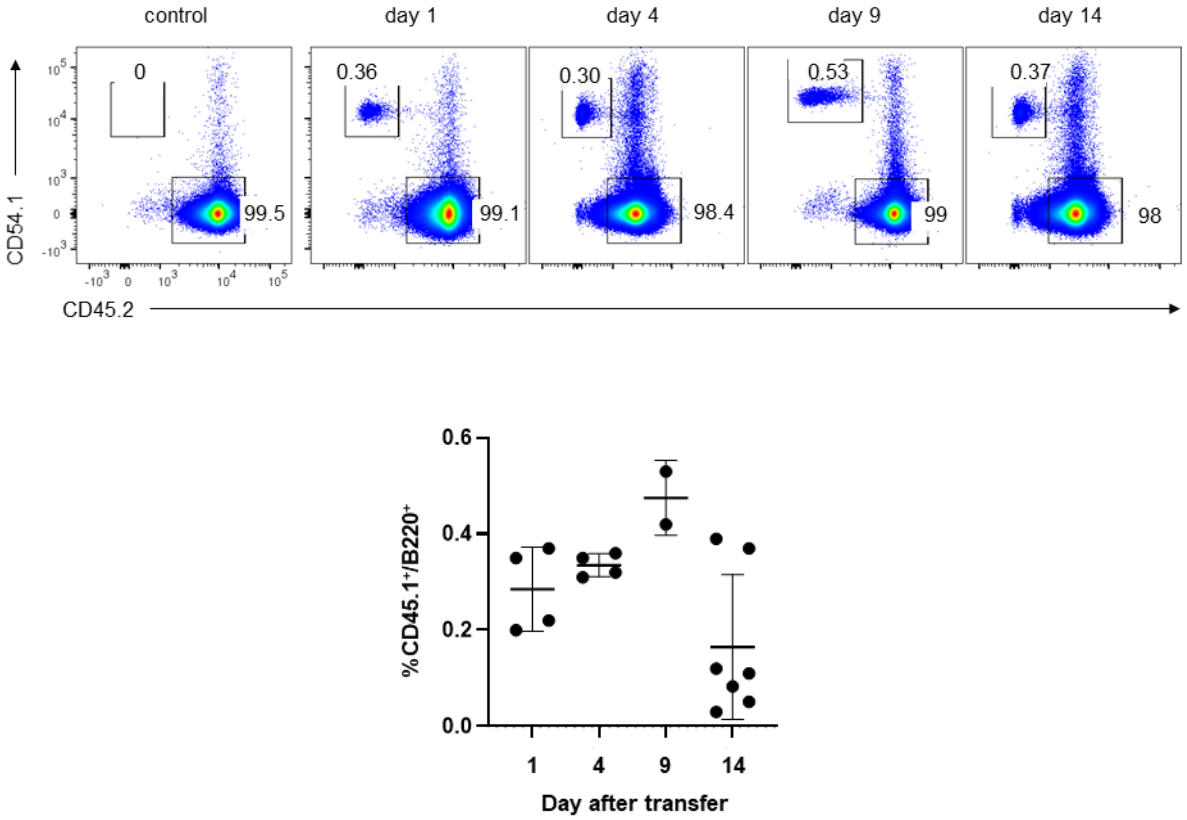

Figure 42: Engraftment efficiency of CD45.1$^+$ donor cells in recipient mice. 5x10^6 CD45.1$^+$ FoB cells were adoptively transferred into CD45.2$^+$ recipient animals. Flow cytometric analysis was performed at the indicated time points after transfer to separate the CD45.1$^+$ donor from CD45.2$^+$ recipient cells. Representative FACS plots are pre-gated on B220$^+$ total B cells and show the separation of CD45.1$^+$ donor cells from CD45.2$^+$ recipient cells. A non-transplanted CD45.2$^+$ control mouse was included to verify the specificity of the anti-CD45.1 antibody staining. The summary below summarizes the percentage of CD45.1$^+$ cells within B220$^+$ splenic B cells. Plotted are all values with means +SD. This staining panel for CD45.1 and CD45.2 was applied on all subsequent flow cytometric analyses. Similar figure in Lechner et al. 2021.

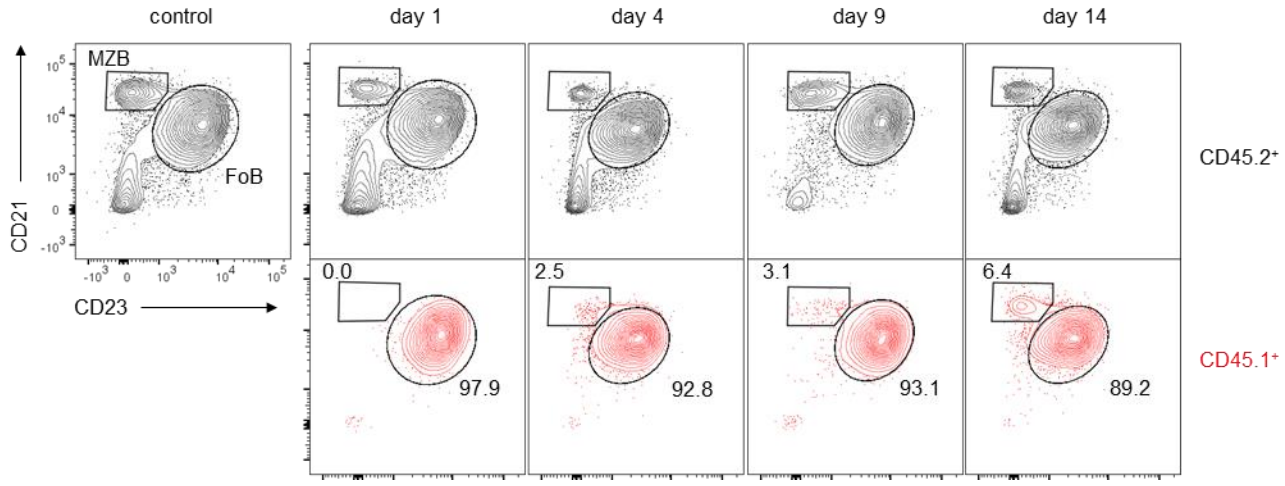

Figure 43: Phenotyping of CD45.1$^+$ cells at indicated time points after adoptive transfer into CD45.2$^+$ congenic recipient mice. MZB/FoB phenotyping based on CD23 and CD21 expression levels was defined in the CD45.2$^+$ population (top row) and applied on the CD45.1$^+$ engrafted cells (bottom row). Numbers in the bottom row indicate the percentages of CD23^{low} CD21^{high} MZB cells and CD23^{high} CD21$^+$ FoB cells among transplanted CD45.1$^+$ cells. All plots were pre-gated on B220$^+$ splenic B cells. Representative data of all experiments summed up in Figure 44. Similar figure in Lechner et al. 2021.

Phenotyping of transplanted FoB cells over time showed that 1 day after transfer, almost all engrafted B cells still had the FoB cell phenotype, but none (0.0%) a MZB cell phenotype. Two weeks after transfer, a subpopulation of cells was clearly identified as mature CD23^{low} CD21^{high} MZB cells (Figure 43) and closely resembled its CD45.2$^+$ counterparts. The intermediate time point of 4 days after transfer showed, that a smaller percentage of cells were located within the MZB gate and seemed to protrude from the FoB gate, with most of the MZB-gated cells still retaining higher levels of CD23 compared to the majority of CD45.2$^+$ MZB cell population. Phenotypic transition of a subset of CD45.1$^+$ cells from FoB to MZB phenotype was consistent in all independent experiments (Figure 44).

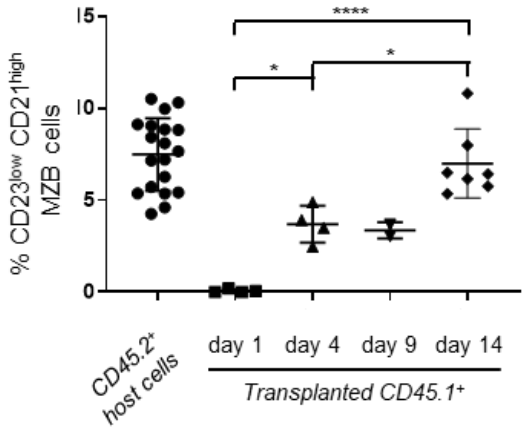

Figure 44: Quantification of cells in the MZB cell gate at the indicated time points after adoptive transfer. CD45.2$^+$ MZB cells (CD23^{low} CD21^{high}) from each recipient mouse are shown as reference. (*p<0.05; ****p<0.0001; one-way ANOVA, multiple comparison test). Similar figure in Lechner et al. 2021.

The finding that a small subfraction of CD45.1$^+$ cells protruded into the MZB gate using the CD23/CD21 staining (Figure 44) was confirmed in a second staining using the known MZB marker CD1d. Gating of CD45.1$^+$ cells for CD21^{high} CD1d^{high} MZB cells (Figure 45, Figure 46) confirmed the previous results.

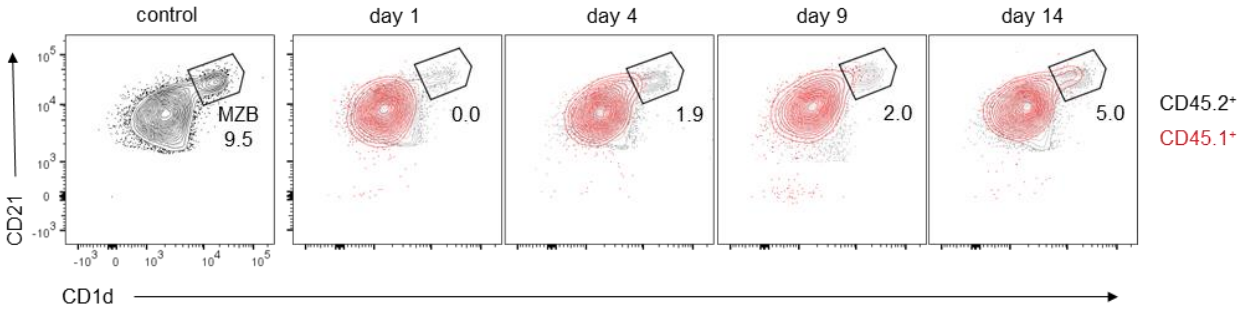

Figure 45: Overlay plot visualizes the trans-differentiation of a CD45.1$^+$ subpopulation over time. CD45.2$^+$ host cells (gray) are overlaid with the respective CD45.1$^+$ transferred cells (red) at the indicated time points after adoptive transfer. Gating visualizes the CD1d^{high}CD21^{high} MZB cells. Numbers refer to percentages of MZB cells in control B cells (left) and in CD45.1$^+$ B cells at days 1 to 14 after transfer. Plots were pre-gated on B220$^+$ B cells and are representative for all experiments summed up in Figure 46. Similar figure in Lechner et al. 2021.

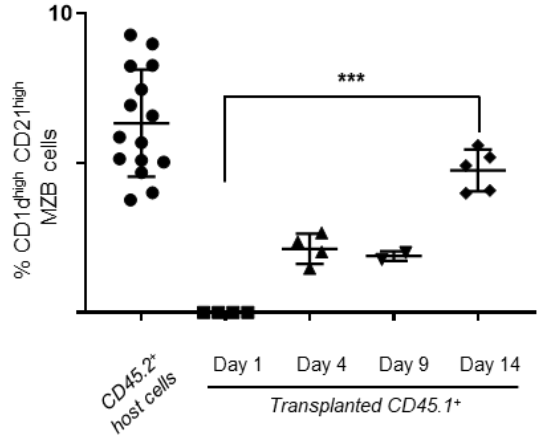

Figure 46: Summary of CD1d^{high}CD21^{high} CD45.1^{+} cells at the indicated time points after adoptive transfer. CD45.2^{+} MZB cells from each recipient mouse are shown as reference. One-way ANOVA did not result in significant p values in multiple comparisons apart from day 14 versus day 1 (***p=0.0002), mainly due to low replicate data points (n=2) for day 9. Similar figure in Lechner et al. 2021.

Interestingly, the time frame of surface protein changes regarding the expression of CD21, CD23 and CD1d very much resembled the previously observed conversion of surface marker expression as shown in the time series experiment (Figure 19) after induction of Notch2IC-expression. Moreover, the early onset of CD21 and delayed upregulation of CD1d and downregulation of CD23 was also reflected on RNA levels of *Cr2* (CD21), *Fcer2a* (CD23) and *Cd1d1* (CD1d). The RNA fold changes over time are depicted in Figure 47.

Taken together, these results show that a subset of mature wild type FoB cells completely trans-differentiated to fully mature MZB cells (regarding all surface markers) within a time window of 14 after adoptive transfer into congenic mice.

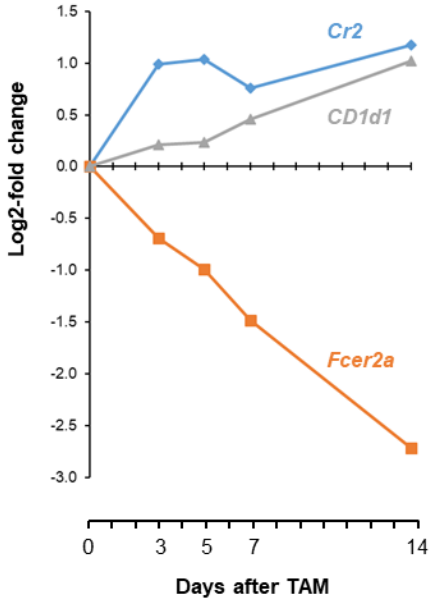

Figure 47: Transcriptomic data of selected FoB versus MZB surface marker gene changes over time after Notch2IC expression. Log2-fold changes at time points 3, 5, 7 and 14 days of $hCD2^+$ versus $hCD2^-$ cells after tamoxifen treatment in Notch2IC/CD19creERT2:hom mice are shown for the genes *Cr2* (CD21), *Fcer2a* (CD23), *Cd1d1* (CD1d).

3.2.3 Identification of an intermediate B cell phenotype

The FoB-to-MZB cell trans-differentiation was shown to be a rather slow process. Over a time frame of two weeks, the expression levels of many surface proteins were altered, with some proteins being regulated rapidly (such as CD21), while others were only found to be sufficiently changed between day 9 and 14 after transfer (CD23, CD1d).

Other groups have tried to identify intermediate B cell subsets somehow in between mature FoB and MZB cells, namely a marginal zone B cell precursor (MZP) phenotype (Zhang, Zhu, et al. 2017; Srivastava, Quinn, et al. 2005; Adori et al. 2018). The function and developmental stage of this subset remains unclear, but most authors claim that MZP cells directly derive from immature transitional B cells and then develop further into fully differentiated MZB cells. Our findings lead us to the hypothesis that maybe these MZP cells might (at least in part) be mature B cells in intermediate phenotypic stages during a transition between FoB and MZB cells.

To see how this MZP cell phenotype might correlate with cell phenotypes during our observed transition phase, we tried to adapt already published staining protocols for MZP cells to the

transplanted CD45.1^{+} cells of the adoptive transfer experiments (Srivastava, Quinn, et al. 2005; Allman and Pillai 2008). First, a subpopulation of IgM^{high}, CD21^{high} B cells was identified within mature B cells (B220^{+}, CD93/AA4^{-}) and then subsequently divided into CD23^{+} MZP and CD23^{low} MZB cells. This gating strategy was implemented on wild type B cell controls, resulting in cell frequencies within the consecutive gating strategy (Figure 48A, left column). When applying the IgM/CD21 gate as identified in the CD45.2^{+} host cells onto the CD45.1^{+} engrafted cells (Figure 48A, right column), it was found almost no cells were present within the IgM/CD21 gate at the first day of analysis after transfer (day 1) and the few cells within the gate were free of mature MZB cells. A comparable separation of MZB/MZP cells was found to be applicable using the mature MZB marker CD1d (Figure 48B).

When analyzing later time points after adoptive transfer of FoB cells, it was found that the population of IgM^{high} CD21^{high} cells expanded over time until CD45.1^{+} and CD45.2^{+} cell frequencies were levelled at day 14 after transfer (Figure 49).

Downstream gating of the IgM^{high} CD21^{high} population in the CD45.1^{+} cells visualized the appearance of larger quantities of MZP cells at day 9 (summarized in histograms in Figure 50). Here, opposed to the wild type situation where MZP cells are only a minor fraction, IgM^{high} CD21^{high} cells were subdivided in half, identifying a appearing wave of large numbers of CD23^{+} MZP cells, while the other half of CD45.1^{+} cells already downregulated CD23 and are therefore considered MZB cells. On day 14 after transfer, the majority of IgM^{high} CD21^{high} cells successfully downregulated CD23 while upregulating CD1d to become MZB cells. The upregulation of CD1d followed similar kinetics when analyzed in parallel but appeared to happen slightly delayed when compared to the downregulation of CD23.

The progressive upregulation of CD1d was better seen when plotting all CD45.1^{+} cells with CD21 against CD1d as previously depicted in Figure 45. Here (Figure 51), a CD21^{high} CD1d^{mid} intermediate population was gated between FoB cells and CD21^{high}CD1d^{high} MZB cells. The quantification of percentages of CD1d^{int} intermediate B confirms an initial wave of differentiation from the FoB phenotype to a IgM^{high} CD21^{high} CD1d^{int} MZP intermediate stage, before cells further upregulate CD1d to eventually become fully differentiated MZB cells (Figure 52).

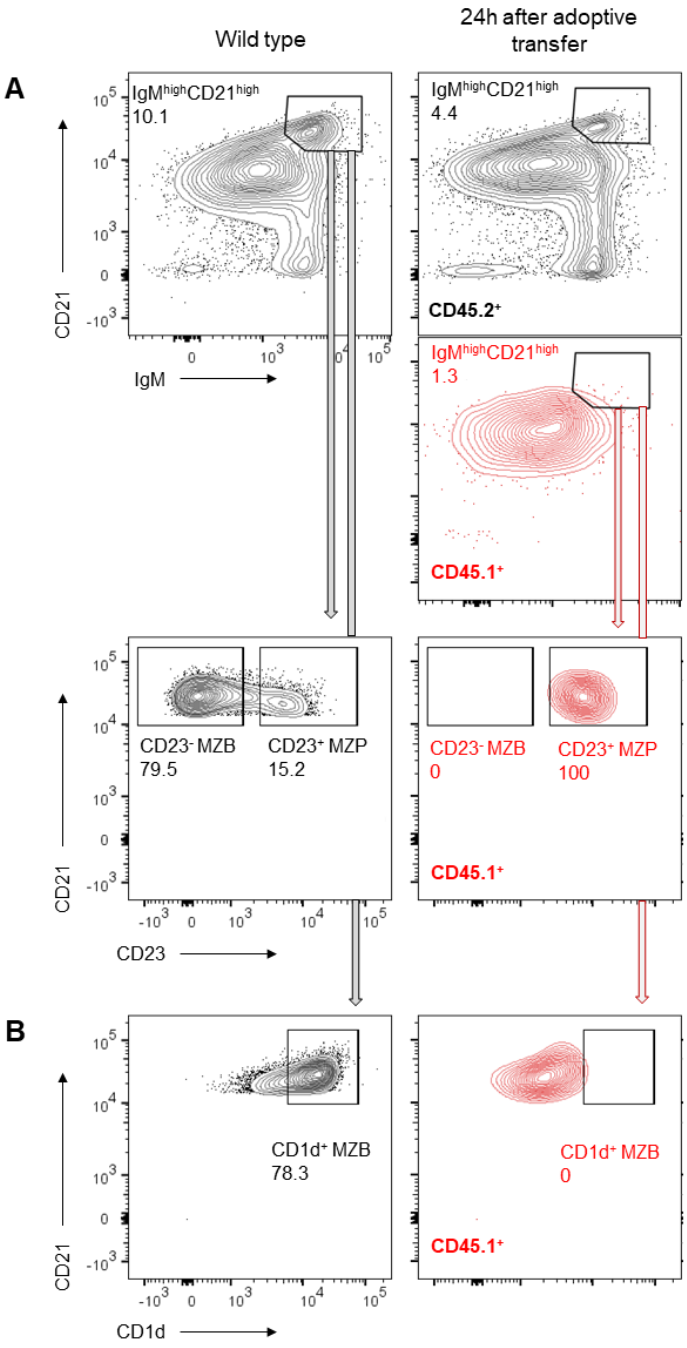

Figure 48: Sequential gating on MZB and MZP cells via a IgM^{high} CD21^{high} cell gate among mature splenic B cells. Wild type B cells were used as a positive control. Plots are sequentially gated as indicated with arrows, starting from splenic B220^{+} B cells in the first row. IgM^{high} CD21^{high} cells comprise MZB and MZP cells that are subdivided in downstream gating. Engrafted CD45.1^{+} cells are shown in red. The IgM^{high} CD21^{high} gate was almost completely absent when gating on recovered CD45.1^{+} cells 24 hours after adoptive transfer of purified FoB cells (second row). Downstream gating on CD23^{-} MZB cells (A) or CD1d^{high} MZB cells (B) revealed similar percentages of mature CD23^{low} CD1d^{high} MZB cells in both gating strategies in control cells while no MZB cells were present 24 hours after transfer among CD45.1^{+} cells. Numbers indicate percentages of cells within the drawn gates. Representative data for four experiments.

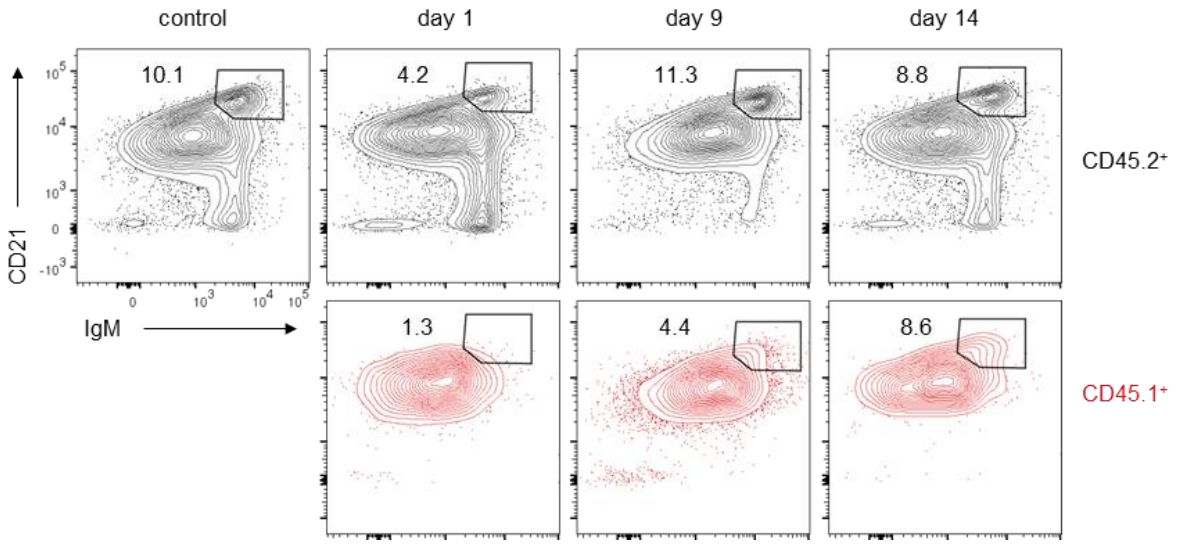

Figure 49: Increase of IgM^{high} CD21^{high} cell percentages among recovered CD45.1^{+} cells after transfer of mature FoB cells. FACS gating on IgM^{high} CD21^{high} cells, comprising MZB and MZP cells, within control B cells (left) and within transplanted CD45.1^{+} FoB cells over time. Plots are pre-gated on B220^{+} B cells and engrafted CD45.1^{+} cells are additionally shown in red (second row). Numbers indicate the percentage of IgM^{high} CD21^{high} cells. Representative data for experiments summarized in Figure 42. Similar figure in Lechner et al. 2021.

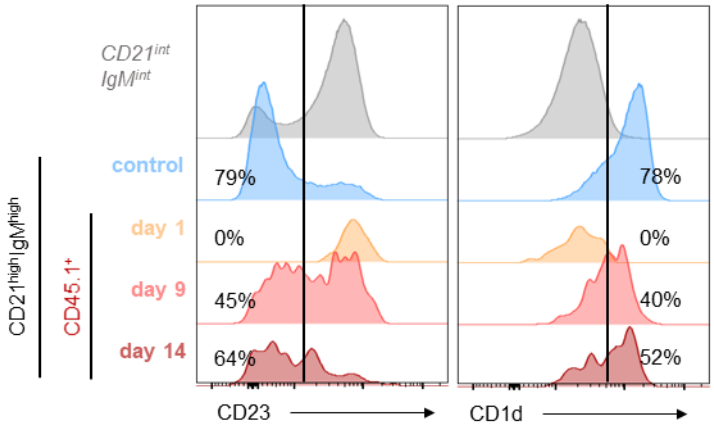

Figure 50: Representative offset histograms summarize the downstream gating of IgM^{high}CD21^{high} cells in transferred CD45.1^{+} cells over time, separating CD23^{-}, CD1d^{high} mature MZB cells from CD23^{+}, CD1d^{int} MZP cells. Depicted histograms were gated according to the gating strategy depicted in Figure 48. Similar figure in Lechner et al. 2021.

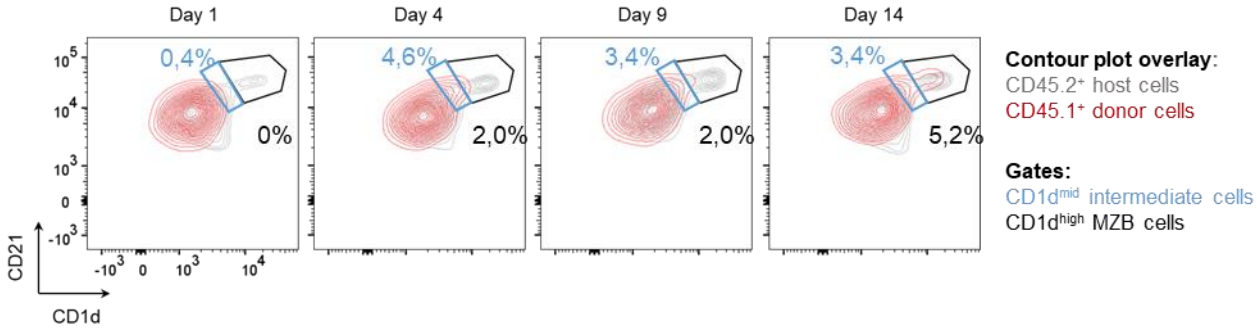

Figure 51: Gating on CD21 and CD1d enables the identification of an intermediate CD1d^{int} population. Overlay of engrafted CD45.1^{+} donor cells (red) over CD45.2^{+} host B cells (gray). Indicated frequencies are median values for the gated populations over all experiments. FACS plots are pre-gated on B220^{+} B cells. Blue gate: CD1d^{mid} intermediate cells, black gate: CD1d^{high} MZB cells. Representative data of experiments summarized in Figure 52.

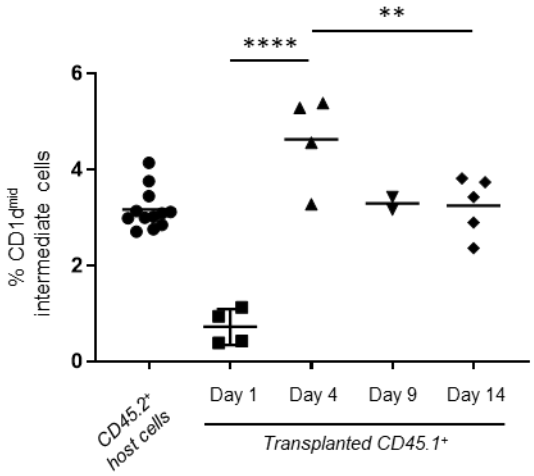

Figure 52: Quantification of CD1d^{int} intermediate MZP cells as gated in Figure 51. **p=0.0095; ****p<0.0001, one-way ANOVA, multiple comparisons. Similar figure in Lechner et al. 2021.

These findings show a more fine-tuned expression pattern of CD1d between FoB, MZP and MZB cells. The intermediate expression level of CD1d was so far not described as an attribute of MZP cells, as they were only described as CD1d^{+} (Wang et al. 2010; Allman and Pillai 2008). We showed before with the inducible Notch2IC system that a high CD1d expression level is only reached at very late stages of MZB differentiation (Figure 47) and it can therefore be beneficial for an additional discrimination of MZP from MZB cells.

3.2.4 Phenotyping of marginal zone B cells after adoptive transfer

For verification of FoB-to-MZB trans-differentiation and exclusion of a possible outgrowth of proliferating MZB cells which might have been transplanted as contamination during FACS sorting, additional adoptive transfer experiments with purified MZB cells were conducted. Two open questions were addressed here: i) Do purified MZB cells show differences in engraftment efficiency or proliferation after transfer? and ii) Are MZB cells also subject to the already described peripheral B cell plasticity? Thus, do transplanted cells lose their MZB identity to become FoB cells?

To answer the first question, MZB cells were purified in parallel to FoB by cell sorting from the same pool of donor splenocytes. Naturally, MZB percentages among splenocytes and the subsequent cell yield after sorting was much lower compared to FoB cells. Therefore, the number of transferred cells was adapted for the MZB experiments. $5x10^6$ purified FoB and $1x10^6$ MZB cells were transferred into recipient sibling mice and analyzed 14 days after transfer. Staining for $CD45.1^+$ engrafted cells showed that while 0.11% $CD45.1^+$ cells were found among B cells after FoB transplantation, 0.022% and 0.023% were found after MZB transfer, thus exactly matching the relative differences in initially transferred cell counts (Figure 53). These results prove that naïve mature MZB cells do not exhibit differences in engraftment efficiency compared to their FoB counterparts or showed spontaneous proliferation after transfer. This finding in turn verifies the above described findings: the consistent MZB population 14 days after FoB transplantation has emerged from trans-differentiated FoB cells and was not the result of sorting impurities and subsequent outgrowth of a small MZB contamination.

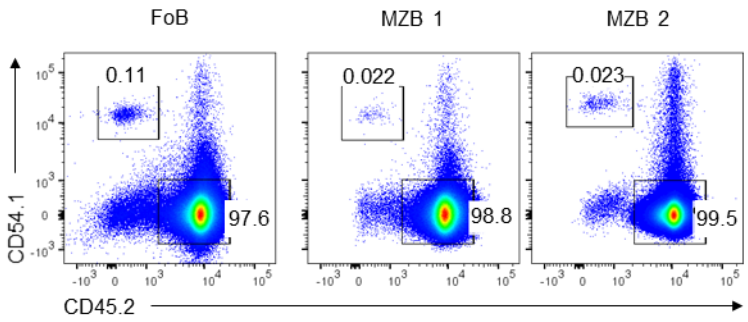

Figure 53: Engraftment efficiencies of purified FoB and MZB cell fractions, 14 days after adoptive transfer. FoB and MZB cells were purified from one cell purification experiment. $5x10^6$ FoB cells and $1x10^6$ MZB cells were transferred. Plots are pre-gated on $B220^+$ B cells. Numbers indicate the gated populations of $CD45.2^+$ host cells and $CD45.1^+$ engrafted FoB and MZB cells. Data show 3 recipient sibling mice transplanted with either FoB cells or MZB cells. Transplanted cells were from pooled purified cell populations, sorted from 3 donor mice in one experiment.

Phenotyping of engrafted MZB cells 14 days after transfer revealed that MZB cells also exhibited a certain degree of plasticity: Around half of the transferred MZB cells lost their $CD23^{low}CD21^{high}CD1d^{high}$ phenotype (Figure 54, Figure 55), but the surface expression levels of CD21 and CD1d remained slightly higher than the host FoB cell compartment. The observed changes in surface phenotype were therefore not characterized as a complete trans-differentiation to FoB identity. Yet, a remarkable proportion of cells undergoing phenotypic changes remains evident and adds further significance to the described model of peripheral B cell plasticity.

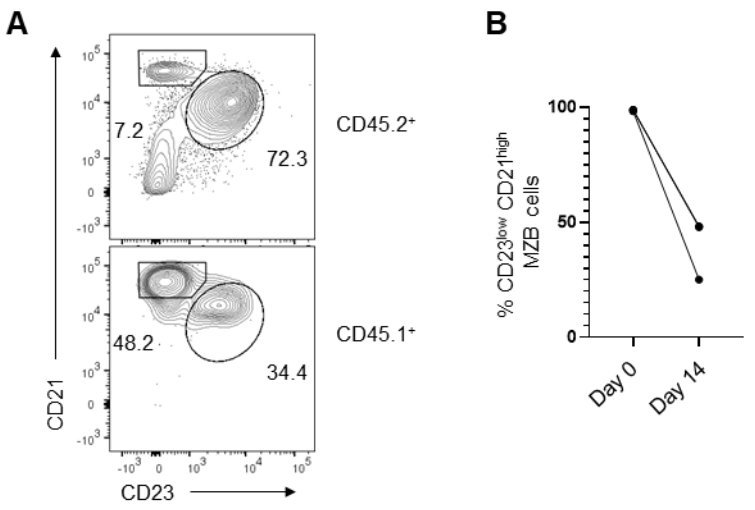

Figure 54: CD45.1$^+$ transferred MZB cells partially lose their CD23^{low}CD21^{high} phenotype 14 days after transfer. (**A**) Representative FACS plots of CD45.2$^+$ host cells and CD45.1$^+$ engrafted splenic cells. Plots are pre-gated on B220$^+$ B cells. Gates and numbers indicate percentages of CD23^{high} CD21$^+$ FoB cells and CD23^{low} CD21^{high} MZB cells among CD45.2$^+$ recipient and CD45.1$^+$ donor cells. Percentages of CD45.1$^+$ cells in the MZB gate from re-sort analysis before transfer (day 0) and at day 14 after transfer are summarized in (B). (n=3 transplanted mice)

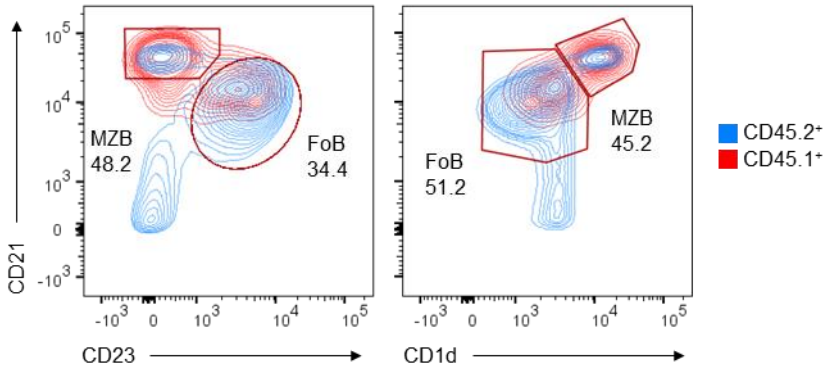

Figure 55: Overlays of CD45.2$^+$ host cells and engrafted CD45.1$^+$ MZB cells visualize the phenotypic drift of transplanted MZB cells into the wild type FoB gates. Overlay plots show B cell phenotypes of donor (red) and recipient B cells (blue) with regard to their expression of CD21 (y-axis) versus CD23 (left) or CD1d (right) to separate CD23^{high} CD21$^+$ CD1d$^+$ FoB cells from CD23^{low} CD21^{high} CD1d^{high} MZB cells. Gating was executed on the donor CD45.2$^+$ population (blue) and applied on the CD45.1$^+$ transplanted cells (red). The depicted gates and frequencies relate to the CD45.1$^+$ cells. Representative data of n=3 transplantation experiments.

These results show that the capacity to convert the functional B cell phenotype seems not to be limited to the FoB-to-MZB transition. Transplantation of MZB cells showed that a subset of engrafted cells lose the expression of typical MZB surface markers and gradually get indistinguishable from FoB cells, indicating a MZB-to-FoB conversion. The data gathered from

adoptive transfer experiments finally prove the hypothesis of a functional plasticity among mature B cell subsets, with identity conversion being a cell-intrinsic mode of action between FoB and MZB cells.

In summary, the adoptive transfer experiments showed for the first time that mature peripheral B cells are equipped with the intrinsic capacity of trans-differentiation. They can become MZB cells, thereby passing through intermediate stages of IgM^{high} $CD21^{high}$ $CD23^{high}$ $CD1d^{int}$ MZP cell identity, even if transferred into the competitive environment of B cell proficient hosts. The trans-differentiation was found to be a rather slow process that was not completed before 9 days after adoptive transfer, thereby following similar kinetics as we found in FoB-to-MZB conversion through induction of Notch2IC-expression. Vice versa, data from transplanted MZB cells hint to a potential MZB-to-FoB conversion, thus further strengthening the hypothesis of peripheral B cell plasticity.

4. Discussion

The cellular mechanisms that affect cell fate decisions during hematopoiesis have been studied extensively. Today we know about the importance of the cellular microenvironment providing specific stimuli and signaling receptor ligation during maturation and differentiation processes. Starting in the bone marrow, the site where hematopoiesis in the postnatal animal roots, cellular signaling pathways have to be activated and repressed, often in concert with others, to provide the basis for the diverse and complex multicellular network of immune cells. At the end of the diverged roads of differentiation, a plethora of different mature immune cells with distinct cellular phenotypes, functions and often specific localization behaviors have been identified in the last decades of immunologic research and our knowledge on lymphocyte diversity is still growing.

The developmental and functional properties of the two mature splenic B cell subsets, follicular B and marginal zone B cells, have been studied extensively in mouse models. The common textbook picture of final B cell differentiation to either FoB or MZB cell identity is drawn as a branching event taking place in immature transitional B cells upon splenic influx. However, several studies have challenged this view of lineage determination and fate decision, thus starting a discussion about peripheral fate decision versus plasticity.

This work adds crucial experimental data collected in transgenic and wild type mouse experiments to strongly support the view of peripheral B cell differentiation as being a dynamic process of functional plasticity between two specialized mature B cell phenotypes. Changes of gene regulation and surface receptor expression within this plasticity are enabling B cells to home at different splenic sites and to execute distinct functional tasks. The results from this work finally prove the B cell-intrinsic capacity of phenotypic and functional transition, driven by the onset of a single cell signaling pathway, Notch2.

4.1 Activation of Notch2 signaling in mature FoB cells is sufficient to drive a complete trans-differentiation to MZB cells

Previous results from several experimental mouse models identified the activation of the Notch2 signaling pathway as one of the crucial events for MZB differentiation (Saito et al. 2003; Kanayama, Cascalho, and Ohmori 2005; Hampel et al. 2011; Oyama et al. 2007; Hozumi et al. 2004). However, the data left some ambiguity about the specific cellular context, where this differentiation process to MZB identity is determined. Others have provided important discussion to a potential plasticity between peripheral B cell subtypes (Allman, Srivastava, and Lindsley 2004; Pillai and Cariappa 2009).

We aimed to finally prove that FoB are capable of a trans-differentiation into MZB cells if they receive an above threshold Notch2 signal. The Notch2IC/CD19CreERT2:hom transgenic mouse model allowed us to guarantee the tamoxifen-triggered induction of Notch2IC expression specifically in mature FoB cells. The simultaneous expression of the hCD2 surface marker enabled the tracking of Notch2IC-expressing cells over time with regard to surface phenotype and splenic localization. With this transgenic system, we were able to finally prove that Notch2 signaling can induce trans-differentiation of FoB cells to MZB cells. The phenotypic conversion was accompanied by a spatial re-localization of Notch2IC-expressing B cells to the marginal zone. The phenotypic conversion and altered B cell homing behavior through the onset of Notch2 signaling was a cell-intrinsic ability that resulted in a rather slow but progressive conversion of one functional B cell subset into another. Two weeks after onset of Notch2IC expression, the vast majority of tamoxifen-responding cells exhibited all characteristics of MZB cells, even in a competitive setting of an already preoccupied MZ microenvironment in CD19-proficient Notch2IC/CD19CreERT2:het mice.

4.2 Advantages of the inducible transgenic mouse model

The inducible Cre system used with the CD19CreERT2:hom mouse showed rather low efficiencies of STOP-cassette deletion after tamoxifen treatment with only around 1% of $B220^+$ splenic B cells successfully expressing hCD2 and Notch2IC, three days after a single tamoxifen treatment. The low efficiency of Cre-activation was beneficial for this study. Although the yield of transgene-expressing B cells was able to be enhanced with repeated doses of tamoxifen, the single dose protocol was strongly preferred for two reasons: First, the availability of the active tamoxifen-metabolite 4-OHT is limited with a serum half-life of around 6 hours (Robinson et al. 1991). The short time window of available 4-OHT after a single tamoxifen dose resulted in a population of cells which have activated the Cre recombinase almost synchronously. This near synchronous activation of Notch2IC expression allowed us to track the $hCD2^+$ cells in narrow time series data points and pinpoint early phenotypic and transcriptomic effects of Notch2IC expression in reporter-positive B cells. Second, the low frequencies of tamoxifen-responding cells led to differentiation of FoB cells to MZB cells with an outcome that vaguely resembled the wild type FoB-to-MZB ratios. This finding was especially appreciated as trans-differentiation to MZB cells resulted in comparable splenic architecture and LPS-responses of Notch2IC-expressing mice 14 days after tamoxifen treatment when compared to controls.

The phenotypic conversion of FoB-to-MZB identity was found to be comparable in Notch2IC/CD19CreERT2:hom and Notch2IC/CD19CreERT2:het mice, suggesting that the process is independent of pre-existing MZB populations or the CD19 signaling pathway.

4.3 The frequency of Notch2IC-expressing B cells over time

With the knowledge on limited availability of 4-OHT after a single tamoxifen dose in mind, the finding of increasing frequencies of $hCD2^+$ splenic B cells within the first two weeks after tamoxifen treatment can be attributed to proliferation of initially recombined B cells. This additionally affirms the acquired data from the BrdU-incorporation experiment, showing that Notch2IC-expressing B cells but not CAR-expressing B cells proliferated within the first week after tamoxifen treatment. Hampel et al. (2011) showed that the expression of Notch2IC in B cells

upregulated protein levels of c-Myc, a known driver of proliferation. mRNA levels of *myc* were also found to be upregulated in our RNA Seq data by factor 2 at day 14 versus day 0 after tamoxifen treatment. This might indicate a role of Myc in physiological MZB differentiation and proliferation. Moreover, influx and splenic homing of $hCD2^+$ B cells from other peripheral sites is very probable, as the initially detected $hCD2^+$ cells in lymph nodes, peritoneal cavity and bone marrow were absent two weeks after tamoxifen treatment. Notch2IC-expression may direct B cells to the splenic marginal zone by upregulation of homing genes such as S1P receptors.

The percentages of $hCD2^+$ B cells after a single dose of tamoxifen showed large variances, especially when analyzing the later time points day 14 and day 30. One reason for this are differences in tamoxifen concentration per mouse. The route of administration – oral gavage – is subject to deviations regarding the administered amount and proper uptake of the applied tamoxifen. We found that the standard deviations of percentages of $hCD2^+$ B cells further increased over time. This could be caused by the individual mouse-specific immune system and its activation status, thus influencing overall B cell activation and proliferation of B cell subsets. After the initial proliferation of $hCD2^+$ B cells and without an endogenous supply of MZB differentiation from transitional or FoB cells, the percentage of $hCD2^+$ B cells will naturally decline in this system.

Moreover, our data showed that the expression of Notch2IC initiated proliferation in B cells, most likely due to the adoption of a MZB cell phenotype, as earlier findings stated a self-renewal of MZB cells (Martin and Kearney 2002). The current knowledge on naïve B cell half-life states around 90-130 days for FoB cells and at least 150 days for MZB cells (Hao and Rajewsky 2001; Jones, Wilmore, and Allman 2015). Hao and Rajewsky postulated that MZB cells show an unlimited life span in their experimental setting of conditional *RAG2*-knockout. Using this, they observed a decline in FoB numbers while MZB numbers stayed relatively constant. With our here presented knowledge, it seems very likely that the remaining FoB cells constantly trans-differentiated into the MZB pool as soon as the niche for Notch2-driven identity conversion was available.

The gradual loss of reporter-positive cells following the peak two weeks after tamoxifen treatment was clearly faster than the published turnover rates of naïve B cells and could be attributed to a

limited life span of Notch2IC-expressing cells. The constitutive activation of Notch2 signaling in trans-differentiated MZB cells might have increased the terminal differentiation into short-lived plasmablasts. What is more, constant Notch2IC expression might lead to enhanced apoptosis. Data from a previous publication from our laboratory suggested increased apoptosis in NotchIC-expressing cells (Kohlhof et al. 2009). Overall, MZB cells expressing Notch2IC and lacking CD19 can not be compared to wild type MZB cells with regard to their half-life.

4.4 Acquired functional traits of trans-differentiated MZB cells

The functional differences between mature FoB and MZB cells have been presented in many studies and reviews (Oliver et al. 1997; Martin, Oliver, and Kearney 2001; Cerutti, Cols, and Puga 2013; Fairfax et al. 2008; Rubtsov et al. 2008). One feature of MZB cells is their rapid TLR4-mediated response to the bacterial cell wall component LPS in vitro and in vivo, while FoB cells are known to also respond to LPS in vitro, but typically exhibit a delayed and less pronounced blasting behavior (Martin, Oliver, and Kearney 2001; Martin and Kearney 2002). This functional difference between FoB and MZB cells upon stimulation with LPS in vitro was first described by Oliver e*t al* (Oliver, Martin, and Kearney 1999). We used this increased LPS sensitivity of MZB cells as a readout to study the functionality of trans-differentiated Notch2IC MZB cells. LPS stimulation for 48 hours in vitro triggered proliferation and plasmablast differentiation in purified B cells of Notch2IC/CD19CreERT2:hom only after tamoxifen treatment, thereby proving that plasmablast differentiation was exclusive to trans-differentiated $hCD2^+$ MZB cells.

Similarly, in vivo a blasting response after LPS immunization was clearly detectable in control animals while being completely absent in CD19-deficient negative controls. Again, trans-differentiated MZB cells in tamoxifen-treated Notch2IC/CD19CreERT2:hom animals fully rescued the defect of rapid blasting response to LPS.

In summary, coherent data was gained from in vitro and in vivo experiments, confirming that the reconstituted Notch2IC-expressing MZB cells fully adopted the MZB-specific rapid response to LPS treatment as shown in literature (Cerutti, Cols, and Puga 2013; Ramstead et al. 2016).

4.5 Transcriptomic regulation of identity conversion and MZB differentiation

Whole transcriptome RNA sequencing (RNA Seq) was identified as an essential pillar in this study. To do this, a comprehensive experimental plan was set up in collaboration with the group of Prof. Dr. Roland Rad from the TranslaTUM in Munich. We aimed to analyze the transcriptomes of highly purified B cell samples in a narrow time course after tamoxifen treatment until 14 days after tamoxifen treatment. The previous findings from flow cytometric analyses and histology strongly suggested a phenotypic and functional trans-differentiation of FoB to MZB cells within this period of time.

The RNA Seq should answer two major questions: Is the trans-differentiation of mature FoB cells to fully functional MZB cells also reflected in a transcriptomic shift when compared to wild type FoB and MZB samples as reference transcriptomes? Additionally, can so far unknown genes be identified that might play a role in MZB differentiation or/and are mediated by Notch2 signaling?

4.5.2 The transcriptomic shift and the influence of CD19 deficiency

The MDS plot as an initial readout functions as an unbiased description of overall transcriptomic relationships between samples. This method already showed a good clustering of the individual data points within one sample group. Moreover, clear and consistent separation of sample clusters from each other was found. The overall shift of global transcriptomic distance within the Notch2IC expression time series from $hCD2^-$ cells to the cell cluster 14 days after treatment nicely resembles the distance between wild type FoB and MZB control samples.

For a better visualization of this, vectors X and X' were added. The equality in vector length and direction in the MDS plot can be an indicator for shared transcriptomic differences between the two compared cluster pairs of FoB/MZB and $hCD2^-$/ $hCD2^+$ (day 14). The basic offset Y = Y' between wild type control groups and Notch2IC/CD19CreERT2:hom samples showed to be unchanged throughout the gene induction time series. This finding indicated that this basic transcriptomic difference between the two mouse strains did not interfere with the identity conversion from FoB-like $hCD2^-$ cells to MZB-like $hCD2^+$ (day 14) cells.

The origin of this basic transcriptomic offset Y could be explained with the fact that two different mouse strains were being compared in this analysis. First, established inbred mouse strains are known to entail certain degrees of interstrain variability on transcriptomic level (Turk et al. 2004; Mostafavi et al. 2014). Second, and probably of more weight in this discussion, all cells from Notch2IC/CD19CreERT2:hom mice used for this experiment harbor a CD19-knockout, while the control MZB and FoB cells have intact *Cd19* alleles. As CD19 is involved in BCR signaling and therefore is part of a gene regulatory network, a deletion of CD19 very likely influences the expression of a variety of genes.

Apart from the visibly striking offset of all Notch2IC/CD19CreERT2:hom cells from controls the Notch2IC-expressing FoB cells clearly shifted their transcriptome from a FoB-like to a MZB-like phenotype. The CD19-deficient background was used to be able to track the newly formed MZB cells in the absence of a pre-existing MZB cell pool. In earlier experiments, our laboratory could show that MZB cells are comparably generated in the presence or absence of CD19 in transgenic mice expressing Notch2IC dependent on CD19Cre (Hampel et al. 2011). This finding is in accord with the results presented here, showing that the kinetic of MZB cell generation and numbers of newly generated MZB cells are comparable in Notch2IC/CD19CreERT2:hom and Notch2IC/CD19CreERT2:het mice. Together, these findings exclude that the CD19-deficiency had any effect on the generation of MZB cells after the induction of Notch2IC expression.

This observed transcriptomic shift in MDS was calculated in an unbiased whole-transcriptome approach, in which the regulation of individual signature genes of the respective target populations was not described. To specify the adoption of a MZB-like transcriptome, cell-specific gene sets were designed for FoB and MZB cells to be able to verify the transcriptomic shift by looking at the regulation of know identity (or “signature”) genes using GSEA. The results of the GSEA showed the strong increase in the enrichment of MZB-specific genes amongst the top-upregulated genes over a time course of two weeks, while the FoB-specific genes were progressively ranked amongst the strongest downregulated genes. The results were of striking statistical significance and successfully proved the adoption of a complete MZB-like transcriptomic profile, independent of a CD19 expression.

4.5.3 Notch2-mediated target gene regulation and indications of a Notch2-KLF2 gene regulation axis

A deeper analysis of the individually top-regulated genes after induction of Notch2IC expression should help to identify the regulatory and functional network of target genes, which execute the phenotypic changes in hCD2^{+} B cells over time.

The analysis of the individual top-regulated target genes of activated Notch2 signaling in follicular B cells revealed that many known and expected MZB or FoB signature genes were found. This again proved the complete shift of cellular identity. When comparing hCD2^{+} cells 14 days after tamoxifen treatment versus hCD2^{-} cells and wild type MZB versus FoB cells, most of the top-regulated genes were regulated uniformly in both comparisons. Many of those genes such as *Fcer2a, S1pr1, S1pr3, Fcrl5, Dph5, Plac8, Emp3, Hvcn1, Rgs10* or *Klf2* were contained in the signature gene sets used for the GSEA and were also described in various recent publications analyzing MZB transcriptomic data (Mabbott and Gray 2014; Newman et al. 2017; Kleiman et al. 2015). As described in the result section, many of the top-regulated genes such as genes encoding for the S1P receptors are known regulators of MZB cell migration and homing and therefore help in understanding the transcriptomic basis of the observed phenotypic alterations. The great correlation of co-regulated genes between trans-differentiated and wild type MZB versus FoB cells strongly supports the argument that we are looking at a physiologically occurring process and that our genetic system of Notch2 activation does not result in an artificially dysregulated (over-) expression of target genes.

However, some genes were significantly up- or downregulated in only one of the two comparisons and have not been associated with MZB biology so far. *Epcam* was found to be upregulated in control MZB versus FoB cells and downregulated in hCD2^{+} versus hCD2^{-} cells. A specific function of Epcam in lymphocytes or even B cells has not been published, while preliminary results from our lab showed a trend of higher Epcam expression on plasmablasts and plasma cells when compared to naïve B cells. A direct regulatory network involving Notch2 signaling in Epcam regulation remains elusive, but the above discussed possibility of Notch2IC-driven enhanced plasmablast differentiation could link both findings. On the other side, several genes involved in Immunoglobulin production such as *Igkv3-4, Iglv1* and *Jchain* were only found upregulated in hCD2^{+} versus hCD2^{-} cells and not in wild type MZB versus FoB cells. Although the sorting step

for $B220^+$ $hCD2^+$ cells for the RNA sequencing was set up to only include naïve B cells, a minor contamination of a small population of B220-positive, early plasmablasts cannot be fully excluded and as again, this finding indicates that the expression of Notch2IC might additionally prime $hCD2^+$ MZB cells for plasmablast differentiation. A small number of Ig-producing early plasmablast cells may therefore account for the upregulation of this group of genes.

The gene that was subject to the biggest differential regulation after the onset of Notch2 signaling in both p-value and relative expression level was *Klf2*. This finding was very interesting, as previously published mouse models suggest that a constitutive activation of Notch2 signaling results in comparable phenotypes as a knockout of KLF2 (Winkelmann et al. 2014; Hart et al. 2011; Winkelmann et al. 2011; Hampel et al. 2011). A direct regulation of KLF2 expression via Notch2 signaling has not been shown so far, but the idea of a direct repression of *Klf2* through Notch2 seems very likely. Some authors have described potential crosstalk between NOTCH and KLF signaling components (Zheng et al. 2009), but a regulatory network is missing. GSEA performed with a KLF2 signature gene set support the idea that a plethora of transcriptomic alterations detected after Notch2 activation were mediated through the repression of KLF2. Amongst the genes that were found co-regulated in a similar fashion by both Notch2 activation and KLF2-knockout were many of the known B cell homing and cell trafficking genes such as *S1pr3*, *Ccr5*, *S1pr4*, *Sema7a*, *Itgb7* and *Sell*. Thus, many of the phenotypic effects of Notch2 activation on B cell identity and location could mechanistically be executed by the downregulation of KLF2 as a major transcription factor.

Interestingly a study of Hart and colleagues (Hart et al. 2011) showed only few genes that did not resemble a MZB-like upregulation after KLF2 knockout in FoB cells, but were rather slightly downregulated compared to control FoB cells. Amongst these were the two best-known Notch2 target genes *Hes1* and *Dtx1*. This very interesting finding presumably excludes a reciprocal regulation of KLF2 inactivation and Notch2 activation in B cells. The comparison of our results to those of Hart and colleagues strengthened our hypothesis of gene regulation after Notch2 activation through the downstream suppression of KLF2.

Summing up, the deeper analysis of the transcriptional alterations induced by Notch2IC induction helped in understanding the regulation of gene expression that finally induces the transition of

FoB to MZB cells. Moreover, a regulatory network was drawn with the suppression of KLF2 expression through Notch2 signaling. This strong downregulation of *Klf2* in turn could be the key event in the transcriptomic regulation of a larger group of genes involved in B cell migration and homing downstream of Notch2 activation.

Although MZB identity and lineage progression in humans is not clearly understood so far, very recent publications discuss comparable roles of Notch2 signaling and KLF2 repression in MZB cell differentiation in humans (Tull et al. 2021; Kibler et al. 2021). This is important in the understanding of tumorigenesis, as loss-of-function mutations in *KLF2* along with *NOTCH2* mutations that increase the intracellular signaling domain are the most commonly found mutations in human MZB cell lymphoma (Campos-Martin et al. 2017).

4.6 B cell plasticity among mature splenic B cell subsets

The last set of transplantation experiments was conducted to answer the question whether the observed trans-differentiation can also physiologically occur in a non-transgenic setting. Overall, the transplantation experiments presented in section 4.2 resulted in highly reproducible data showing that mature FoB cells indeed are capable of trans-differentiation to MZB cells and vice versa in a time window of around two weeks.

Although the percentage of engrafted $CD45.1^{+}$ cells amongst $B220^{+}$ splenic B cells varied especially at the later time points of the experiment, phenotypic analysis of $CD45.1^{+}$ cells were very similar and confirmed the differentiation of a consistent subset of transplanted FoB cells into bona fide $CD23^{low}$ $CD21^{high}$ $CD1d^{high}$ MZB cells.

4.6.1 The concern of an outgrowth of a contaminated cell population

A stringent cell sorting strategy was developed to exclude the contamination of transplanted FoB cells with immature B or MZB cells. With an observed contamination of below 0.1% MZB cells amongst transplanted FoB cells, there still was the possibility that the newly generated MZB cells originated from a low number of erroneously transplanted MZB cells. However, it is very unlikely

that the differentiation of MZB cells after FoB cell transplantation is due to the outgrowth of contaminating MZB cells as outlined below.

First, overall engraftment efficiency of transplanted B cells was found to be very poor. 24 hours after transplantation only around 0.3% of splenic B cells were CD45.1-positive. The amount of transplanted cells ($5x10^6$) was very high in comparison to the estimated number of splenic host B cells of around $1\text{-}3x10^7$ cells. With this in mind, a rough estimation of only 30.000-90.000 $CD45.1^+$ cells were located in the host spleen which corresponds to only 0.6% - 1.8% of transplanted cells. If engraftment of MZB and FoB cells would be comparable, this game of numbers would cut down the number of possibly engrafted $CD45.1^+$ MZB cells to an almost imperceptible number of 30-90. Outgrowth of a population this small of erroneously co-transplanted MZB cells to around 4% of splenic B cells at day 4 would only be possible if engrafted MZB cells would proliferate at unrealistically high division rates.

Secondly, and more important, phenotyping of $CD45.1^+$ cells at different time points after engraftment showed that virtually no MZB cells were detected 24 hours after transplantation. Of course, not all splenic cells were analyzed in this flow cytometry experiments, but data were consistent and proved that the development of MZB cells occurs through an intermediate precursor state and not by the outgrowth of a pre-existing MZB population.

Lastly, transplantation of purified MZB cells showed that the percentage of engrafted MZB cells 14 days after transfer was indeed comparable to that of FoB cells, thus showing that engrafted MZB cells were not subject to a rapid expansion after transfer.

These points all add up to the statement that an outgrowth of a contaminated population of MZB cells can definitely be excluded as the source of an emerging MZB population after transfer of purified FoB cells.

4.6.2 Intermediate phenotypes and a theory of cell selection for trans-differentiation

Section 4.2.3 describes the identification of intermediate B cell phenotypes that were found during the process of FoB-to-MZB trans-differentiation. The upregulation of the MZB marker CD1d occurred only at the later stages of identity conversion, whereas the upregulation of IgM and CD21

were rather fast. The here described IgM^{high} CD21^{high} CD1d^{int} cells resemble an already described marginal zone B cell precursor (MZP) phenotype (Srivastava, Quinn, et al. 2005; Zhang, Zhu, et al. 2017; Wang et al. 2010). Adding some complexity to the description of intermediate B cell populations, so-called FoB-II cells were discussed by Cariappa and colleagues (Cariappa et al. 2007).

As this work finally proves, MZB cells can also develop directly from FoB cells and it is therefore of great interest to study the question of how cells and which subset of FoB cells are selected for the process of trans-differentiation. Of note, the experimental data provided here do not challenge or replace the "traditional" view of MZB development from transitional B cell precursors. The results from transplantation experiments showed that only a small but stable proportion of engrafted cells was subject to MZB differentiation. This work and previous data from our lab identified activation of Notch2 signaling as the determining force to drive MZB differentiation (Hampel et al. 2011). Interestingly, Liu and colleagues provided evidence that a stronger initiation of Notch2 signaling activity occurs in a subset of FoB cells compared to the bulk of immature T2 cells (Liu et al. 2015). If this Notch2 activation would serve as a threshold signal to initiate MZB differentiation, this piece of data from Liu et al would nicely merge with our findings of FoB-to-MZB conversion via activation of Notch2 in a subset of FoB cells.

MZP cells (and CD21^{high} FoB-II cells) were described to derive from transitional T1 and T2 B cells (Loder et al., 1999, Srivastava et al., 2005; Kleiman et al., 2015). Combining these findings, the feeding into the MZB-precursor cell pool is probably a shared trait of transitional B cells and a subset of mature FoB cells. The physiological balance of T2 or FoB precursor differentiation is very likely a multifactorial interplay of availability and competition between FoB and T2 cells for Notch2 receptor activation in the spleen and the overall systemic immunological status of the animal. The latter can dramatically influence the production of bone marrow precursors and influx into the spleen on the one hand and B cell activation, migration and terminal differentiation of mature FoB and MZB cells on the other.

The requirements needed to select a FoB cell to get a threshold Notch2 activation signal remain an unanswered question. Previous work showed that inactivation of one allele of the Notch2 receptor or one allele of the Notch-Ligand DLL-1 in fibroblasts was sufficient to significantly

reduce the percentage of MZB cells (Saito et al. 2003; Hozumi et al. 2004). These results strengthen the signaling threshold theory: MZB development is sensitive to the number of receptor-ligand pairs on a single cell and identified the Notch2-DLL-1 interaction between B cells (FoB and T1/T2 B cells) and splenic fibroblasts as the decisive signaling niche.

In our transplantation model, donor FoB and recipient B cells equally compete for DLL1 interaction. In earlier transplantation models studying B cell development, purified B cells were frequently transplanted into immunodeficient recipient mice, where competition for DLL1 binding was absent. This lead to enhanced regeneration of a MZB cell pool after transfer of total splenic B cells and even purified FoB cells (Srivastava, Quinn, et al. 2005; Oliver, Martin, and Kearney 1999; Hao and Rajewsky 2001; Agenès and Freitas 1999; Vinuesa et al. 2003). As we here describe the FoB-to-MZB conversion in immunocompetent mice as a rather slow process that was not completed before 14 days after transfer, Srivastava et al. could not see a trans-differentiation of FoB cells to MZB cells when they transplanted purified FoB cells into wild type recipients, as they only tracked the engrafted cells until day 8.5.

As stated in the introduction, BCR signaling seems to act upstream of Notch2 signaling in some aspects, with activated BCR signaling inducing the expression of the critical Notch2-cleaving protease Adam10 (Hammad et al. 2017). Moreover, experiments conducted by Tea Babushku in our lab showed that Notch2 expression levels on the cell surface can be strongly upregulated (about tenfold) by BCR stimulation of FoB cells *in vitro* (Lechner et al. 2021).

The best-fitting model to describe the occurrence of an above-threshold Notch2 signaling activation can be drawn by defining the DLL-1 interaction within splenic follicles as the limiting niche factor and FoB cells compete for their spot to reach the threshold Notch2 signal. Previous activation of BCR signaling and subsequent upregulation of Notch2 receptor and Notch2 signaling machinery might prime FoB cells to eventually reach the signaling threshold. As presented in this work, activation of Notch2 is then capable to trigger a plethora of phenotypic and transcriptomic changes and is the key switch to initiate the FoB-to-MZB trans-differentiation.

Vice versa, inhibition of Notch2 signaling was shown to re-organize MZB cells into the splenic follicle to be indistinguishable from FoB cells (Simonetti et al. 2013). Our data from transplanting mature MZB cells also showed the loss of MZB phenotype within 14 days to a large extent. As

MZB cells undergo follicular shuttling behavior and therefore leave the S1P-rich marginal zone, they potentially need to re-gain Notch2 activation for the maintenance of sufficient expression levels of MZ-homing receptors. In this view, engrafted MZB cells are therefore again competing for limited spots of DLL1 interaction in the splenic follicles.

Collectively, this work finally proves a remarkable plasticity among mature B cell subsets and rectifies the view of lineage commitment during B cell development as a dead-end road.

4.7 A glance beyond B cells: The emerging concepts of lymphocyte plasticity

In recent years, the paradigm of lineage stability has been challenged and concepts of cellular and functional plasticity amongst mature immune cells were developed. Plasticity of T cells, especially amongst $CD4^+$ T_H cells, has first been lively discussed (Bluestone et al. 2009) and later gained broad acceptance as important cellular mechanisms to rapidly adapt to changing environments in the presence of infection (DuPage and Bluestone 2016; Ivanova and Orekhov 2015). DuPage and colleagues even criticize "the use of terms such as lineage, specification and master regulator as terms best aligned with developmental programs, such as in *Caenorhabditis elegans*, in which the fate of each cell is predetermined and irreversible." (DuPage and Bluestone 2016), favoring the use of a more flexible term to describe the endpoints of differentiation to fully functional immune cell subset and eventually introduce a descriptor that leaves room for flexibility amongst T cells – "*polarized*" T cell subsets (DuPage and Bluestone 2016). Interestingly, in this model of polarization and plasticity, the local cytokine microenvironment and Notch signaling processes were identified to be critically involved. Notch signaling was found to regulate T cell polarization by mechanisms such as regulation of TCR antigen sensitivity as well as metabolic and transcriptional regulation (Yamane and Paul 2013; Laky et al. 2015).

Our understanding of immune cell diversity still broadens and as recent as in the last decade, a whole subset of non-T cell, non-B cells and natural killer (NK) cell like- lymphocytes were described and termed innate lymphoid cells (ILCs) in 2013 (Spits et al. 2013). ILCs are tissue-resident lymphocytes, which can be categorized into several subgroups defined by their surface phenotypes and cytokine production. The new knowledge on ILCs was just summarized in two

well reputed reviews (Vivier et al. 2018; Bal, Golebski, and Spits 2020). ILCs show tremendous phenotypic and functional plasticity depending on their local cytokine microenvironment (Zhang, Xu, et al. 2017; Klose and Artis 2020). Again, Notch signaling is critically involved and induces lineage plasticity and cytokine production in ILCs (Rankin et al. 2013; Zhang, Xu, et al. 2017).

This short excursion should emphasis how our current understanding of lymphocyte development is being broadened and shows that Notch signaling plays a key role in immune cell plasticity.

Bibliography

Adori, M., G. K. Pedersen, C. Adori, E. Erikson, S. Khoenkhoen, J. M. Stark, J. H. Choi, P. Dosenovic, M. C. I. Karlsson, B. Beutler, and G. B. Karlsson Hedestam. 2018. 'Altered Marginal Zone B Cell Selection in the Absence of IkappaBNS', *J Immunol*, 200: 775-87.

Agenès, F., and A. A. Freitas. 1999. 'Transfer of small resting B cells into immunodeficient hosts results in the selection of a self-renewing activated B cell population', *J Exp Med*, 189: 319-30.

Allman, D., and M. P. Hardy. 1999. 'Commitment to the B Lymphoid Lineage Occurs before D H -J H Recombination'.

Allman, D., and S. Pillai. 2008. 'Peripheral B cell subsets', *Curr Opin Immunol*, 20: 149-57.

Allman, D., B. Srivastava, and R. C. Lindsley. 2004. 'Alternative routes to maturity: branch points and pathways for generating follicular and marginal zone B cells', *Immunol Rev*, 197: 147-60.

Allman, David, R. Coleman Lindsley, William DeMuth, Kristina Rudd, Susan A. Shinton, and Richard R. Hardy. 2001. 'Resolution of Three Nonproliferative Immature Splenic B Cell Subsets Reveals Multiple Selection Points During Peripheral B Cell Maturation', *The Journal of Immunology*, 167: 6834-40.

Anzelon, A. N., H. Wu, and R. C. Rickert. 2003. 'Pten inactivation alters peripheral B lymphocyte fate and reconstitutes CD19 function', *Nat Immunol*, 4: 287-94.

Arnon, T. I., R. M. Horton, I. L. Grigorova, and J. G. Cyster. 2013. 'Visualization of splenic marginal zone B-cell shuttling and follicular B-cell egress', *Nature*, 493: 684-8.

Arnon, T. I., Y. Xu, C. Lo, T. Pham, J. An, S. Coughlin, G. W. Dorn, and J. G. Cyster. 2011. 'GRK2-dependent S1PR1 desensitization is required for lymphocytes to overcome their attraction to blood', *Science*, 333: 1898-903.

Arnon, Tal I., and Jason G. Cyster. 2014. 'Blood, Sphingosine-1-Phosphate and Lymphocyte Migration Dynamics in the Spleen.' in, *Sphingosine-1-Phosphate Signaling in Immunology and Infectious Diseases*.

Bal, S. M., K. Golebski, and H. Spits. 2020. 'Plasticity of innate lymphoid cell subsets', *Nat Rev Immunol*.

Batten, M., J. Groom, T. G. Cachero, F. Qian, P. Schneider, J. Tschopp, J. L. Browning, and F. Mackay. 2000. 'BAFF mediates survival of peripheral immature B lymphocytes', *J Exp Med*, 192: 1453-66.

Baumgarth, N. 2017. 'A Hard (y) Look at B-1 Cell Development and Function', *J Immunol*, 199: 3387-94.

Bluestone, J. A., C. R. Mackay, J. J. O'Shea, and B. Stockinger. 2009. 'The functional plasticity of T cell subsets', *Nat Rev Immunol*, 9: 811-6.

Bretscher, P. A. 1999. 'A two-step, two-signal model for the primary activation of precursor helper T cells', *Proc Natl Acad Sci U S A*, 96: 185-90.

Campos-Martin, Y., N. Martinez, A. Martinez-Lopez, L. Cereceda, F. Casado, P. Algara, D. Oscier, F. J. Menarguez, J. F. Garcia, M. A. Piris, and M. Mollejo. 2017. 'Clinical and diagnostic relevance of NOTCH2-and KLF2-mutations in splenic marginal zone lymphoma', *Haematologica*, 102: e310-e12.

Cancro, Michael P. 2009. 'Signalling crosstalk in B cells: managing worth and need', *Nature reviews. Immunology*, 9: 657-61.

Cariappa, A., C. Boboila, S. T. Moran, H. Liu, H. N. Shi, and S. Pillai. 2007. 'The Recirculating B Cell Pool Contains Two Functionally Distinct, Long-Lived, Posttransitional, Follicular B Cell Populations', *The Journal of Immunology*, 179: 2270-81.

Cariappa, A., H. C. Liou, B. H. Horwitz, and S. Pillai. 2000. 'Nuclear factor kappa B is required for the development of marginal zone B lymphocytes', *The Journal of Experimental Medicine*, 192: 1175-82.

Cariappa, A., M. Tang, C. Parng, E. Nebelitskiy, M. Carroll, K. Georgopoulos, and S. Pillai. 2001. 'The follicular versus marginal zone B lymphocyte cell fate decision is regulated by Aiolos, Btk, and CD21', *Immunity*, 14: 603-15.

Cerutti, A., M. Cols, and I. Puga. 2013. 'Marginal zone B cells: virtues of innate-like antibody-producing lymphocytes', *Nat Rev Immunol*, 13: 118-32.

Chan, T. D., D. Gatto, K. Wood, T. Camidge, A. Basten, and R. Brink. 2009. 'Antigen affinity controls rapid T-dependent antibody production by driving the expansion rather than the differentiation or extrafollicular migration of early plasmablasts', *J Immunol*, 183: 3139-49.

Chaudhry, Mohammed S., and Anastasios Karadimitris. 2014. 'Role and regulation of CD1d in normal and pathological B cells', *Journal of immunology (Baltimore, Md. : 1950)*, 193: 4761-68.

Chen, J., J. J. Limon, C. Blanc, S. L. Peng, and D. A. Fruman. 2010. 'Foxo1 regulates marginal zone B-cell development', *Eur J Immunol*, 40: 1890-6.

Chung, J. B., R. A. Sater, M. L. Fields, J. Erikson, and J. G. Monroe. 2002. 'CD23 defines two distinct subsets of immature B cells which differ in their responses to T cell help signals', *International Immunology*, 14: 157-66.

Cinamon, G., M. Matloubian, M. J. Lesneski, Y. Xu, C. Low, T. Lu, R. L. Proia, and J. G. Cyster. 2004. 'Sphingosine 1-phosphate receptor 1 promotes B cell localization in the splenic marginal zone', *Nat Immunol*, 5: 713-20.

Cinamon, G., M. A. Zachariah, O. M. Lam, F. W. Foss, Jr., and J. G. Cyster. 2008. 'Follicular shuttling of marginal zone B cells facilitates antigen transport', *Nat Immunol*, 9: 54-62.

Clark, M. R., M. Mandal, K. Ochiai, and H. Singh. 2014. 'Orchestrating B cell lymphopoiesis through interplay of IL-7 receptor and pre-B cell receptor signalling', *Nat Rev Immunol*, 14: 69-80.

Clayton, E., G. Bardi, S. E. Bell, D. Chantry, C. P. Downes, A. Gray, L. A. Humphries, D. Rawlings, H. Reynolds, E. Vigorito, and M. Turner. 2002. 'A crucial role for the p110delta subunit of phosphatidylinositol 3-kinase in B cell development and activation', *J Exp Med*, 196: 753-63.

Cooper, M. D., R. D. Peterson, and R. A. Good. 1965. 'Delineation of the Thymic and Bursal Lymphoid Systems in the Chicken', *Nature*, 205: 143-6.

Cooper, Max D. 2015. 'The early history of B cells', *Nature Reviews Immunology*, 15: 191-97.

Cornejo, M. G., V. Mabialah, S. M. Sykes, T. Khandan, C. Lo Celso, C. K. Lopez, P. Rivera-Munoz, P. Rameau, Z. Tothova, J. C. Aster, R. A. DePinho, D. T. Scadden, D. G. Gilliland, and T. Mercher. 2011. 'Crosstalk between NOTCH and AKT signaling during murine megakaryocyte lineage specification', *Blood*, 118: 1264-73.

Cyster, J. G. 2000. 'B cells on the front line', *Nat Immunol*, 1: 9-10.

———. 2005. 'Chemokines, sphingosine-1-phosphate, and cell migration in secondary lymphoid organs', *Annu Rev Immunol*, 23: 127-59.

Cyster, J. G., and S. R. Schwab. 2012. 'Sphingosine-1-phosphate and lymphocyte egress from lymphoid organs', *Annu Rev Immunol*, 30: 69-94.

Cyster, Jason G. 2010. 'B cell follicles and antigen encounters of the third kind', *Nature Immunology*, 11: 989-96.

Cyster, Jason G., Theresa T. Lu, and Charles G. Lo. 2003. 'Integrin-dependence of Lymphocyte Entry into the Splenic White Pulp', *Journal of Experimental Medicine*, 197: 353-61.

Dammers, P. M., N. K. de Boer, G. J. Deenen, P. Nieuwenhuis, and F. G. Kroese. 1999. 'The origin of marginal zone B cells in the rat', *Eur J Immunol*, 29: 1522-31.

Dengler, H. S., G. V. Baracho, S. A. Omori, S. Bruckner, K. C. Arden, D. H. Castrillon, R. A. DePinho, and R. C. Rickert. 2008. 'Distinct functions for the transcription factor Foxo1 at various stages of B cell differentiation', *Nat Immunol*, 9: 1388-98.

Dominguez-Sola, D., J. Kung, A. B. Holmes, V. A. Wells, T. Mo, K. Basso, and R. Dalla-Favera. 2015. 'The FOXO1 Transcription Factor Instructs the Germinal Center Dark Zone Program', *Immunity*, 43: 1064-74.

DuPage, M., and J. A. Bluestone. 2016. 'Harnessing the plasticity of CD4 (+) T cells to treat immune-mediated disease', *Nat Rev Immunol*, 16: 149-63.

Dustin, M. L. 2014. 'The immunological synapse', *Cancer Immunol Res*, 2: 1023-33.

Fairfax, K. A., A. Kallies, S. L. Nutt, and D. M. Tarlinton. 2008. 'Plasma cell development: from B-cell subsets to long-term survival niches', *Semin Immunol*, 20: 49-58.

Fasnacht, N., H. Y. Huang, U. Koch, S. Favre, F. Auderset, Q. Chai, L. Onder, S. Kallert, D. D. Pinschewer, H. R. MacDonald, F. Tacchini-Cottier, B. Ludewig, S. A. Luther, and F. Radtke. 2014. 'Specific fibroblastic niches in secondary lymphoid organs orchestrate distinct Notch-regulated immune responses', *J Exp Med*, 211: 2265-79.

Feil, R., J. Wagner, D. Metzger, and P. Chambon. 1997. 'Regulation of Cre recombinase activity by mutated estrogen receptor ligand-binding domains', *Biochem Biophys Res Commun*, 237: 752-7.

Feil, S., N. Valtcheva, and R. Feil. 2009. 'Inducible Cre mice', *Methods Mol Biol*, 530: 343-63.

Feng, J., H. Wang, D. M. Shin, M. Masiuk, C. F. Qi, and H. C. Morse, 3rd. 2011. 'IFN regulatory factor 8 restricts the size of the marginal zone and follicular B cell pools', *J Immunol*, 186: 1458-66.

Ferguson, A. R., and R. B. Corley. 2005. 'Accumulation of marginal zone B cells and accelerated loss of follicular dendritic cells in NF-kappaB p50-deficient mice', *BMC Immunol*, 6: 8.

Forster, R., A. Schubel, D. Breitfeld, E. Kremmer, I. Renner-Muller, E. Wolf, and M. Lipp. 1999. 'CCR7 coordinates the primary immune response by establishing functional microenvironments in secondary lymphoid organs', *Cell*, 99: 23-33.

Förster, Reinhold, Ana Clara Davalos-Misslitz, and Antal Rot. 2008. 'CCR7 and its ligands: balancing immunity and tolerance', *Nature Reviews Immunology*, 8: 362-71.

Genestier, L., M. Taillardet, P. Mondiere, H. Gheit, C. Bella, and T. Defrance. 2007. 'TLR Agonists Selectively Promote Terminal Plasma Cell Differentiation of B Cell Subsets Specialized in Thymus-Independent Responses', *The Journal of Immunology*, 178: 7779-86.

Gibb, D. R., M. El Shikh, D. J. Kang, W. J. Rowe, R. El Sayed, J. Cichy, H. Yagita, J. G. Tew, P. J. Dempsey, H. C. Crawford, and D. H. Conrad. 2010. 'ADAM10 is essential for Notch2-dependent marginal zone B cell development and CD23 cleavage in vivo', *J Exp Med*, 207: 623-35.

Glick, Bruce, Timothy S. Chang, and R. George Jaap. 1956. 'The Bursa of Fabricius and Antibody Production', *Poultry Science*, 35: 224-25.

Grasseau, A., M. Boudigou, L. Le Pottier, N. Chriti, D. Cornec, J. O. Pers, Y. Renaudineau, and S. Hillion. 2020. 'Innate B Cells: the Archetype of Protective Immune Cells', *Clin Rev Allergy Immunol*, 58: 92-106.

Groeneveld, P. H., T. Erich, and G. Kraal. 1985. 'In vivo effects of LPS on B lymphocyte subpopulations. Migration of marginal zone-lymphocytes and IgD-blast formation in the mouse spleen', *Immunobiology*, 170: 402-11.

Gutierrez, A., and A. T. Look. 2007. 'NOTCH and PI3K-AKT pathways intertwined', *Cancer Cell*, 12: 411-3.

Hammad, H., M. Vanderkerken, P. Pouliot, K. Deswarte, W. Toussaint, K. Vergote, L. Vandersarren, S. Janssens, I. Ramou, S. N. Savvides, J. J. Haigh, R. Hendriks, M. Kopf, K. Craessaerts, B. de Strooper, J. F. Kearney, D. H. Conrad, and B. N. Lambrecht. 2017. 'Transitional B cells commit to marginal zone B cell fate by Taok3-mediated surface expression of ADAM10', *Nat Immunol*, 18: 313-20.

Hampel, F., S. Ehrenberg, C. Hojer, A. Draeseke, G. Marschall-Schroter, R. Kuhn, B. Mack, O. Gires, C. J. Vahl, M. Schmidt-Supprian, L. J. Strobl, and U. Zimber-Strobl. 2011. 'CD19-independent instruction of murine marginal zone B-cell development by constitutive Notch2 signaling', *Blood*, 118: 6321-31.

Hao, Z., and K. Rajewsky. 2001. 'Homeostasis of peripheral B cells in the absence of B cell influx from the bone marrow', *J Exp Med*, 194: 1151-64.

Hardy, R. R., and K. Hayakawa. 2001. 'B cell development pathways', *Annu Rev Immunol*, 19: 595-621.

Hardy, R. R., K. Hayakawa, D. R. Parks, and L. A. Herzenberg. 1983. 'Demonstration of B-cell maturation in X-linked immunodeficient mice by simultaneous three-colour immunofluorescence', *Nature*, 306: 270-72.

Hart, G. T., X. Wang, K. A. Hogquist, and S. C. Jameson. 2011. 'Kruppel-like factor 2 (KLF2) regulates B-cell reactivity, subset differentiation, and trafficking molecule expression', *Proc Natl Acad Sci U S A*, 108: 716-21.

Heger, K., M. Kober, D. Riess, C. Drees, I. de Vries, A. Bertossi, A. Roers, M. Sixt, and M. Schmidt-Supprian. 2015. 'A novel Cre recombinase reporter mouse strain facilitates selective and efficient infection of primary immune cells with adenoviral vectors', *Eur J Immunol*, 45: 1614-20.

Heng, T. S., M. W. Painter, and Consortium Immunological Genome Project. 2008. 'The Immunological Genome Project: networks of gene expression in immune cells', *Nat Immunol*, 9: 1091-4.

Hikida, M., S. Johmura, A. Hashimoto, M. Takezaki, and T. Kurosaki. 2003. 'Coupling between B cell receptor and phospholipase C-gamma2 is essential for mature B cell development', *J Exp Med*, 198: 581-9.

Hoek, K. L., L. E. Gordy, P. L. Collins, V. V. Parekh, T. M. Aune, S. Joyce, J. W. Thomas, L. Van Kaer, and E. Sebzda. 2010. 'Follicular B cell trafficking within the spleen actively restricts humoral immune responses', *Immunity*, 33: 254-65.

Hozumi, K., N. Negishi, D. Suzuki, N. Abe, Y. Sotomaru, N. Tamaoki, C. Mailhos, D. Ish-Horowicz, S. Habu, and M. J. Owen. 2004. 'Delta-like 1 is necessary for the generation of marginal zone B cells but not T cells in vivo', *Nat Immunol*, 5: 638-44.

Inoue, T., R. Shinnakasu, W. Ise, C. Kawai, T. Egawa, and T. Kurosaki. 2017. 'The transcription factor Foxo1 controls germinal center B cell proliferation in response to T cell help', *J Exp Med*.

Ivanova, Ekaterina A., and Alexander N. Orekhov. 2015. 'T Helper Lymphocyte Subsets and Plasticity in Autoimmunity and Cancer: An Overview', *BioMed Research International*, 2015: 1-9.

Johnson, Kristen, Julie Chaumeil, Mariann Micsinai, Joy M. H. Wang, Laura B. Ramsey, Gisele V. Baracho, Robert C. Rickert, Francesco Strino, Yuval Kluger, Michael A. Farrar, and Jane A. Skok. 2012. 'IL-7 Functionally Segregates the Pro-B Cell Stage by Regulating Transcription of Recombination Mediators across Cell Cycle', *The Journal of Immunology*, 188: 6084-92.

Jones, Derek D., Joel R. Wilmore, and David Allman. 2015. 'Cellular Dynamics of Memory B Cell Populations: IgM⁺ and IgG⁺ Memory B Cells Persist Indefinitely as Quiescent Cells', *The Journal of Immunology*, 195: 4753-59.

Jun-ichi, Miyazaki, Takaki Satoshi, Araki Kimi, Tashiro Fumi, Tominaga Akira, Takatsu Kiyoshi, and Yamamura Ken-ichi. 1989. 'Expression vector system based on the chicken β-actin promoter directs efficient production of interleukin-5', *Gene*, 79: 269-77.

Kadoch, C., and G. R. Crabtree. 2013. 'Reversible disruption of mSWI/SNF (BAF) complexes by the SS18-SSX oncogenic fusion in synovial sarcoma', *Cell*, 153: 71-85.

Kageyama, R., T. Ohtsuka, and T. Kobayashi. 2007. 'The Hes gene family: repressors and oscillators that orchestrate embryogenesis', *Development*, 134: 1243-51.

Kageyama, Ryoichiro, and Toshiyuki Ohtsuka. 1999. 'The Notch-Hes pathway in mammalian neural development', *Cell Research*, 9: 179-88.

Kaji, T., A. Ishige, M. Hikida, J. Taka, A. Hijikata, M. Kubo, T. Nagashima, Y. Takahashi, T. Kurosaki, M. Okada, O. Ohara, K. Rajewsky, and T. Takemori. 2012. 'Distinct cellular pathways select germline-encoded and somatically mutated antibodies into immunological memory', *J Exp Med*, 209: 2079-97.

Kanayama, N., M. Cascalho, and H. Ohmori. 2005. 'Analysis of Marginal Zone B Cell Development in the Mouse with Limited B Cell Diversity: Role of the Antigen Receptor Signals in the Recruitment of B Cells to the Marginal Zone', *The Journal of Immunology*, 174: 1438-45.

Katakai, T., T. Hara, M. Sugai, H. Gonda, and A. Shimizu. 2004. 'Lymph node fibroblastic reticular cells construct the stromal reticulum via contact with lymphocytes', *J Exp Med*, 200: 783-95.

Kearney, J. F., W. J. Won, C. Benedict, C. Moratz, P. Zimmer, A. Oliver, F. Martin, and F. Shu. 1997. 'B cell development in mice', *Int Rev Immunol*, 15: 207-41.

Kibler, Artur, Bettina Budeus, Ekaterina Homp, Kevin Bronischewski, Victoria Berg, Ludger Sellmann, Florian Murke, Andreas Heinold, Falko M. Heinemann, Monika Lindemann, Isabelle Bekeredjian-Ding, Peter A. Horn, Carsten J. Kirschning, Ralf Küppers, and Marc Seifert. 2021. 'Systematic memory B cell archiving and random display shape the human splenic marginal zone throughout life', *Journal of Experimental Medicine*, 218.

Kleiman, E., D. Salyakina, M. De Heusch, K. L. Hoek, J. M. Llanes, I. Castro, J. A. Wright, E. S. Clark, D. M. Dykxhoorn, E. Capobianco, A. Takeda, J. C. Renauld, and W. N. Khan. 2015. 'Distinct Transcriptomic Features are Associated with Transitional and Mature B-Cell Populations in the Mouse Spleen', *Front Immunol*, 6: 30.

Klein, U., S. Casola, G. Cattoretti, Q. Shen, M. Lia, T. Mo, T. Ludwig, K. Rajewsky, and R. Dalla-Favera. 2006. 'Transcription factor IRF4 controls plasma cell differentiation and class-switch recombination', *Nat Immunol*, 7: 773-82.

Klose, C. S. N., and D. Artis. 2020. 'Innate lymphoid cells control signaling circuits to regulate tissue-specific immunity', *Cell Res*, 30: 475-91.

Kohlhof, H., F. Hampel, R. Hoffmann, H. Burtscher, U. H. Weidle, M. Holzel, D. Eick, U. Zimber-Strobl, and L. J. Strobl. 2009. 'Notch1, Notch2, and Epstein-Barr virus-encoded nuclear antigen 2 signaling differentially affects proliferation and survival of Epstein-Barr virus-infected B cells', *Blood*, 113: 5506-15.

Kopan, R., and M. X. Ilagan. 2009. 'The canonical Notch signaling pathway: unfolding the activation mechanism', *Cell*, 137: 216-33.

Kovall, R. A., B. Gebelein, D. Sprinzak, and R. Kopan. 2017. 'The Canonical Notch Signaling Pathway: Structural and Biochemical Insights into Shape, Sugar, and Force', *Dev Cell*, 41: 228-41.

Kraal, G. 1992. 'Cells in the marginal zone of the spleen', *Int Rev Cytol*, 132: 31-74.

Kumararatne, D. S., H. Bazin, and I. C. MacLennan. 1981. 'Marginal zones: the major B cell compartment of rat spleens', *Eur J Immunol*, 11: 858-64.

Laky, K., S. Evans, A. Perez-Diez, and B. J. Fowlkes. 2015. 'Notch signaling regulates antigen sensitivity of naive CD4+ T cells by tuning co-stimulation', *Immunity*, 42: 80-94.

Larson, Erik D., and Nancy Maizels. 2004. 'Transcription-coupled mutagenesis by the DNA deaminase AID', *Genome Biology*, 5: 211.

Lechner, M., T. Engleitner, T. Babushku, M. Schmidt-Supprian, R. Rad, L. J. Strobl, and U. Zimber-Strobl. 2021. 'Notch2-mediated plasticity between marginal zone and follicular B cells', *Nat Commun*, 12: 1111.

Lewis, S. M., A. Williams, and S. C. Eisenbarth. 2019. 'Structure and function of the immune system in the spleen', *Science Immunology*, 4.

Liao, Wenhua, Zhaolin Hua, Can Liu, Lin Lin, Rui Chen, and Baidong Hou. 2017. 'Characterization of T-Dependent and T-Independent B Cell Responses to a Virus-like Particle', *The Journal of Immunology*, 198: 3846-56.

Lin, W. H., W. C. Adams, S. A. Nish, Y. H. Chen, B. Yen, N. J. Rothman, R. Kratchmarov, T. Okada, U. Klein, and S. L. Reiner. 2015. 'Asymmetric PI3K Signaling Driving Developmental and Regenerative Cell Fate Bifurcation', *Cell Rep*, 13: 2203-18.

Liu, Z., E. Brunskill, B. Varnum-Finney, C. Zhang, A. Zhang, P. Y. Jay, I. Bernstein, M. Morimoto, and R. Kopan. 2015. 'The intracellular domains of Notch1 and Notch2 are functionally equivalent during development and carcinogenesis', *Development*, 142: 2452-63.

Loder, F., B. Mutschler, R. J. Ray, C. J. Paige, P. Sideras, R. Torres, M. C. Lamers, and R. Carsetti. 1999. 'B cell development in the spleen takes place in discrete steps and is determined by the quality of B cell receptor-derived signals', *The Journal of Experimental Medicine*, 190: 75-89.

Love, M. I., W. Huber, and S. Anders. 2014. 'Moderated estimation of fold change and dispersion for RNA-seq data with DESeq2', *Genome Biol*, 15: 550.

Mabbott, N. A., and D. Gray. 2014. 'Identification of co-expressed gene signatures in mouse B1, marginal zone and B2 B-cell populations', *Immunology*, 141: 79-95.

MacLennan, and Vinuesa. 2003. 'Extrafollicular antibody responses', *Immunological Reviews*.

MacLennan, I. C., D. Gray, D. S. Kumararatne, and H. Bazin. 1982. 'The lymphocytes of splenic marginal zones: a distinct B-cell lineage', *Immunol Today*, 3: 305-7.

MacLennan, I. C., A. Gulbranson-Judge, K. M. Toellner, M. Casamayor-Palleja, E. Chan, D. M. Sze, S. A. Luther, and H. A. Orbea. 1997. 'The changing preference of T and B cells for partners as T-dependent antibody responses develop', *Immunol Rev*, 156: 53-66.

Macosko, E. Z., A. Basu, R. Satija, J. Nemesh, K. Shekhar, M. Goldman, I. Tirosh, A. R. Bialas, N. Kamitaki, E. M. Martersteck, J. J. Trombetta, D. A. Weitz, J. R. Sanes, A. K. Shalek, A. Regev, and S. A. McCarroll. 2015. 'Highly Parallel Genome-wide Expression Profiling of Individual Cells Using Nanoliter Droplets', *Cell*, 161: 1202-14.

Martin, F., and J. F. Kearney. 2000. 'Positive selection from newly formed to marginal zone B cells depends on the rate of clonal production, CD19, and btk', *Immunity*, 12: 39-49.

———. 2002. 'Marginal-zone B cells', *Nat Rev Immunol*, 2: 323-35.

Martin, F., A. M. Oliver, and J. F. Kearney. 2001. 'Marginal zone and B1 B cells unite in the early response against T-independent blood-borne particulate antigens', *Immunity*, 14: 617-29.

Mead, A. 1992. 'Review of the Development of Multidimensional Scaling Methods', *Journal of the Royal Statistical Society: Series D (The Statistician)*, 41: 27-39.

Mesin, L., J. Ersching, and G. D. Victora. 2016. 'Germinal Center B Cell Dynamics', *Immunity*, 45: 471-82.

Meyer-Bahlburg, A., A. D. Bandaranayake, S. F. Andrews, and D. J. Rawlings. 2009. 'Reduced c-myc expression levels limit follicular mature B cell cycling in response to TLR signals', *J Immunol*, 182: 4065-75.

Morgan, T. H. 1917. 'The Theory of the Gene', *The American Naturalist*, 51: 513-44.

Moriyama, Y., C. Sekine, A. Koyanagi, N. Koyama, H. Ogata, S. Chiba, S. Hirose, K. Okumura, and H. Yagita. 2008. 'Delta-like 1 is essential for the maintenance of marginal zone B cells in normal mice but not in autoimmune mice', *Int Immunol*, 20: 763-73.

Mostafavi, Sara, Adriana Ortiz-Lopez, Molly A. Bogue, Kimie Hattori, Cristina Pop, Daphne Koller, Diane Mathis, and Christophe Benoist. 2014. 'Variation and Genetic Control of Gene Expression in Primary Immunocytes across Inbred Mouse Strains', *The Journal of Immunology*, 193: 4485-96.

Muramatsu, M., K. Kinoshita, S. Fagarasan, S. Yamada, Y. Shinkai, and T. Honjo. 2000. 'Class switch recombination and hypermutation require activation-induced cytidine deaminase (AID), a potential RNA editing enzyme', *Cell*, 102: 553-63.

Murphy, Kenneth. 2012. *Janeway's Immunobiology* (Garland Science: New York).

Newman, R., H. Ahlfors, A. Saveliev, A. Galloway, D. J. Hodson, R. Williams, G. S. Besra, C. N. Cook, A. F. Cunningham, S. E. Bell, and M. Turner. 2017. 'Maintenance of the marginal-zone B cell compartment specifically requires the RNA-binding protein ZFP36L1', *Nat Immunol*, 18: 683-93.

Ochiai, K., M. Maienschein-Cline, G. Simonetti, J. Chen, R. Rosenthal, R. Brink, A. S. Chong, U. Klein, A. R. Dinner, H. Singh, and R. Sciammas. 2013. 'Transcriptional regulation of germinal center B and plasma cell fates by dynamical control of IRF4', *Immunity*, 38: 918-29.

Oliver, A. M., F. Martin, G. L. Gartland, R. H. Carter, and J. F. Kearney. 1997. 'Marginal zone B cells exhibit unique activation, proliferative and immunoglobulin secretory responses', *Eur J Immunol*, 27: 2366-74.

Oliver, A. M., F. Martin, and J. F. Kearney. 1999. 'IgMhighCD21high lymphocytes enriched in the splenic marginal zone generate effector cells more rapidly than the bulk of follicular B cells', *J Immunol*, 162: 7198-207.

Oracki, S. A., J. A. Walker, M. L. Hibbs, L. M. Corcoran, and D. M. Tarlinton. 2010. 'Plasma cell development and survival', *Immunol Rev*, 237: 140-59.

Osipo, C., T. E. Golde, B. A. Osborne, and L. A. Miele. 2008. 'Off the beaten pathway: the complex cross talk between Notch and NF-kappaB', *Lab Invest*, 88: 11-7.

Otero, D. C., A. N. Anzelon, and R. C. Rickert. 2003. 'CD19 function in early and late B cell development: I. Maintenance of follicular and marginal zone B cells requires CD19-dependent survival signals', *J Immunol*, 170: 73-83.

Otero, D. C., S. A. Omori, and R. C. Rickert. 2001. 'Cd19-dependent activation of Akt kinase in B-lymphocytes', *J Biol Chem*, 276: 1474-8.

Oyama, T., K. Harigaya, A. Muradil, K. Hozumi, S. Habu, H. Oguro, A. Iwama, K. Matsuno, R. Sakamoto, M. Sato, N. Yoshida, and M. Kitagawa. 2007. 'Mastermind-1 is required for Notch signal-dependent steps in lymphocyte development in vivo', *Proc Natl Acad Sci U S A*, 104: 9764-9.

Parekh, S., C. Ziegenhain, B. Vieth, W. Enard, and I. Hellmann. 2016. 'The impact of amplification on differential expression analyses by RNA-seq', *Sci Rep*, 6: 25533.

Paus, D., T. G. Phan, T. D. Chan, S. Gardam, A. Basten, and R. Brink. 2006. 'Antigen recognition strength regulates the choice between extrafollicular plasma cell and germinal center B cell differentiation', *J Exp Med*, 203: 1081-91.

Peng, X., A. Kasran, P. A. Warmerdam, M. de Boer, and J. L. Ceuppens. 1996. 'Accessory signaling by CD40 for T cell activation: induction of Th1 and Th2 cytokines and synergy with interleukin-12 for interferon-gamma production', *Eur J Immunol*, 26: 1621-7.

Pillai, S., and A. Cariappa. 2009. 'The follicular versus marginal zone B lymphocyte cell fate decision', *Nat Rev Immunol*, 9: 767-77.

Pillai, S., A. Cariappa, and S. T. Moran. 2005. 'Marginal zone B cells', *Annu Rev Immunol*, 23: 161-96.

Radtke, F., N. Fasnacht, and H. R. Macdonald. 2010. 'Notch signaling in the immune system', *Immunity*, 32: 14-27.

Radtke, F., H. R. MacDonald, and F. Tacchini-Cottier. 2013. 'Regulation of innate and adaptive immunity by Notch', *Nat Rev Immunol*, 13: 427-37.

Ramos-Perez, W. D., V. Fang, D. Escalante-Alcalde, M. Cammer, and S. R. Schwab. 2015. 'A map of the distribution of sphingosine 1-phosphate in the spleen', *Nat Immunol*, 16: 1245-52.

Ramstead, A. G., A. Robison, A. Blackwell, M. Jerome, B. Freedman, K. J. Lubick, J. F. Hedges, and M. A. Jutila. 2016. 'Roles of Toll-Like Receptor 2 (TLR2), TLR4, and MyD88 during Pulmonary Coxiella burnetii Infection', *Infect Immun*, 84: 940-49.

Rankin, Lucille C., Joanna R. Groom, Michaël Chopin, Marco J. Herold, Jennifer A. Walker, Lisa A. Mielke, Andrew N. J. McKenzie, Sebastian Carotta, Stephen L. Nutt, and Gabrielle T. Belz. 2013. 'The transcription factor T-bet is essential for the development of NKp46+ innate lymphocytes via the Notch pathway', *Nature Immunology*, 14: 389-95.

Rawlings, D. J., M. A. Schwartz, S. W. Jackson, and A. Meyer-Bahlburg. 2012a. 'Integration of B cell responses through Toll-like receptors and antigen receptors', *Nat Rev Immunol*, 12: 282-94.

Rawlings, David J., Marc A. Schwartz, Shaun W. Jackson, and Almut Meyer-Bahlburg. 2012b. 'Integration of B cell responses through Toll-like receptors and antigen receptors', *Nature Reviews Immunology*, 12: 282-94.

Robinson, S. P., S. M. Langan-Fahey, D. A. Johnson, and V. C. Jordan. 1991. 'Metabolites, pharmacodynamics, and pharmacokinetics of tamoxifen in rats and mice compared to the breast cancer patient', *Drug Metab Dispos*, 19: 36-43.

Rubtsov, A. V., C. L. Swanson, S. Troy, P. Strauch, R. Pelanda, and R. M. Torres. 2008. 'TLR agonists promote marginal zone B cell activation and facilitate T-dependent IgM responses', *J Immunol*, 180: 3882-8.

Saito, T., S. Chiba, M. Ichikawa, A. Kunisato, T. Asai, K. Shimizu, T. Yamaguchi, G. Yamamoto, S. Seo, K. Kumano, E. Nakagami-Yamaguchi, Y. Hamada, S. Aizawa, and H. Hirai. 2003. 'Notch2 is preferentially expressed in mature B cells and indispensable for marginal zone B lineage development', *Immunity*, 18: 675-85.

Sander, S., V. T. Chu, T. Yasuda, A. Franklin, R. Graf, D. P. Calado, S. Li, K. Imami, M. Selbach, M. Di Virgilio, L. Bullinger, and K. Rajewsky. 2015. 'PI3 Kinase and FOXO1 Transcription Factor Activity Differentially Control B Cells in the Germinal Center Light and Dark Zones', *Immunity*, 43: 1075-86.

Sangphech, N., B. A. Osborne, and T. Palaga. 2014. 'Notch signaling regulates the phosphorylation of Akt and survival of lipopolysaccharide-activated macrophages via regulator of G protein signaling 19 (RGS19)', *Immunobiology*, 219: 653-60.

Sasaki, Y., E. Derudder, E. Hobeika, R. Pelanda, M. Reth, K. Rajewsky, and M. Schmidt-Supprian. 2006. 'Canonical NF-kappaB activity, dispensable for B cell development, replaces BAFF-receptor signals and promotes B cell proliferation upon activation', *Immunity*, 24: 729-39.

Sato, S., D. A. Steeber, and T. F. Tedder. 1995. 'The CD19 signal transduction molecule is a response regulator of B-lymphocyte differentiation', *Proc Natl Acad Sci U S A*, 92: 11558-62.

Savage, H. P., V. M. Yenson, S. S. Sawhney, B. J. Mousseau, F. E. Lund, and N. Baumgarth. 2017. 'Blimp-1-dependent and -independent natural antibody production by B-1 and B-1-derived plasma cells', *J Exp Med*, 214: 2777-94.

Schiemann, B., J. L. Gommerman, K. Vora, T. G. Cachero, S. Shulga-Morskaya, M. Dobles, E. Frew, and M. L. Scott. 2001. 'An essential role for BAFF in the normal development of B cells through a BCMA-independent pathway', *Science*, 293: 2111-4.

Shaffer, A. L., K. I. Lin, T. C. Kuo, X. Yu, E. M. Hurt, A. Rosenwald, J. M. Giltnane, L. Yang, H. Zhao, K. Calame, and L. M. Staudt. 2002. 'Blimp-1 orchestrates plasma cell differentiation by extinguishing the mature B cell gene expression program', *Immunity*, 17: 51-62.

Sic, H., H. Kraus, J. Madl, K. A. Flittner, A. L. von Münchow, K. Pieper, M. Rizzi, A. K. Kienzler, K. Ayata, S. Rauer, B. Kleuser, U. Salzer, M. Burger, K. Zirlik, V. Lougaris, A. Plebani, W. Römer, C. Loeffler, S. Scaramuzza, A. Villa, E. Noguchi, B. Grimbacher, and H. Eibel. 2014. 'Sphingosine-1-phosphate receptors control B-cell migration through signaling components associated with primary immunodeficiencies, chronic lymphocytic leukemia, and multiple sclerosis', *J Allergy Clin Immunol*, 134: 420-8.

Siebenlist, U., K. Brown, and E. Claudio. 2005. 'Control of lymphocyte development by nuclear factor-kappaB', *Nat Rev Immunol*, 5: 435-45.

Silverstein, A. M., and A. A. Bialasiewicz. 1980. 'History of immunology. A history of theories of acquired immunity', *Cell Immunol*, 51: 151-67.

Simmons, S., and M. Ishii. 2014. 'Sphingosine-1-phosphate: a master regulator of lymphocyte egress and immunity', *Arch Immunol Ther Exp (Warsz)*, 62: 103-15.

Simonetti, G., A. Carette, K. Silva, H. Wang, N. S. De Silva, N. Heise, C. W. Siebel, M. J. Shlomchik, and U. Klein. 2013. 'IRF4 controls the positioning of mature B cells in the lymphoid microenvironments by regulating NOTCH2 expression and activity', *J Exp Med*, 210: 2887-902.

Song, H., and J. Cerny. 2003. 'Functional heterogeneity of marginal zone B cells revealed by their ability to generate both early antibody-forming cells and germinal centers with hypermutation and memory in response to a T-dependent antigen', *J Exp Med*, 198: 1923-35.

Song, J., Z. Lokmic, T. Lammermann, J. Rolf, C. Wu, X. Zhang, R. Hallmann, M. J. Hannocks, N. Horn, M. A. Ruegg, A. Sonnenberg, E. Georges-Labouesse, T. H. Winkler, J. F. Kearney, S. Cardell, and L. Sorokin. 2013. 'Extracellular matrix of secondary lymphoid organs impacts on B-cell fate and survival', *Proc Natl Acad Sci U S A*, 110: E2915-24.

Sonoda, Koh-Hei, and Joan Stein-Streilein. 2002. 'CD1d on antigen-transporting APC and splenic marginal zone B cells promotes NKT cell-dependent tolerance', *European Journal of Immunology*, 32: 848-57.

Spits, H., D. Artis, M. Colonna, A. Diefenbach, J. P. Di Santo, G. Eberl, S. Koyasu, R. M. Locksley, A. N. McKenzie, R. E. Mebius, F. Powrie, and E. Vivier. 2013. 'Innate lymphoid cells--a proposal for uniform nomenclature', *Nat Rev Immunol*, 13: 145-9.

Srivastava, B., R. C. Lindsley, N. Nikbakht, and D. Allman. 2005. 'Models for peripheral B cell development and homeostasis', *Semin Immunol*, 17: 175-82.

Srivastava, B., W. J. Quinn, 3rd, K. Hazard, J. Erikson, and D. Allman. 2005. 'Characterization of marginal zone B cell precursors', *J Exp Med*, 202: 1225-34.

Subramanian, A., P. Tamayo, V. K. Mootha, S. Mukherjee, B. L. Ebert, M. A. Gillette, A. Paulovich, S. L. Pomeroy, T. R. Golub, E. S. Lander, and J. P. Mesirov. 2005. 'Gene set enrichment analysis: a knowledge-based approach for interpreting genome-wide expression profiles', *Proc Natl Acad Sci U S A*, 102: 15545-50.

Takamatsu, Hyota, and Atsushi Kumanogoh. 2012. 'Diverse roles for semaphorin−plexin signaling in the immune system', *Trends in Immunology*, 33: 127-35.

Tan, J. B., K. Xu, K. Cretegny, I. Visan, J. S. Yuan, S. E. Egan, and C. J. Guidos. 2009. 'Lunatic and manic fringe cooperatively enhance marginal zone B cell precursor competition for delta-like 1 in splenic endothelial niches', *Immunity*, 30: 254-63.

Tanigaki, K., H. Han, N. Yamamoto, K. Tashiro, M. Ikegawa, K. Kuroda, A. Suzuki, T. Nakano, and T. Honjo. 2002. 'Notch-RBP-J signaling is involved in cell fate determination of marginal zone B cells', *Nat Immunol*, 3: 443-50.

Tanigaki, Kenji, and Tasuku Honjo. 2007. 'Regulation of lymphocyte development by Notch signaling', *Nature Immunology*, 8: 451-56.

Taylor, Milton W. 2014. 'The History of Immunology.' in, *Viruses and Man: A History of Interactions* (Springer International Publishing Switzerland).

Tedford, K., M. Steiner, S. Koshutin, K. Richter, L. Tech, Y. Eggers, I. Jansing, K. Schilling, A. E. Hauser, M. Korthals, and K. D. Fischer. 2017. 'The opposing forces of shear flow and sphingosine-1-phosphate control marginal zone B cell shuttling', *Nat Commun*, 8: 2261.

Tellier, J., W. Shi, M. Minnich, Y. Liao, S. Crawford, G. K. Smyth, A. Kallies, M. Busslinger, and S. L. Nutt. 2016. 'Blimp-1 controls plasma cell function through the regulation of immunoglobulin secretion and the unfolded protein response', *Nat Immunol*.

Teng, Grace, and F. Nina Papavasiliou. 2007. 'Immunoglobulin Somatic Hypermutation', *Annual Review of Genetics*, 41: 107-20.

Treml, L. S., G. Carlesso, K. L. Hoek, J. E. Stadanlick, T. Kambayashi, R. J. Bram, M. P. Cancro, and W. N. Khan. 2007. 'TLR Stimulation Modifies BLyS Receptor Expression in Follicular and Marginal Zone B Cells', *The Journal of Immunology*, 178: 7531-39.

Tull, Thomas J., Michael J. Pitcher, William Guesdon, Jacqueline H. Y. Siu, Cristina Lebrero-Fernández, Yuan Zhao, Nedyalko Petrov, Susanne Heck, Richard Ellis, Pawan Dhami, Ulrich D. Kadolsky, Michelle Kleeman, Yogesh Kamra, David J. Fear, Susan John, Wayel Jassem, Richard W. Groves, Jeremy D. Sanderson, Michael D. Robson, David P. D'Cruz, Mats Bemark, and Jo Spencer. 2021. 'Human marginal zone B cell development from early T2 progenitors', *Journal of Experimental Medicine*, 218.

Turk, R., P. A. t Hoen, E. Sterrenburg, R. X. de Menezes, E. J. de Meijer, J. M. Boer, G. J. van Ommen, and J. T. den Dunnen. 2004. 'Gene expression variation between mouse inbred strains', *BMC Genomics*, 5: 57.

Vinuesa, C. G., D. M. Sze, M. C. Cook, K. M. Toellner, G. G. Klaus, J. Ball, and I. C. MacLennan. 2003. 'Recirculating and germinal center B cells differentiate into cells responsive to polysaccharide antigens', *Eur J Immunol*, 33: 297-305.

Vivier, E., D. Artis, M. Colonna, A. Diefenbach, J. P. Di Santo, G. Eberl, S. Koyasu, R. M. Locksley, A. N. J. McKenzie, R. E. Mebius, F. Powrie, and H. Spits. 2018. 'Innate Lymphoid Cells: 10 Years On', *Cell*, 174: 1054-66.

Vora, K. A., E. Nichols, G. Porter, Y. Cui, C. A. Keohane, R. Hajdu, J. Hale, W. Neway, D. Zaller, and S. Mandala. 2005. 'Sphingosine 1-phosphate receptor agonist FTY720-phosphate causes marginal zone B cell displacement', *J Leukoc Biol*, 78: 471-80.

Vos, Q., A. Lees, Z. Q. Wu, C. M. Snapper, and J. J. Mond. 2000. 'B-cell activation by T-cell-independent type 2 antigens as an integral part of the humoral immune response to pathogenic microorganisms', *Immunol Rev*, 176: 154-70.

Wang, J. H., J. Li, Q. Wu, P. Yang, R. D. Pawar, S. Xie, L. Timares, C. Raman, D. D. Chaplin, L. Lu, J. D. Mountz, and H. C. Hsu. 2010. 'Marginal zone precursor B cells as cellular agents for type I IFN-promoted antigen transport in autoimmunity', *J Immunol*, 184: 442-51.

Wardemann, Hedda, Thomas Boehm, Neil Dear, and Rita Carsetti. 2002. 'B-1a B Cells that Link the Innate and Adaptive Immune Responses Are Lacking in the Absence of the Spleen', *Journal of Experimental Medicine*, 195: 771-80.

Wehrli, N., D. F. Legler, D. Finke, K. M. Toellner, P. Loetscher, M. Baggiolini, I. C. MacLennan, and H. Acha-Orbea. 2001. 'Changing responsiveness to chemokines allows medullary plasmablasts to leave lymph nodes', *Eur J Immunol*, 31: 609-16.

Weidenreich, Franz. 1901. 'Das gefässsystem der menschlichen Milz', *Archiv für Mikroskopische Anatomie*, 58: 247-376.

Wen, L., J. Brill-Dashoff, S. A. Shinton, M. Asano, R. R. Hardy, and K. Hayakawa. 2005. 'Evidence of marginal-zone B cell-positive selection in spleen', *Immunity*, 23: 297-308.

Wen, R., Y. Chen, L. Xue, J. Schuman, S. Yang, S. W. Morris, and D. Wang. 2003. 'Phospholipase Cgamma2 provides survival signals via Bcl2 and A1 in different subpopulations of B cells', *J Biol Chem*, 278: 43654-62.

Winkelmann, R., L. Sandrock, J. Kirberg, H. M. Jack, and W. Schuh. 2014. 'KLF2--a negative regulator of pre-B cell clonal expansion and B cell activation', *PLoS One*, 9: e97953.

Winkelmann, R., L. Sandrock, M. Porstner, E. Roth, M. Mathews, E. Hobeika, M. Reth, M. L. Kahn, W. Schuh, and H. M. Jack. 2011. 'B cell homeostasis and plasma cell homing controlled by Kruppel-like factor 2', *Proc Natl Acad Sci U S A*, 108: 710-5.

Yamane, H., and W. E. Paul. 2013. 'Early signaling events that underlie fate decisions of naive CD4 (+) T cells toward distinct T-helper cell subsets', *Immunol Rev*, 252: 12-23.

Yasuda, T., T. Wirtz, B. Zhang, T. Wunderlich, M. Schmidt-Supprian, T. Sommermann, and K. Rajewsky. 2013. 'Studying Epstein-Barr virus pathologies and immune surveillance by reconstructing EBV infection in mice', *Cold Spring Harb Symp Quant Biol*, 78: 259-63.

Yu, K., and M. R. Lieber. 2019. 'Current insights into the mechanism of mammalian immunoglobulin class switch recombination', *Crit Rev Biochem Mol Biol*, 54: 333-51.

Zhang, K., X. Xu, M. A. Pasha, C. W. Siebel, A. Costello, A. Haczku, K. MacNamara, T. Liang, J. Zhu, A. Bhandoola, I. Maillard, and Q. Yang. 2017. 'Cutting Edge: Notch Signaling Promotes the Plasticity of Group-2 Innate Lymphoid Cells', *J Immunol*, 198: 1798-803.

Zhang, Y., L. Garcia-Ibanez, and K. M. Toellner. 2016. 'Regulation of germinal center B-cell differentiation', *Immunol Rev*, 270: 8-19.

Zhang, Y., G. Zhu, H. Xiao, X. Liu, G. Han, G. Chen, C. Hou, B. Shen, Y. Li, N. Ma, and R. Wang. 2017. 'CD19 regulates ADAM28-mediated Notch2 cleavage to control the differentiation of marginal zone precursors to MZ B cells', *J Cell Mol Med*, 21: 3658-69.

Zheng, H., D. M. Pritchard, X. Yang, E. Bennett, G. Liu, C. Liu, and W. Ai. 2009. 'KLF4 gene expression is inhibited by the notch signaling pathway that controls goblet cell differentiation in mouse gastrointestinal tract', *Am J Physiol Gastrointest Liver Physiol*, 296: G490-8.

List of abbreviations

4-OHT	4-hydroxytamoxifen
ADAM10	A Disintegrin And Metalloproteinase 10
AID	activation-induced deaminase
APC	antigen presenting cell
BAFF	B cell activating factor
BCR	B cell receptor
BSA	bovine serum albumin
BrdU	Bromodeoxyuidine
BTK	Bruton's tyrosine kinase
CCR	C-C chemokine receptor
CCL	C-C chemokine ligand
CD	cluster of differentiation
CFSE	carboxyfluorescein succinimidyl ester
CLP	common lymphoid progenitor
CSR	class switch recombination
CXCL	chemokine (C-X-C) motif ligand 13
CXCR	C-X-C chemokine receptor type 5
DC	dendritic cell
DLL-1	delta-like ligand 1
DNA	deoxyribonucleic acid
DMSO	dimethyl sulfoxide
EGF	epidermal growth factor
ERT2	tamoxifen inducible estrogen receptor
ES	enrichment score
FACS	fluorescence-activated cell sorting
FCS	fetal calf serum
FDC	follicular dendritic cell
FDR q-val	false discovery rate
FoB	follicular B (cell)
FRC	fibroblastic reticular cell
GC	germinal center
HEL	hen egg lysozyme
ICAM	intercellular adhesion molecules
Ig	immunoglobulin
IL7	interleukin 7
IL7R	interleukin 7 receptor
ILCs	innate lymphoid cells
IRES	internal ribosomal entry site
IRF	interferon regulatory factor
KLF	krueppel-like factor
KO	knock-out
LFA-1	lymphocyte function-associated antigen 1
LoxP	locus of X-over P1

LPS	lipopolysaccharide
MACS	magnetic cell separation
MAML1	mastermind-like protein 1
MDS	multidimensional scaling analysis
MHC	major histocompatibility complex
min	minute
ml	milliliter
MZB	marginal zone B (cell)
NF-κB	nuclear factor κB
NOM p-val	nominal p value
NotchIC/EC	intracellular/extracellular domain of the Notch receptor
nt	nucleotide
PBS	phosphate buffered saline
PCA	principal component analysis
PCR	polymerase chain reaction
PFA	paraformaldehyde
RAG	recombinase-activating genes
RBPjκ	recombining binding protein for immunoglobulin kappa J region
RIN	RNA integrity number
RNA	ribonucleic acid
RNA-Seq	RNA sequencing
rRNA	ribosomal RNA
rpm	revolutions per minute
S1P	sphingosine-1-phosphate
S1PR	sphingosine-1-phosphate receptor
SHM	somatic hypermutation
TACI	transmembrane activator and CAML interactor
TCR	T cell receptor
TD	T cell-dependent
TF	transcription factor
TI	T cell-independent
TLR	toll-like receptor
TNF	tumor necrosis factor
VCAM-1	**v**ascular cell adhesion protein 1
VLA-4	very late antigen 4

Danksagung

Ich danke zu allererst PD Dr. Ursula Zimber-Strobl für die Betreuung meiner Dissertation. Vielen herzlichen Dank für die Bereitstellung dieses interessanten Themas, ihr Vertrauen in mich und meine Arbeit und die Unterstützung über die Jahre im Labor und darüber hinaus. Die vielen Diskussionen und die intensive Zusammenarbeit an Publikationen haben mich als Wissenschaftler geschult und geprägt. Die zuletzt genannten Punkte verbinde ich auch mit Lothar Strobl, dem ich ebenfalls herzlich danke. Durch seine enorme Fachkompetenz zu Notch2 war er für mich stets kompetenter Ideengeber und Antreiber dieses Projekts.

Des Weiteren möchte ich mich bei Prof. Dr. Marc Schmidt-Supprian und Prof. Dr. Oliver Weigert bedanken, die für mich ein großartiges Thesis Advisory Committee bildeten. Besonderer Dank gebührt Marc für die intensive fachliche Zusammenarbeit. Er war früh ein wichtiger Kritiker und Entscheidungshelfer in diesem Projekt und ich danke ihm für zahlreiche Diskussionen und Kommentare, die letztlich in die gemeinsame Publikation mündeten.

Ein großer Dank geht an Dr. Thomas Engleitner, Dr. Ruppert Öllinger und Prof. Dr. Roland Rad für die Möglichkeit und den tatkräftigen Einsatz in einer fruchtbaren Kollaboration.

Ein besonders herzliches Dankeschön geht an die vielen Kolleg*innen der AGV, die meine Jahre im Haematologikum begleitet und bereichert haben. Der erste Dank gilt meinen unmittelbaren Laborkolleginnen Laura, Alex, Tea, Laura und Kris für die super Zusammenarbeit und die mitunter tatkräftige Hilfe wo gebraucht. Ich danke dem Abteilungsleiter der AGV, Prof. Dr. Wolfgang Hammerschmidt für seine Unterstützung und die fachlichen Diskussionen. Besonderer Dank auch an Wiebe und Alina (auch hier seinen nochmals Alex und Laura erwähnt) für deren zumindest teilweise hilfreichen Kommunikationsansätze zu diversen wissenschaftlichen und definitiv nicht-wissenschaftlichen Themen während wichtiger Espressopausen und darüber hinaus.

Ein ganz großes Dankeschön kann ich Michael Hagemann und seinen Mitarbeitern des Tierstalls aussprechen, die besonders nach dem Umzug unserer Labormäuse mit stets bewundernswert guter Laune meine Forschung überhaupt erst ermöglicht haben.

Zuletzt darf ich meiner Freundin Magdalena, meiner Familie und meinen guten Freunden danken, die durch ihr zumeist gut gemeintes, aber doch beharrliches Nachhaken zum aktuellen Stand meiner Doktorarbeit entscheidenden Anteil an der Fertigstellung dieses Manuskripts haben.

Eiddesstattliche Versicherung

Ich erkläre hiermit an Eides statt, dass ich die vorliegende Dissertation mit dem Titel:

Notch2 signaling in B cell plasticity

……

selbständig verfasst, mich außer der angegebenen keiner weiteren Hilfsmittel bedient und alle Erkenntnisse, die aus dem Schrifttum ganz oder annähernd übernommen sind, als solche kenntlich gemacht und nach ihrer Herkunft unter Bezeichnung der Fundstelle einzeln nachgewiesen habe.

Ich erkläre des Weiteren, dass die hier vorgelegte Dissertation nicht in gleicher oder in ähnlicher Form bei einer anderen Stelle zur Erlangung eines akademischen Grades eingereicht wurde.

München, 01.12.2021	Markus Lechner
Ort, Datum	Unterschrift Doktorand